

AD-A047 374

KAMAN SCIENCES CORP COLORADO SPRINGS COLO

F/G 19/4

HUSSAR SWORD SERIES. HUSKY PUP EVENT. DEVELOPMENT AND TESTING O--ETC(U)

SEP 76 H HOLLISTER, E L COLE, M A LEW

DNA001-75-C-0277

UNCLASSIFIED

K-76-112U(R)

DNA-4114F

NL

1 OF 2

AD
A047374



AD A047374

AD-E300 026 ✓

DNA 4114F

(12)

HUSSAR SWORD SERIES HUSKY PUP EVENT

Development and Testing of an
Earth Displacement Sensor

Kaman Sciences Corporation
P.O. Box 7463
Colorado Springs, Colorado 80933

September 1976

Final Report for Period September 1975 — September 1976

CONTRACT NO. DNA 001-75-C-0277

APPROVED FOR PUBLIC RELEASE;
DISTRIBUTION UNLIMITED.

THIS WORK SPONSORED BY THE DEFENSE NUCLEAR AGENCY
UNDER RDT&E RMSS CODE B345076462 J11AAXAX01301 H2590D.

Prepared for
Director
DEFENSE NUCLEAR AGENCY
Washington, D.C. 20305

DDC
RECEIVED
DEC 9 1977
B

DDC FILE COPY

Destroy this report when it is no longer
needed. Do not return to sender.



UNCLASSIFIED

SECURITY CLASSIFICATION OF THIS PAGE (When Data Entered)

REPORT DOCUMENTATION PAGE		READ INSTRUCTIONS BEFORE COMPLETING FORM
1. REPORT NUMBER DNA 4114F	2. GOVT ACCESSION NO.	3. RECIPIENT'S CATALOG NUMBER
4. TITLE (and Subtitle) HUSSAR SWORD SERIES. HUSKY PUP EVENT. Development and Testing of an Earth Displacement Sensor.		5. TYPE OF REPORT & PERIOD COVERED Final Report, for Period Sep 75-Sep 76,
6. AUTHOR(s) Herb (1002)/Hollister, Eldine L./Cole Michael A./Lew		7. PERFORMING ORGANIZATION REPORT NUMBER K-76-112U(R)
8. PERFORMING ORGANIZATION NAME AND ADDRESS Kaman Sciences Corporation P.O. Box 7463 Colorado Springs, Colorado 80933		9. CONTRACT OR GRANT NUMBER(s) DNA 001-75-C-0277
10. CONTROLLING OFFICE NAME AND ADDRESS Director Defense Nuclear Agency Washington, D.C. 20305		11. PROGRAM ELEMENT, PROJECT, TASK AREA & WORK UNIT NUMBERS NWET Subtask J11AAXAX013-01
12. MONITORING AGENCY NAME & ADDRESS (if different from Controlling Office) (12) 160p.		13. REPORT DATE September 1976
		14. NUMBER OF PAGES 170
		15. SECURITY CLASS (of this report) UNCLASSIFIED
16. DISTRIBUTION STATEMENT (of this Report) Approved for public release; distribution unlimited.		15a. DECLASSIFICATION/DOWNGRADING SCHEDULE
17. DISTRIBUTION STATEMENT (of the abstract entered in Block 20, if different from Report) (19) 4114F, AD-E300 026		
18. SUPPLEMENTARY NOTES This work sponsored by the Defense Nuclear Agency under RDT&E RMSS Code B345076462 J11AAXAX01301 H2590D.		
19. KEY WORDS (Continue on reverse side if necessary and identify by block number) EDS Development Project Rainer Mesa Canister Hardware Design Posttest Results Data Compensation		
20. ABSTRACT (Continue on reverse side if necessary and identify by block number) This report describes the effort by Kaman Sciences Corporation toward development of an Earth Displacement Sensor (EDS) for direct measurement of earth particle velocity and displacement in an underground test environment. The objective of this development was a sensor capable of direct measurement of earth displacement thereby avoiding errors associated with integration of acceleration or velocity measurements. The EDS consists of an —> next page		

DD FORM 1 JAN 73 1473

EDITION OF 1 NOV 65 IS OBSOLETE

UNCLASSIFIED

SECURITY CLASSIFICATION OF THIS PAGE (When Data Entered)

389 119

LB

UNCLASSIFIED

SECURITY CLASSIFICATION OF THIS PAGE(When Data Entered)

20. ABSTRACT (Continued)

Cont. Inertially isolated radial field magnet within a long tube which is embedded in the earth. Discrete pickup coils are distributed along the length of the tube. As the tube moves with the earth motion, a signal is induced in the coils moving through the magnetic field. Determination of which coil is producing the signal at any given time yields a direct measurement of the earth position at that time. Additionally, the amplitudes of the signals are proportional to the earth particle velocity. Details of the EDS design and related analysis are described and results of laboratory tests are presented along with field test results from event HUSKY PUP. Several remaining engineering problems are identified that await solution before the EDS can be considered a fieldworthy displacement measuring instrument.

ACCESSION for	
NTIS	White Section <input checked="" type="checkbox"/>
DOC	Dark Section <input type="checkbox"/>
UNANNOUNCED	<input type="checkbox"/>
JUSTIFICATION	
BY	
DISTRIBUTION/AVAILABILITY CODES	
Dist.	Avail. and/or SPECIAL
A	

UNCLASSIFIED

SECURITY CLASSIFICATION OF THIS PAGE(When Data Entered)

TABLE OF CONTENTS

	<u>Page</u>
CHAPTER 1 INTRODUCTION	9
1.1 Background	9
1.2 Project Objectives	10
CHAPTER 2 PROJECT SUMMARY	11
2.1 Design	11
2.1.1 Sensor	11
2.1.2 Canister	13
2.1.3 Response Analysis	13
2.1.4 Cable Transition	14
2.2 Laboratory Tests	14
2.2.1 Calibration	14
2.2.2 Drop Tests	14
2.3 Husky Pup Event	15
2.3.1 Installation	15
2.3.2 Posttest Results	16
2.4 Conclusions and Recommendations	17
CHAPTER 3 ENGINEERING DESIGN AND ANALYSIS	19
3.1 Rigid Body Response Analysis	19
3.2 EDS Canister Survival Analysis	26
3.2.1 Objectives	26
3.2.2 Assumptions	26
3.2.3 Constraints	28
3.2.4 Permissible Designs	38
3.3 Canister Coupling to Media	51
CHAPTER 4 HARDWARE DESIGN	57
4.1 The Transducer	57
4.1.1 Transduction Principle	57
4.1.2 Sensor Geometry	58

TABLE OF CONTENTS (Continued)

	<u>Page</u>
4.1.3 Coil Tube	60
4.1.4 Inertial Slug	61
4.1.5 Latching Mechanism	65
4.1.6 Electrical Circuit	66
4.2 The Canister	66
4.2.1 Outer Case	66
4.2.2 Cable Transition	69
4.3 The EDS	71
CHAPTER 5 PERFORMANCE TESTS	75
5.1 Bench Tests	76
5.1.1 Gravity Fall-Through	76
5.1.2 Sinusoidal Calibration	83
5.2 Shock Tests	84
5.2.1 Series I Drop Tests	86
5.2.2 Series II Drop Tests	90
5.2.3 EDS Test Results and Analysis	104
5.2.4 Crescent Gage Tests and Analysis	111
CHAPTER 6 HUSKY PUP UGT	119
6.1 Installation	119
6.2 Results	121
6.3 Comments	122
CHAPTER 7 SELECTED BIBLIOGRAPHIES	123
REFERENCES	129
APPENDIX A ANALYSIS OF EDS WITH DAMPING	131
A.1 Introduction	131
A.2 Analysis by Hartenbaum and Shunk	131
A.2.1 Purpose of Analysis	131
A.2.2 Mathematical Model	131

TABLE OF CONTENTS (Continued)

	<u>Page</u>
A.2.3 Data Compensation	136
A.2.4 Example	137
A.2.5 Conclusions	137
A.3 Analysis by Keeffe	139
A.3.1 Analytic Predictions	139
A.3.2 Evaluation of Viscous Damping Coefficient	140
A.3.3 Interpretation of Damped EDS Data	143
APPENDIX B FREE-FIELD GROUND MOTION FOR EDS ANALYSIS . . .	145
APPENDIX C NUMERICAL ANALYSIS OF DROP TEST RESULTS . . .	153
C.1 Configuration of EDS Drop Test	153
C.2 Canister Motions	153
C.3 EDS Equations of Motion	155
C.3.1 Slug Free-Body	155
C.3.2 Equations of Motion	155
C.3.3 Slug Breakaway	157
C.4 Slug Response	158
C.5 Data Presentation	159

LIST OF ILLUSTRATIONS

<u>Figure</u>	<u>Page</u>
2.1 Earth displacement sensor (EDS)	12
3.1 EDS geometry for rigid-body response analysis . . .	20
3.2 Sensitivity of breakaway acceleration to off-axis acceleration	22
3.3 Free-field waveforms for ground motion	24
3.4 Percent error in EDS displacement output	27
3.5 Pressure-time data trace from Dido Queen (Ref- erence 3)	29
3.6 Cross-section of a long tube subjected to uniform, lateral external pressure (P)	31
3.7 Geometry of the bending constraint problem	34
3.8 Survivability design constraints for 4130 steel at 0.5 kbar	39
3.9 Survivability design constraints for 4130 steel at 1 kbar	40
3.10 Survivability design constraints for 4130 steel at 2 kbar	41
3.11 Survivability design constraints for 4130 steel at 3 kbar	42
3.12 Survivability design constraints for 4130 steel at 4 kbar	43
3.13 Survivability design constraints for 4130 steel at 5 kbar	44
3.14 Minimum canister thickness versus pressure for 4130 steel	45
3.15 Survivability design constraints for 7075-T6 alu- minum at 0.5 kbar	47
3.16 Survivability design constraints for 7075-T6 alu- minum at 1 kbar	48
3.17 Survivability design constraints for 7075-T6 alu- minum at 1.5 kbar	49
3.18 Survivability design constraints for 7075-T6 alu- minum at 2 kbar	50
3.19 Minimum canister thickness versus pressure for 7075-T6 aluminum	52

LIST OF ILLUSTRATIONS (Continued)

<u>Figure</u>	<u>Page</u>
4.1 Cutaway view of EDS core geometry	59
4.2 Photograph of EDS coil tube during assembly	62
4.3 Photograph of EDS inertial slug with latching mechanism	63
4.4 Details of solenoid latch for inertial slug	64
4.5 EDS circuit diagram	67
4.6 Photograph at EDS assembly	68
4.7 Drawing of EDS canister	70
4.8 Cross-sectional drawing of EDS	72
5.1 Oscilloscope traces for gravity fall-through tests	77
5.2 Calibration of EDS from gravity fall-through test data	78
5.3 Velocity versus time for EDS slug in free fall	79
5.4 Displacement versus time for EDS slug in free fall	81
5.5 Effective coefficient of friction for prototype EDS	82
5.6 EDS drop test geometry	85
5.7 EDS drop test fixture	87
5.8 SLA vertical drop tester (DT-1) 45 degree test configuration for EDS	88
5.9 EDS signal, 300 g at zero degrees	94
5.10 Crescent signal, 300 g at zero degrees	95
5.11 Table accelerometer (A-1) signal, 300 g at zero degrees	96
5.12 Axial accelerometer (A-2) signal, 300 g at zero degrees	97
5.13 Transverse accelerometer (A-3) signal, 300 g at zero degrees	98
5.14 EDS signal, 300 g at 45 degrees	99
5.15 Crescent signal, 300 g at 45 degrees	100
5.16 Table accelerometer (A-1) signal, 300 g at 45 degrees	101
5.17 Axial accelerometer (A-2) signal, 300 g at 45 degrees	102

LIST OF ILLUSTRATIONS (Continued)

<u>Figure</u>	<u>Page</u>
5.18 Transverse accelerometer (A-3) signal, 300 g at 45 degrees	103
5.19 Table velocity and displacement for the zero degree, 100 g drop test	106
5.20 Table velocity and displacement for the 45 degree 100 g drop test	107
5.21 EDS output for the zero degree, 100 g drop test	109
5.22 EDS output for the 45 degree, 100 g drop test	110
5.23 Photograph of Crescent velocity gage	112
5.24 Crescent gage output signal from Operation Diamond Dust (Reference 11, Figure A.21)	113
5.25 Integrated Crescent gage output signals, 300 g at zero and 45 degrees	115
5.26 Crescent gage drop test results, 300 g at zero degrees	117
5.27 Crescent gage drop test results, 300 g at 45 degrees	118
6.1 EDS placement on Husky Pup event	120
A.1 EDS model for analysis	132
A.2 Direct readout of ground displacement versus shuttle displacement for 2.54 cm coil spacing (uncertainty in shuttle position ± 1.27 cm)	135
A.3 Comparison of true displacement with shuttle output	138
A.4 Vertical free fall experiment	141
A.5 EDS slug velocity-time history	142
B.1 Typical free-field motion	146
B.2 Parametric plot for determining X_R or t_d	152
C.1 EDS drop test configuration	154
C.2 Slug free-body diagram	156

LIST OF TABLES

<u>Table</u>	<u>Page</u>
3.1 Typical free-field motion parameters	25
3.2 Density, maximum shear stress, and seismic impedance for the grout candidates	54
5.1 EDS test matrix - Series II	92
5.2 Test data index	93

CHAPTER 1

INTRODUCTION

This report describes the effort by Kaman Sciences Corporation (KSC) toward development of an earth displacement sensor (EDS) for direct measurement of the particle velocity and displacement in an underground test (UGT) environment. The work has been sponsored by the Defense Nuclear Agency (DNA) under Contract No. DNA001-75-C-0277.

1.1 BACKGROUND

Direct measurement of the earth particle displacement associated with the UGT environment has long been a subject of interest to the experimenter concerned with ground motion studies. Many devices and schemes have been investigated in the past years in search for a satisfactory solution to this measurement problem. All of these have had serious drawbacks and most have fallen into disuse.

The most prevalent methods of determining earth displacement are the numerical double integration of an accelerometer or single integration of a velocity gage output. These methods have drawbacks as the effects of noise, zero shifts, and frequency response often contribute to large errors, especially at late times. There is great appeal for a sensor such as the EDS with possibility for a direct and independent temporal measure of both velocity and displacement.

The Time-Resolving and Integrating Momentum (TRIM) gage manufactured by KSC has proven to be highly successful for measuring impulse and momentum in specimens exposed to the UGT environment. Reference 1 is a report describing the TRIM gage. Modification of the TRIM design for application to ground displacement and velocity measurement appeared to be a straightforward

problem in design engineering with no major obstacles to overcome. This report shows that such was not the case. Several rather difficult engineering problems await solutions before the EDS will be a fieldworthy displacement transducer.

1.2 PROJECT OBJECTIVES

The EDS development project included: (1) Canister Design and Survival Analysis, (2) Sensor Design and Response Analysis, (3) Prototype Fabrication, (4) Response Tests and Analysis, (5) Field Test Unit Fabrication, (6) Husky Pup Field Support and (7) Posttest Analysis and Evaluation. The project objectives were the analysis, design, fabrication, qualification, and proof tests of an instrument suitable for measurement of the earth displacements associated with earth stress in the range from 0.2 kbar up to 1 or 2 kbar.

Viscous damping was considered as a method for reducing the length required for close-in measurements. Step one of the EDS project was the development of an undamped instrument. Efforts toward a damped model were curtailed early in the project with only a cursory investigation into the feasibility of such a design. Considerations of a damped EDS are presented in Appendix A.

CHAPTER 2

PROJECT SUMMARY

This chapter presents a very brief condensation of KSC's efforts to develop an EDS.

The EDS concept is derived from an extension of the principles of the highly successful TRIM gage manufactured by KSC. During early planning and proposal stages of the project, it was anticipated that the sensing element would be a rather straightforward modification of the TRIM with the protective canister as the major design problem. Hindsight has shown the inverse to be true.

Drop tests at the shock test facility at Sandia Laboratories showed the EDS transient response to be inadequate due to excessive frictional effects. While these data were still being analyzed, field test results from Husky Pup event came in with no useful data from either of the two channels fielded.

Salient points from development, fielding and test results are given in the chapters to follow, along with conclusions and recommendations.

2.1 DESIGN

Major problems and decisions associated with design of the EDS are broadly classed in one of four categories: Sensor, Canister, Response Analysis, and Cable Transition. Skipping intermediate details, the final design will be described. Figure 2.1 is a photograph of the EDS ready for field installation.

2.1.1 Sensor. The EDS is a self-generating transducer whose output is generated by an inertial magnet passing through a series of discrete coils under the influence of axial ground motion. Much of the EDS design was directly abstracted from the

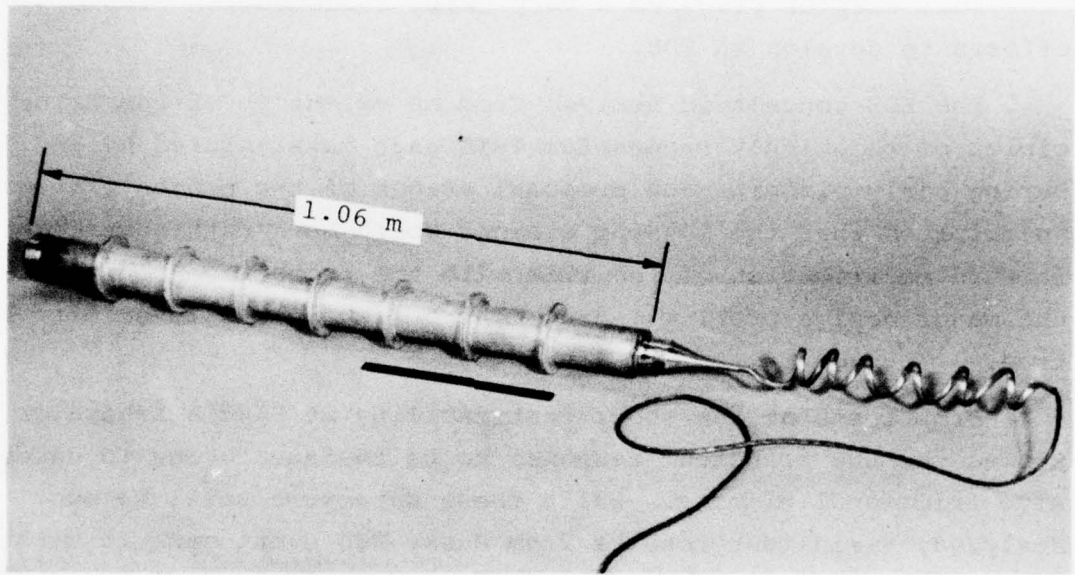


Figure 2.1. Earth displacement sensor (EDS).

TRIM gage to capitalize on past experience and existing technology.

Increasing the length by a factor of four presented an unexpected major obstacle in fabrication of the coil tube from polycarbonate within the dimensional tolerances required. The final design used tubes that were fabricated from precision honed and highly polished aluminum. The EDS was built and tested with a displacement range of 91 cm.

The radial field magnet rides on two bearings of nylon loaded with MoS_2 . Laboratory experiments in selecting this system indicated the coefficient of friction would be easily less than 0.1, approaching 0.05 under ideal conditions. The final design resulted in measured values approximately twice the expected value.

2.1.2 Canister. The canister serves a dual role in the measurement of earth displacement. First, it protects the sensing mechanism from distortion and physical damage by the environment and second, provides a means of coupling the sensor to the media. The canister is essentially a piece of heat treated steel pipe with seven external welded rings that served to enhance coupling to the surrounding grout.

The predicted failure mode was excessive buckling deformation above 1.4 kbar static pressure level. Deformation represents a major constraint if the canister is rigidly coupled to the coil form tube. A satisfactory solution was reached by decoupling the outer canister shell from the active sensing elements. A liner of silicone rubber serves to isolate the coil form from effects of external case distortion and also to suppress shock induced vibrations of the coil tube.

2.1.3 Response Analysis. Parametric studies of EDS response were carried out to better understand the frictional

effects on gage error. Sensitivity to off-axis acceleration was also studied. These studies showed the error to be acceptably low if the coefficient of friction could be kept well below 0.1.

A mathematical model of the EDS was developed for use in computer aided analysis and predictions. With known frictional values and the acceleration environment the indicated displacement can be corrected to improve the accuracy of the measurement.

2.1.4 Cable Transition. The interface between canister and cable is recognized as a particularly vulnerable area for failure of the cable in shear. To relieve this problem, a graded strength transition between the two elements was designed. An aluminum end piece approximately 10 cm long was attached to the canister with a threaded section. This piece was tapered in a somewhat concave fashion to a feather edge at the extreme end to meet a 75 cm section of aluminum tubing formed in a spiral. This allowed for axial motion of the cable relative to the canister. The cable was inside of the aluminum tubing.

The details of this design are believed to be sound and worthy of consideration for application to similar situations where cable survival is a problem.

2.2 LABORATORY TESTS

2.2.1 Calibration. The EDS was calibrated using a reciprocating connecting rod drive on the inertial mass. By moving the magnet past the coils at a known velocity, the sensitivity was measured to be a nominal 4.8 mv/cm/sec.

The slug was also allowed to drop through the coils in a free fall under the influence of gravity. The coefficient of friction indicated by this experiment was 0.16.

2.2.2 Drop Tests. The EDS was tested on a vertical drop test machine (DT-1) in the Shock Testing Facility at Sandia

Laboratories. Test objectives were twofold: (1) proof test at 125 percent of maximum predicted shock levels and, (2) characterize the gage response and sensitivity to cross-axis acceleration. The tests represented a reasonable compromise with consideration for availability of equipment for simulation of the desired environments. An exact simulation of the environment the EDS is designed to measure is not the best test for characterization of the gage transfer function. Another important constraint was a very limited budget of both money and time.

The EDS drop test matrix included shock levels of 300 and 100 g peak (10 ms half-sine) at angles of 0, 27 and 45 degrees. Results of these tests were disappointing, indicating a much larger error than was expected or acceptable for a useful instrument. The large error associated with the zero degree test led to the conclusion that the inertial slug was probably moving through the tube with a "rattling" motion.

Analysis of these laboratory test data showed the EDS was not yet refined to a fieldworthy state. However, the overall schedule did not allow this determination prior to a commitment to field two units on Husky Pup event.

2.3 HUSKY PUP EVENT

2.3.1 Installation. Two gages were installed, one at 104 meters and the other at 137 meters from the working point. Several difficulties were encountered during installation of the higher level unit. The plan was to place it at 95 meters but debris in the drill hole forced placement further back. Also, a portion of the tunnel wall broke out during pressurization of the grout. During subsequent regrouting the pressure was maintained at 40 psi maximum. The 137 meter unit was successfully pressurized to 120 psi.

This and several other aspects of the installation are now academic in view of the failure of both EDS gages.

2.3.2 Posttest Results. No useful data were obtained from either EDS channel on Husky Pup event. Since the canisters have not been recovered, one can only speculate the cause for complete failure. In retrospect, the most probable cause for total failure appears to be leakage of fluid during the grouting operation. If the fluid penetrated the vinyl jacket of the cable there is good probability it could follow the wires into the canister interior. While the EDS is potted internally (except for inside the coil tube) the RTV would not be expected to act as a pressure seal since its adhesion is poor and it is quite compressible. Assuming this failure mode explains all of the subsequent experiences. First, there was no positive indication that the inertial slug was released when the latching solenoid was energized. Second, no meaningful data was recorded during the ground motion from Husky Pup event. There was no indication of any signal that could be interpreted as motion of the coil tube relative to the magnet.

Failure of the solenoid to respond would cause an error of the output signal by delaying initial movement of the inertial slug. The locking mechanism consisted of a 1.5 mm diameter steel pin inserted behind a 0.8 mm aluminum lip. However, it is unlikely that this lip would not fail in shear at or before the peak acceleration level.

A less likely but possible alternative failure mode is the canister distortion. Undue crushing of the canister would result in seizure of the slug with no output as a consequence.

The cable transition seems to have survived at least for several hundred milliseconds as seen from studying the baseline noise level.

2.4 CONCLUSIONS AND RECOMMENDATIONS

Quite aside from the UGT failure, based on drop test results, it is obvious that the EDS is not yet ready for field application in the environment for which it is has been designed. The coefficient of friction (or apparent frictional effects) must be reduced to an acceptable level and the fluid pressure integrity of the canister improved. The latter presents no special problem while the drag on the slug could be much more troublesome.

The apparent frictional effects could be caused by the combination of a short shuttle and relatively loose clearance between sliding bearings and the coil tube. When the EDS is shocked, vibrations in the tube may cause the shuttle to rattle from side to side as it moves down the tube. Analysis of the drop test data indicates that the error is not induced by any simple interpretation of coulomb friction.

As mentioned previously, without recovery of at least one of the EDS canisters it is impossible to make positive determination of the failure mode. It would seem worthwhile to consider recovery if mining is being done in the immediate vicinity. The recovery would permit assessment of canister survival, cable transition survival and a positive determination of the cause of failure. The first two benefits could have direct application to other projects while the third may be only of academic value depending upon the fate of this EDS project.

While the primary objective of this project (successful development of an earth displacement sensor) was not satisfied, several worthwhile byproducts of this effort have direct application to other projects. These will be emphasized in this report along with the lessons learned in studying and working with the EDS concept. Of particular significance is the cable transition design described in Chapter 4. The canister survival

analysis has general applicability to other thick walled cylinder design problems.

The response analysis and damping considerations are not as general in nature yet could apply to instruments with similar designs.

One day the principle of the EDS will doubtless be applied in some modified form to another problem for which it is more suitable. It is hoped that the lessons learned on this project and reported herein will serve as stepping stones and for guidance to that project. For this reason, many details are reported that are otherwise irrelevant history.

CHAPTER 3
ENGINEERING DESIGN AND ANALYSIS

3.1 RIGID BODY RESPONSE ANALYSIS

A rigid-body analysis was performed to determine the sensitivity of the induced motion $X(t)$ of the EDS inertial slug to values of the angle α between the direction of motion of the shock front and the axis of the EDS.

For this analysis, it was assumed that: (1) the EDS canister is rigid and installed horizontally in the earth, (2) the radial shock (with respect to the source) propagates slightly off the horizontal axis at an angle α , (3) the only force acting on the slug at the coil tube interface arises from coulomb (sliding) friction (i.e., no damping) and, (4) there is perfect coupling between the earth and the canister. Displacements X and X_1 are referenced to a fixed ground point. The geometry is shown in Figure 3.1.

Quantities and parameters in the figure are defined:

$X_1(t)$ = free-field motion of the earth and canister,

$X(t)$ = induced motion of the inertial slug,

α = off-axis angle of radial shock front with the horizontal

m = mass of the inertial slug, and

f = frictional force

The frictional force $f = \mu N$, where

N = the normal force on the slug

μ = the coefficient of friction

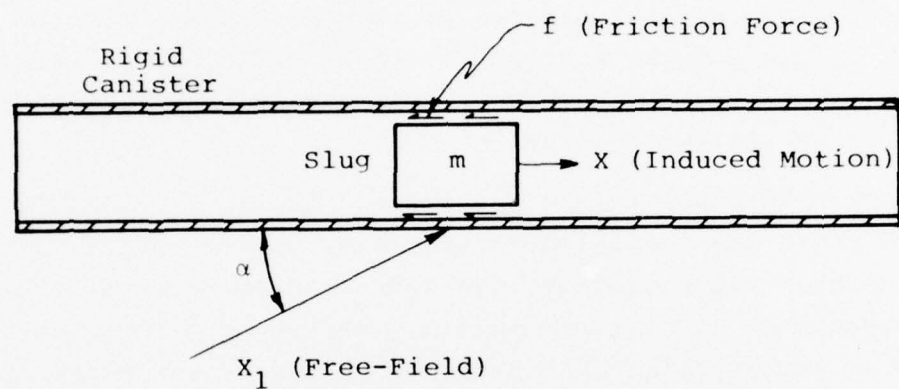


Figure 3.1. EDS geometry for rigid-body response analysis.

Subscripts are used for

μ_1 = coefficient of static friction $\dot{X}_1 = \dot{X}$

μ_2 = coefficient of dynamic friction $\dot{X}_1 \neq \dot{X}$

At very early times the slug moves with the canister due to static friction, but at some time t_0 , the breakaway time, the slug will break loose from the canister and relative movement will commence. At t_0 , the free-field acceleration $\ddot{X}_1(t_0)$ satisfies the condition

$$\frac{\ddot{X}_1(t_0)}{g} = \frac{\mu_1}{\cos\alpha - \mu_1 \sin\alpha} \quad (3.1)$$

Figure 3.2 shows the sensitivity of the free-field breakaway acceleration to various angles of α using Equation (3.1). It may be seen that over a range of angles α from ± 60 degrees, the breakaway acceleration ranges from 0.05 g to 0.2 g for $0.05 \leq \mu_1 \leq 0.1$.

These equations show that the effects of friction on breakaway are small when compared to the built-in value of 1.67 g. This is from the spring restraint clip that holds the slug in place until measurement time. See Chapter 4 for further details of this aspect of the EDS.

The breakaway acceleration values are very small compared to the peak accelerations expected for the EDS free-field environment, so that breakaway should occur very shortly (several microseconds) after the arrival of the shock front.

After breakaway, the slug motion is governed by its initial conditions and frictional drag forces (neglecting any aerodynamic drag). The equation of motion is

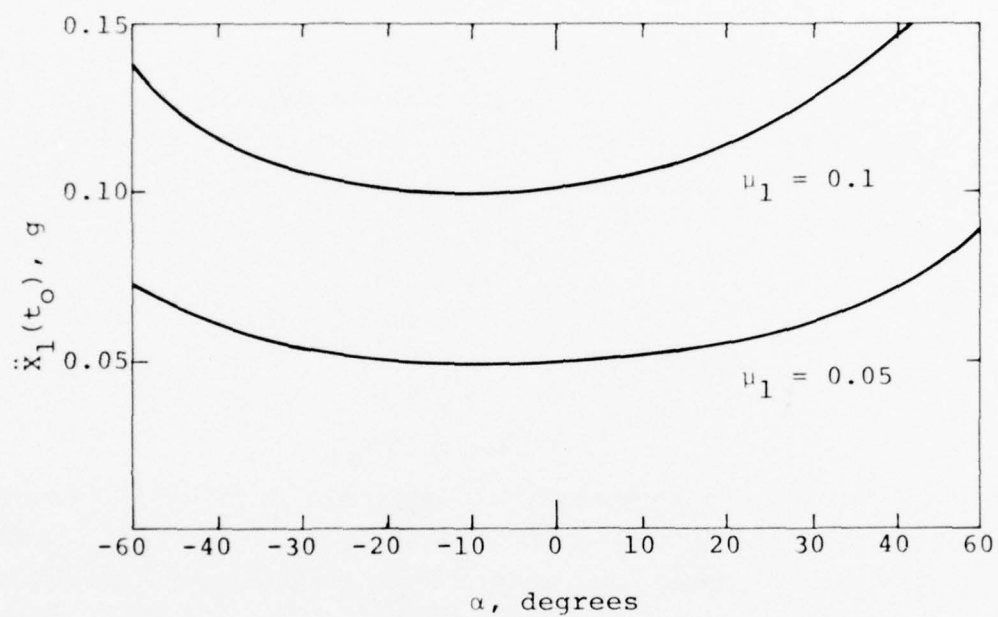


Figure 3.2. Sensitivity of breakaway acceleration to off-axis acceleration.

$$m\ddot{X}(t) - \left| \mu_2 m [g + \ddot{X}_1(t)\sin\alpha] \right| = 0 \quad (3.2)$$

with initial conditions

$$\begin{aligned} \dot{X}(t_0) &= \dot{X}_1(t_0)\cos\alpha \\ X(t_0) &= X_1(t_0)\cos\alpha \end{aligned} \quad (3.3)$$

The parameters of interest are

X_1 = free-field displacement

$X_1\cos\alpha$ = canister displacement

X = slug displacement

$\Delta X = X_1\cos\alpha - X$ = gage output parameter

Gage error = $1 - \frac{\Delta X}{X_1\cos\alpha}$

Equation 3.2 was solved in closed form to obtain velocity $\dot{X}(t)$ and displacement $X(t)$ in terms of the free field environment. The resulting equations were programmed for computer-aided computations of parametric values used in studies of EDS performance and response. DNA furnished data (Reference 2) were used as input for waveforms and peak values of acceleration, velocity, and displacement at various ranges. Figure 3.3 portrays the general nature of the temporal waveforms expected while representative peak values are given in Table 3.1.

Using the DNA predicted environment for guidance, a self-consistent set of piecewise-continuous functions were developed that could be used in the computer code as the input stimulus to the EDS. These equations are given for reference in Appendix B. The code was also developed to accept an arbitrary input such as would be

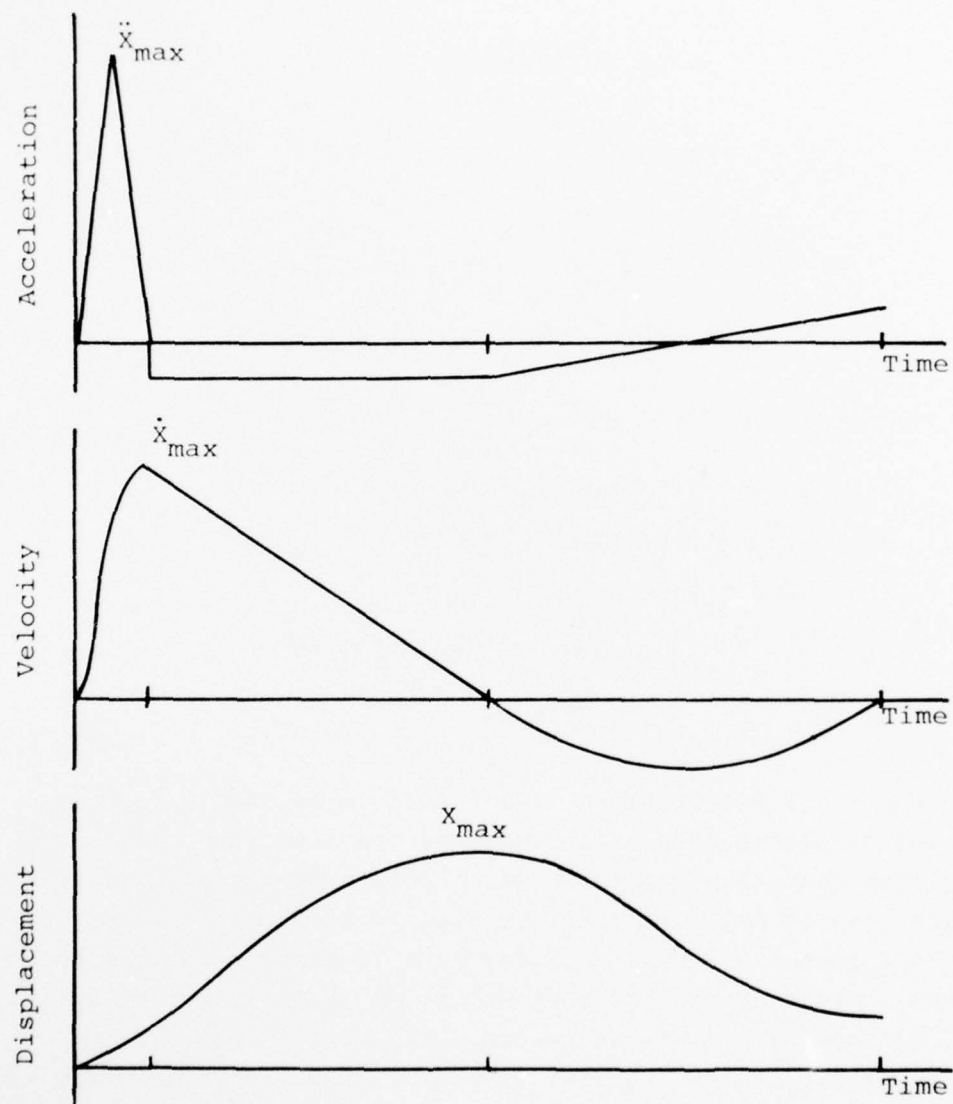


Figure 3.3. Free-field waveforms for ground motion.

Table 3.1. Typical free-field motion parameters.

P_{\max} (kbar)	\ddot{X}_{\max} (g)	\dot{X}_{\max} (m/sec)	X_{\max} (m)
2.8	3350.	75.0	3.60
0.66	350.	14.9	0.96
0.29	96.	5.7	0.44
0.16	38.	2.9	0.26
0.10	19.	1.7	0.17

obtained from digitization of an analog accelerometer measurement.

The results of an error analysis to investigate the sensitivity of the EDS to cross-axis acceleration are shown in Figure 3.4. It is noted from study of the figure that if, μ equals 0.1, a five percent error at peak displacement can be expected for a misalignment on the order of 10 degrees ($\arctan \alpha$ equals 0.8).

It was concluded from the analysis that the EDS requires a low coefficient of friction (μ less than 0.1) to be used satisfactorily without applying any correction for frictional effects if a precision measurement is required. The use of a complementary triaxial accelerometer measurement and a forehand knowledge of the coefficient of friction enables a straightforward and reasonable compensation of the data. Such a procedure would extend the useful range of applications for the EDS and tolerate a larger value of μ .

3.2 EDS CANISTER SURVIVAL ANALYSIS

3.2.1 Objectives. A survivability analysis was performed to determine adequate structural designs for the canister of the EDS. The analysis was performed over a range of peak pressures up to 5 kbar with a specific design objective of determining a canister sure-survival design for a peak pressure of 1 kbar. Several aspects of structural adequacy were considered using static analyses, which in general will tend to yield conservative designs.

3.2.2 Assumptions. It was assumed throughout this analysis that as the pressure shock front traverses the free-field medium and engulfs the canister itself, a state of hydrostatic pressure exists behind the shock front. Thus when the maximum pressure occurs at some point on the canister, that maximum pressure

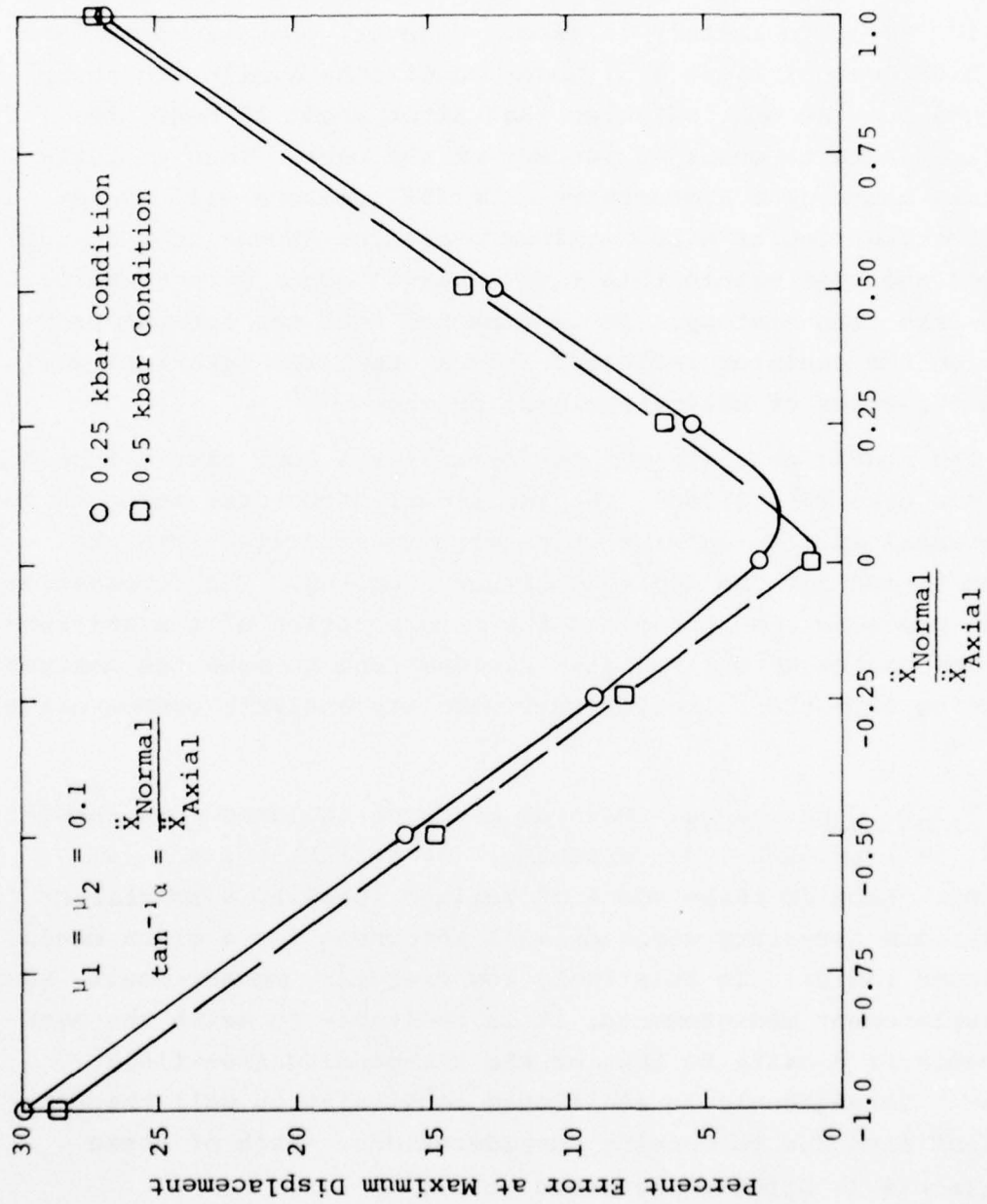


Figure 3.4. Percent error in EDS displacement output.

occurs over the length of the canister engulfed by the shock front. This assumption is reasonable for the first 15 msec after the arrival time since the expected positive acceleration pulse duration is approximately 15 msec. However, pressure-time data from Dido Queen (Figure 3.5) under conditions similar to those expected for the EDS indicates that after about 15 msec, the pressure drops to about 40 percent of the peak. Thus a static analysis assuming a hydrostatic external pressure will yield conservative results since maximum pressures appear to last only 15 msec and even within this time interval occur with a sharp, spike-like time history. It is expected that the lateral pressures on the canister reflected from a quartzite interface will be on the order of half the radial pressure.

The static analysis was performed for a long simple tube and does not take into account the additional structural strength due to external stiffening ribs which were incorporated into the design to enhance the medium/canister coupling. The combination of the pressure assumption and the incorporation of the stiffening ribs on the actual canister fielded tend to make the designs resulting from the following survivability analysis conservative ones.

3.2.3 Constraints. Several modes of failures were considered: (1) buckling, (2) crushing, (3) deflection, and (4) bending. Each of these modes of failure leads to a constraint on the minimum necessary canister wall thickness for a given canister inner radius. In relatively low frequency measurements, such as displacement measurements, it is desirable to match the average canister density to that of the surrounding free-field medium. Consequently an additional constraint on wall thickness is identified due to density considerations. Each of these constraints is briefly discussed below.

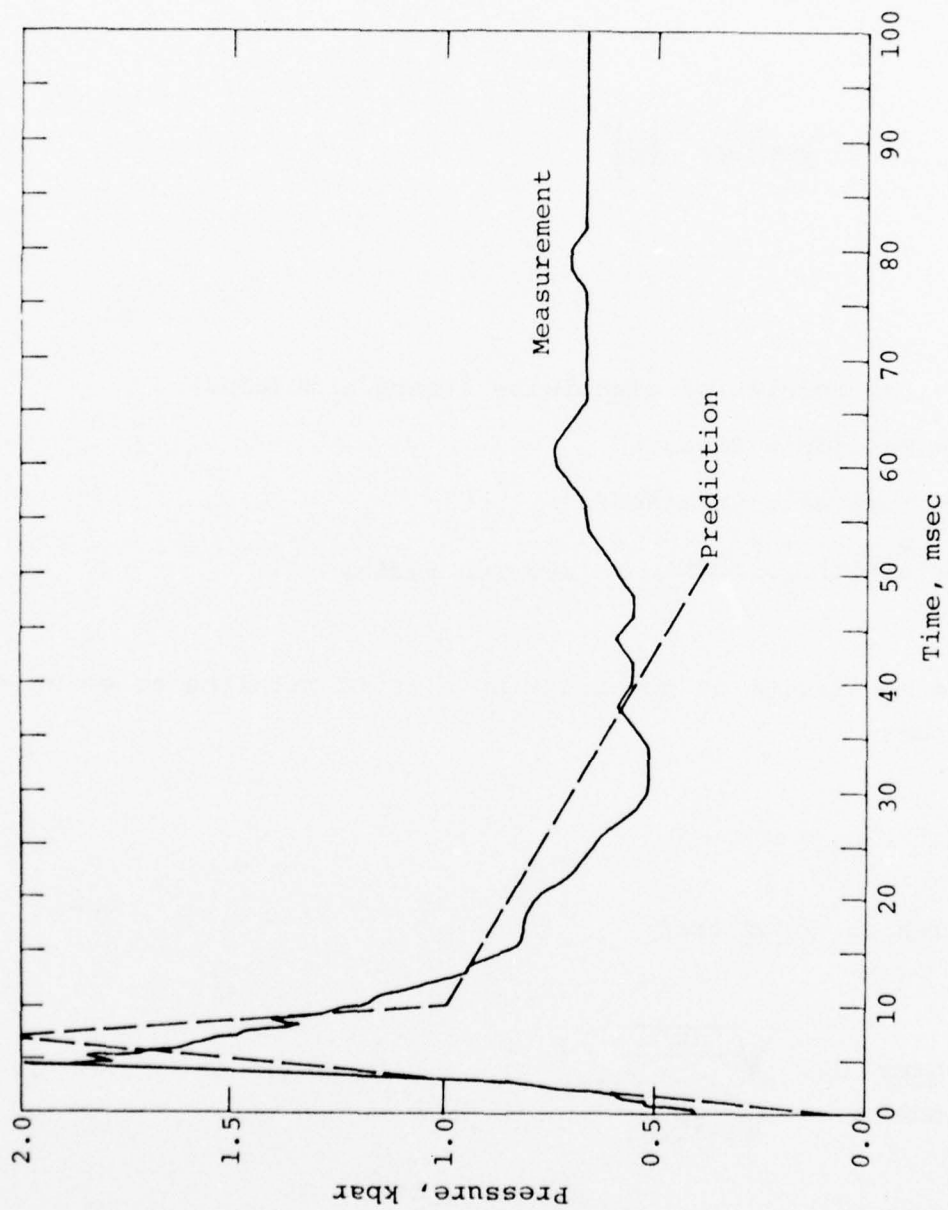


Figure 3.5. Pressure-time data trace from Dido Queen (Reference 3).

1. Buckling Constraint. For a long tube subjected to a uniform lateral external pressure P (see Figure 3.6), the critical pressure P_{crit} at which elastic buckling occurs is (Reference 4, Page 354):

$$P_{crit} = \frac{E}{4(1-\nu^2)} \left(\frac{t}{R} \right)^3$$

where:

E = the modulus of elasticity (Young's Modulus)

ν = Poisson's Ratio

t = Tube wall thickness

$$R = \frac{R_{outer} + R_{inner}}{2} = \text{average radius}$$

The constraint of not allowing elastic buckling to occur requires that

$$P < P_{crit} ,$$

from which is found that:

$$\frac{R_{outer}}{R_{inner}} > \frac{\sqrt[3]{\frac{2E}{P(1-\nu^2)}} + 1}{\sqrt[3]{\frac{2E}{P(1-\nu^2)}} - 1} \quad (3.4)$$

2. Crushing Constraint. For a thick tube subjected to a uniform external pressure P , (as shown in Figure 3.6) at a given

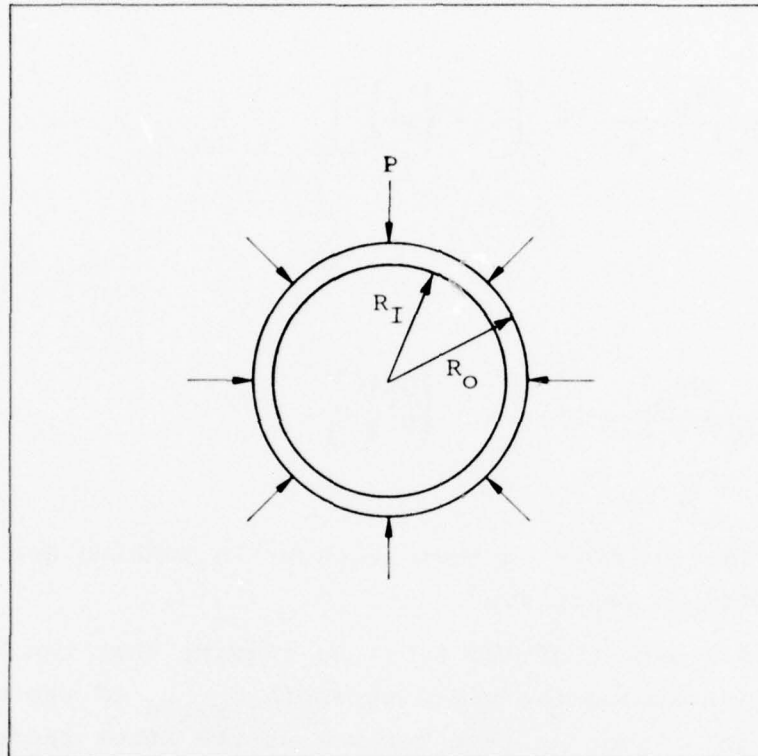


Figure 3.6. Cross-section of a long tube subjected to uniform, lateral external pressure (P).

radius R , the equations for the radial and hoop stress components (Reference 4, Page 308) are:

$$\sigma_r = \frac{PR_o^2}{R_o^2 - R_I^2} \cdot \left[1 - \left(\frac{R_I}{R} \right)^2 \right]$$

and

$$\sigma_\theta = \frac{-PR_o^2}{R_o^2 - R_I^2} \cdot \left[1 + \left(\frac{R_I}{R} \right)^2 \right]$$

The sign convention here is that stresses in tension are positive and in compression negative.

To avoid crushing of the tube, we require that the hoop stress does not exceed the yield strength σ_{yield} of the material in compression. Since σ_θ is a maximum at the inner radius R_I , we require that σ_θ be less (in absolute value) than σ_{yield} , i.e.,

$$\sigma_\theta > -\sigma_{\text{yield}} \quad \text{at } R = R_I$$

The crushing constraint leads to the inequality

$$\frac{R_o}{R_I} > \sqrt{\frac{\sigma_{\text{yield}}}{\sigma_{\text{yield}} - 2P}} \quad (3.5)$$

3. Deflection Constraint. For a thick tube subjected to a uniform external pressure (Figure 3.6), we require that the deflection (change in radial displacement) δ at the inner radius R_I be less than some given deflection of magnitude δ_O . This constraint was to insure that the steel outer coil tube (internal to the canister) would not deform so as to bind up the inertial slug within.

The equation for the deflection of the canister at a given radius R is:

$$\delta = \frac{R}{E} \left(\sigma_{\theta} - \nu \sigma_r \right)$$

where σ_{θ} , σ_r , E and ν are defined as above.

We then require that

$$\delta > -\delta_O = 0.25 \text{ mm at } R = R_I ,$$

where a radial expansion is a positive δ while a contraction is a negative δ . The result is the inequality

$$\frac{R_O}{R_I} > \sqrt{\frac{1}{1 - \frac{2R_I P}{\delta_O E}}} \quad (3.6)$$

4. Bending Constraint. If the shock front traverses the EDS while being inclined at angle θ to the canister axis (Figure 3.7), the non-axisymmetric loading over a length d tends to bend

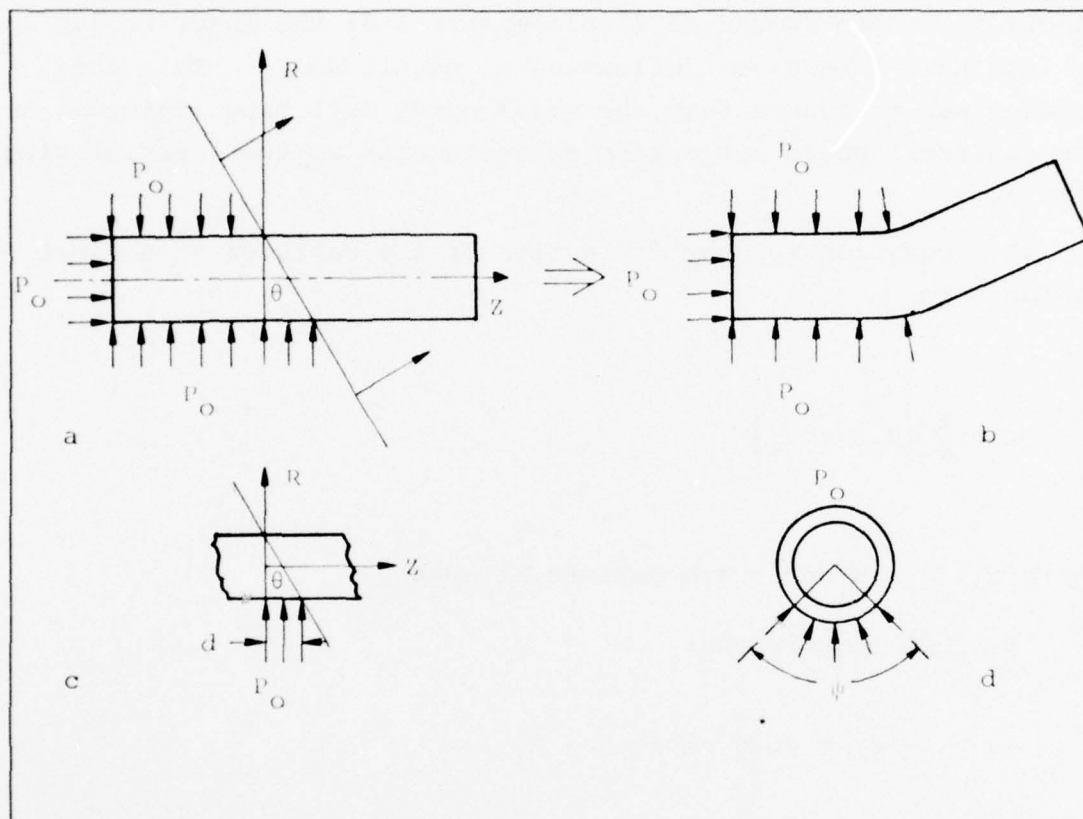


Figure 3.7. Geometry of the bending constraint problem.

the canister. At the end points of this region along the canister, the load passes from zero degrees engulfment to 360 degrees engulfment, while at any point in between the ends, Ψ degrees out of 360 degrees are engulfed. The incremental component of load dP perpendicular to the axis on a cross-sectional "disc" of length dz is given by:

$$dP = \left[\int_{-\Psi/2}^{\Psi/2} P_O R_O \cos \alpha \, d\alpha \right] dz$$

$$= 2P_O R_O \sin \frac{\Psi}{2} dz$$

At $\Psi = 0^\circ$ and $\Psi = 360^\circ$, $P = 0$ as expected. Ψ varies linearly from $z = 0$ to $z = d$ as given by

$$\Psi = \left(\frac{d - z}{d} \right) 2\pi$$

The moment M on the canister is then:

$$dm = zdP$$

Solving for M by integration of both sides

$$M = 2P_O R_O \int_0^d z \sin \left(\frac{\pi}{d} z \right) dz$$

$$= 2P_O R_O \left(\frac{d^2}{\pi} \right)$$

Since $d = 2R_O \tan \theta$, we then have:

$$M = \frac{8P_O R_O^3 \tan^2 \theta}{\pi}$$

For beam bending, the stress component in the z direction due to bending is

$$\sigma_{\text{bending}} = \frac{MR_O}{I} = \frac{4MR_O}{\pi(R_O^4 - R_I^4)}$$

$$= \frac{32P_O R_O^4 \tan^2 \theta}{\pi^2 (R_O^4 - R_I^4)}$$

where

$$I = \frac{\pi(R_O^4 - R_I^4)}{4} = \text{moment of inertia of the tube.}$$

To take into account the effects of the axial load on the end caps, we can first determine the end load P_{end} :

$$P_{\text{end}} = P_O \pi R_O^2$$

This end load causes an axial stress σ_{end} in the tube as given by:

$$\sigma_{\text{end}} = \frac{P_{\text{end}}}{\pi(R_O^2 - R_I^2)} = \frac{P_O R_O^2}{R_O^2 - R_I^2}$$

If we now require that the axial stress be less than the yield strength of the material we have:

$$\sigma_z = \sigma_{\text{end}} + \sigma_{\text{bending}} < \sigma_{\text{yield}}$$

which yields the constraint:

$$\frac{R_O}{R_I} > \sqrt{\frac{-B + \sqrt{B^2 - 4AC}}{2A}} \quad (3.7)$$

where:

$$A = \pi^2 \sigma_{\text{yield}} - 32 P_O \tan^2 \theta - \pi^2 P_O$$

$$B = -\pi^2 P_O \quad \text{and}$$

$$C = -\pi^2 \sigma_{\text{yield}}$$

5. Density Considerations. It is desirable to have an EDS with an average weight density $\bar{\rho}$ equal to the density of the surrounding medium ρ_m (equals 2.0 gm/cm³ for saturated tuff), particularly when relatively low frequency ground motion data are sought. Reference 5 indicates that for a spherical canister

with a density mismatch of 1.35 between the canister and medium, an error of approximately 20 percent in the measured radial velocity from the true free-field velocity can be expected.

Requiring that $\bar{\rho} = \rho_m$, we can obtain a relation for the ratio R_O/R_I that is a function of ρ_m (and the canister dimensions):

$$\frac{R_O}{R_I} = f(\rho_m) \quad (3.8)$$

The function $f(\rho_m)$ is not explicitly given here as it includes all of the formulas for elemental volumes, and densities of the EDS assembly. It is long and unwieldy and would serve no useful purpose to include in this report.

3.2.4 Permissible Designs. Plotting Equations (3.4), (3.5), (3.6), (3.7), and (3.8) on a graph of canister thickness, $t = R_O - R_I$, versus R_I for various external pressures up to 5 kbar, one can readily identify the permissible designs for the EDS canister. High strength 4130 steel was used for fabrication of the EDS canister. The material was heat treated to obtain a yield strength of 117,000 N/cm². The density of the surrounding medium was assumed to be that of saturated tuff with matching grout, viz, $\rho_m = 2.0$ gm/cm³. For pressures of 0.5, 1, 2, 3, 4, and 5 kbar, the resulting plots are shown in Figures 3.8 through 3.13.

Also shown on the plot for 0.5, 1, and 2 kbar are the curves for density ratios $\bar{\rho}/\rho_m$ of 1.25 and 1.5. The areas of permissible designs are shown as the hatched areas with a symbol indicating the EDS design point. Figure 3.14 is a plot of minimum canister thickness versus pressure for various inner radii. This figure indicates that the EDS design is adequate to 1.4 kbar.

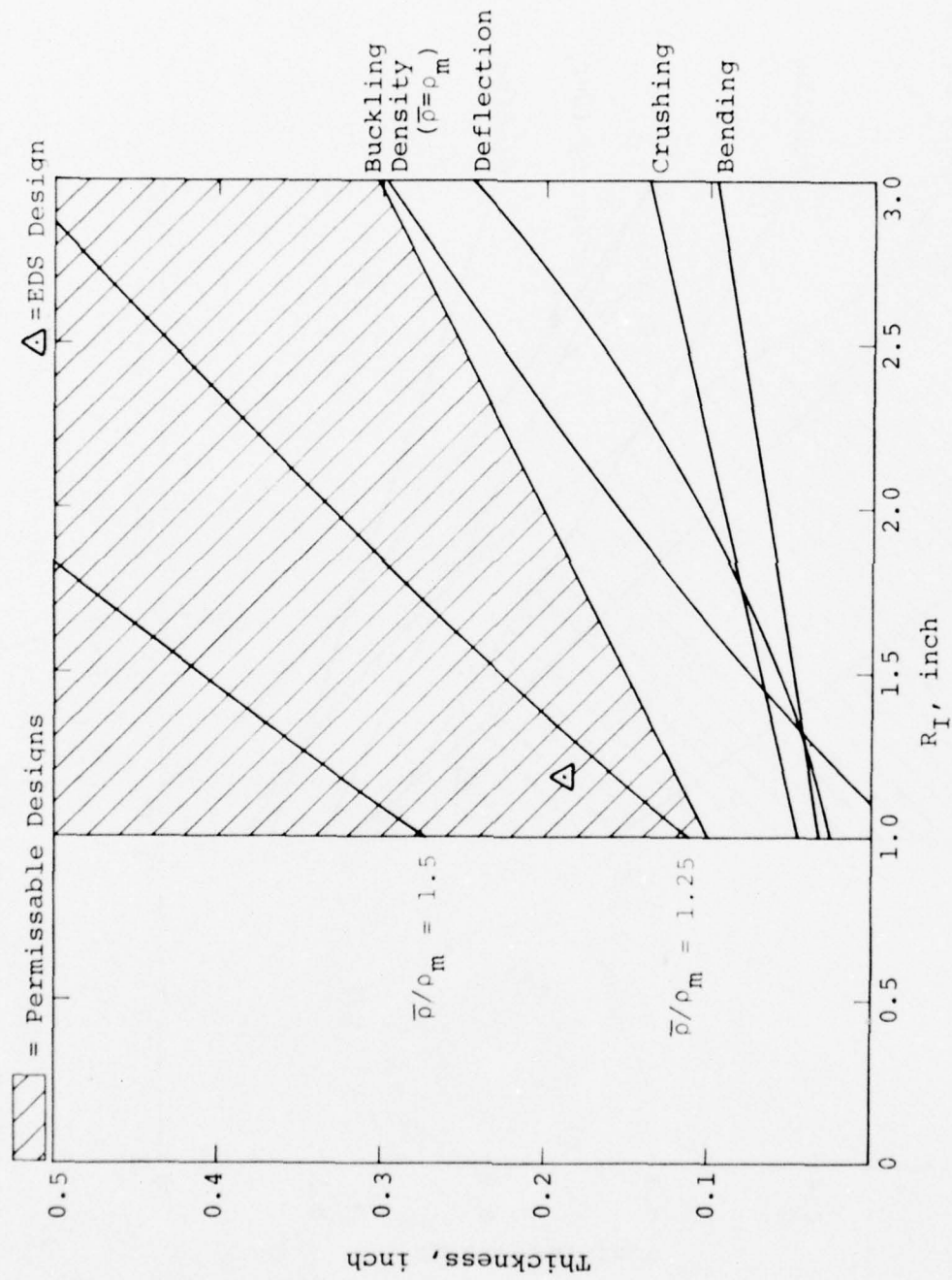


Figure 3.8. Survivability design constraints for 4130 steel at 0.5 kbar.

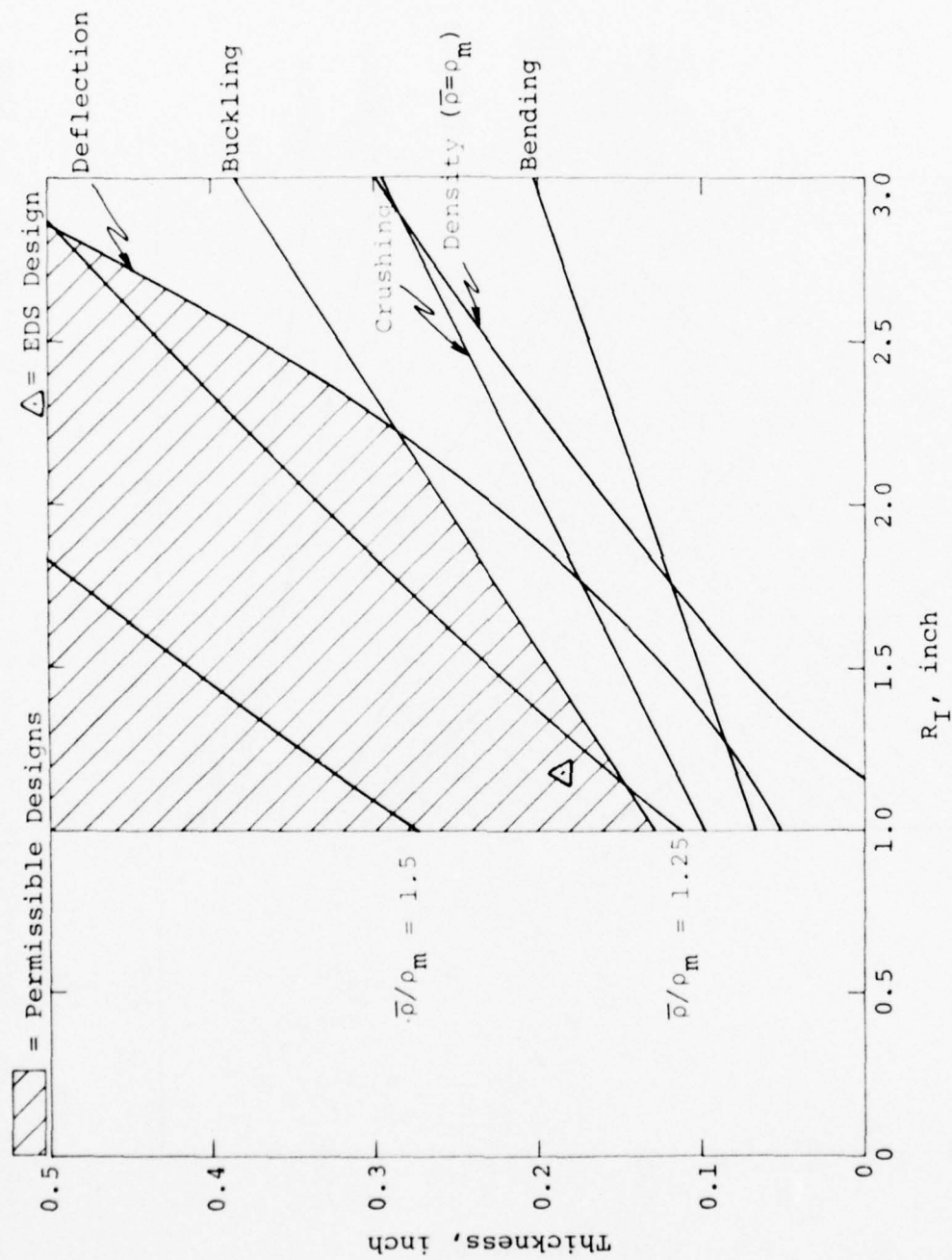


Figure 3.9. Survivability design constraints for 4130 steel at 1 kbar.

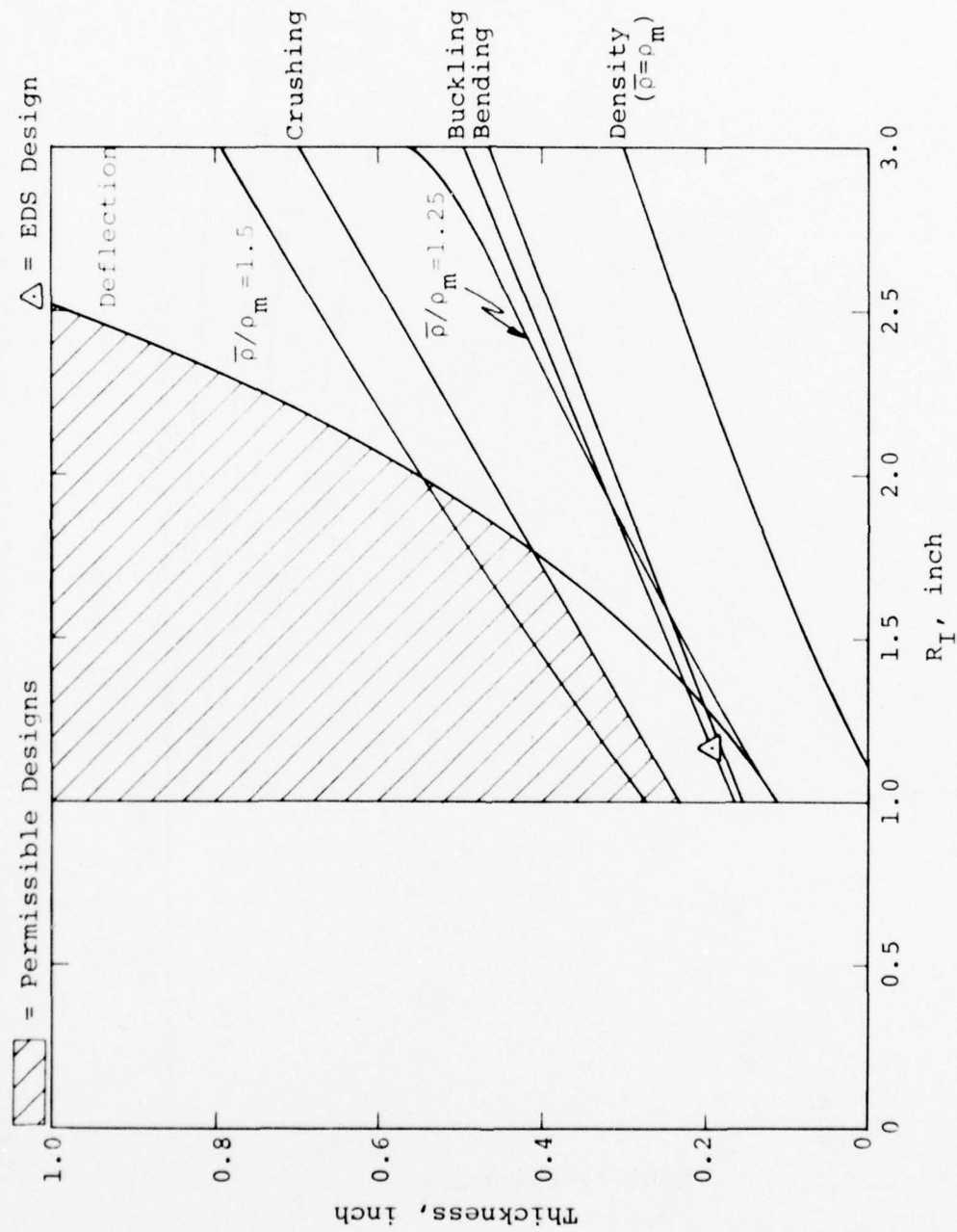


Figure 3.10. Survivability design constraints for 4130 steel at 2 kbar.

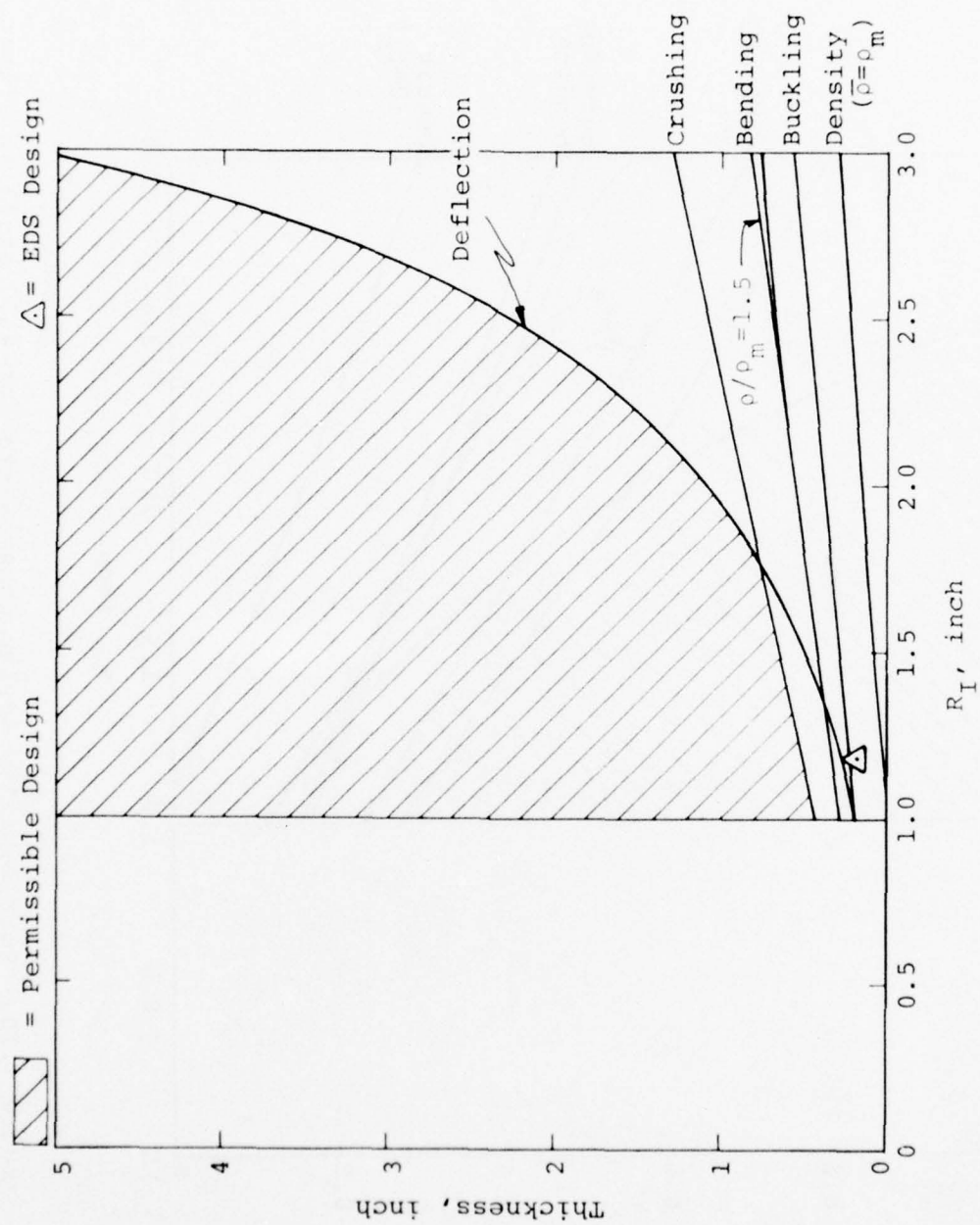


Figure 3.11. Survivability design constraints for 4130 steel at 3 kbar.

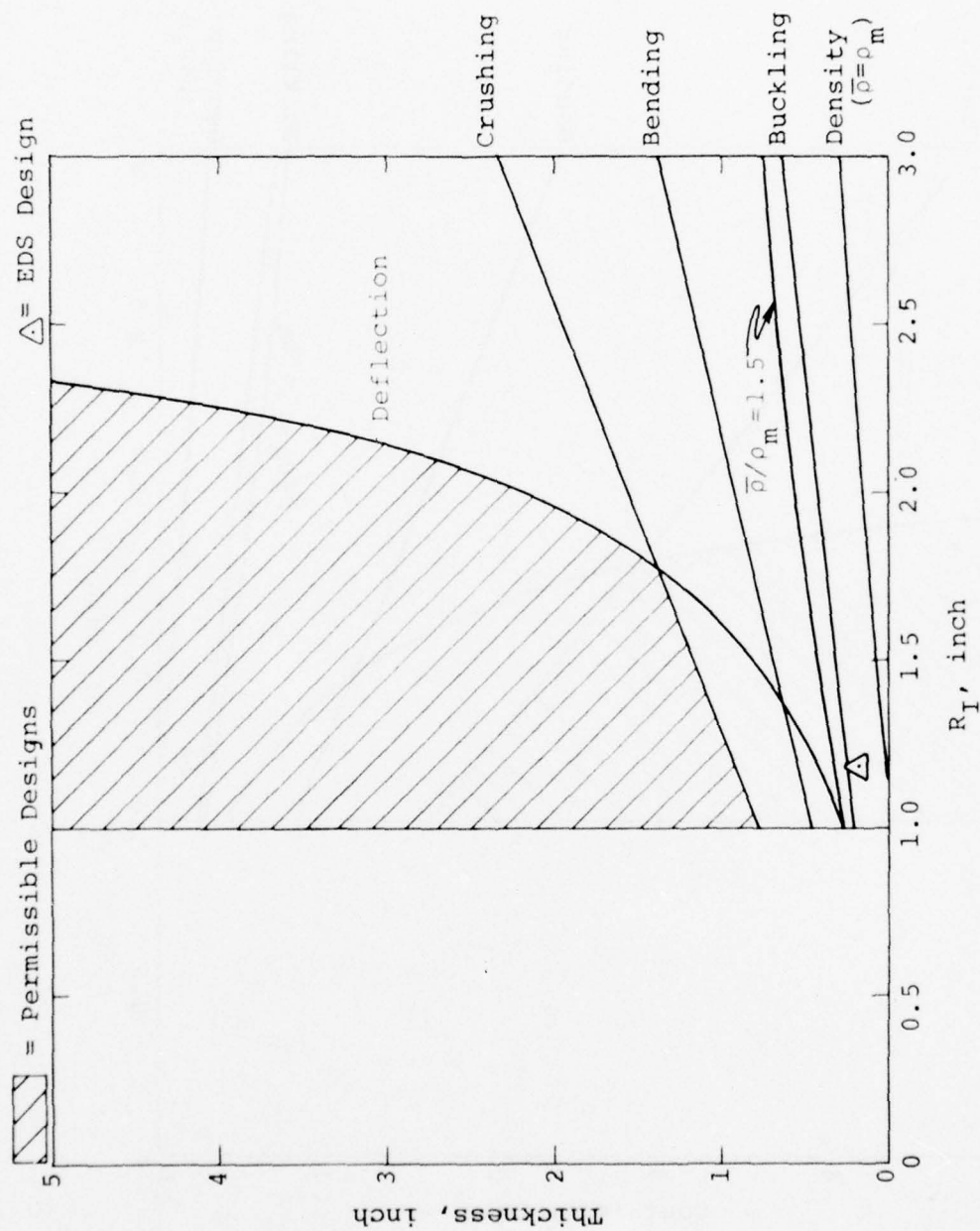


Figure 3.12. Survivability design constraints for 4130 steel at 4 kbar.

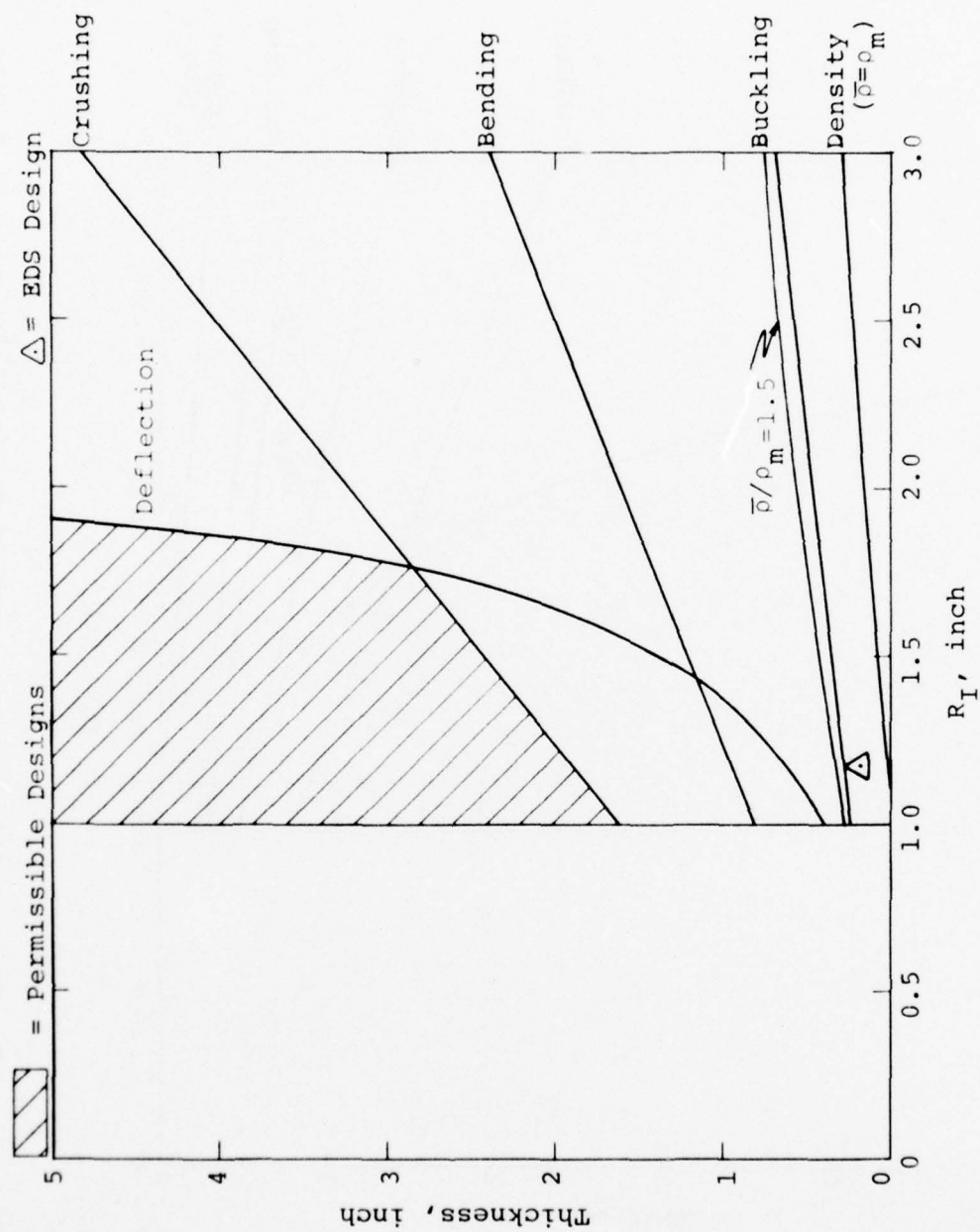


Figure 3.13. Survivability design constraints for 4130 steel at 5 kbar.

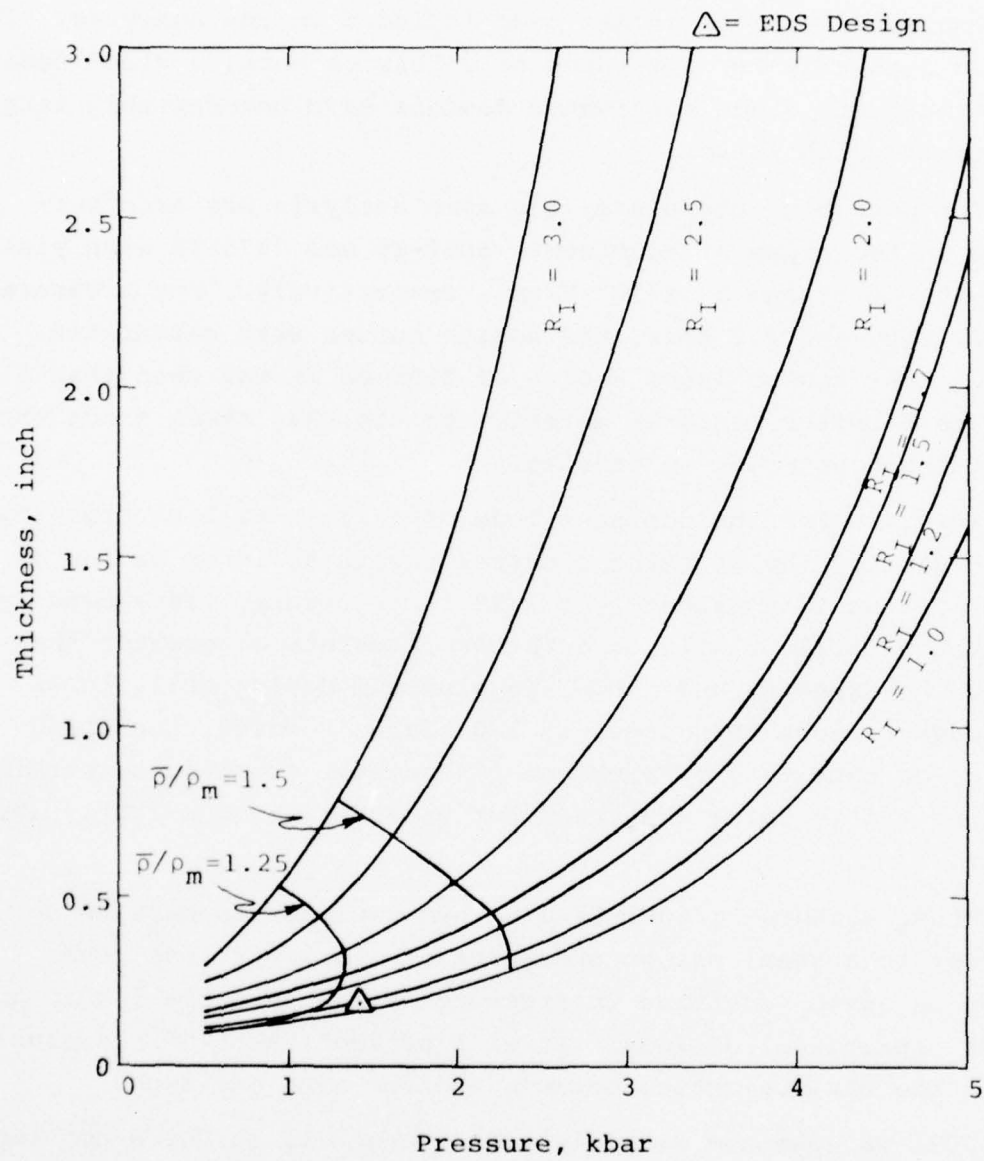


Figure 3.14. Minimum canister thickness versus pressure for 4130 steel.

This sure survival level is considered a conservative estimate since no account of the additional structural strength due to coupling/stiffening rings has been included in the analysis. It is also seen that for pressures of 2 kbar or more, a steel design is not adequate since survivable designs have unacceptably large density mismatch ratios.

For possible future use, the same analysis was also performed on two types of aluminum: 6061-T6 and 7075-T6 with yield strengths of 28 and $50 \times 10^3 \text{ N/cm}^2$, respectively. For pressures of 0.5, 1.0, and 1.2 kbar, the design curves were calculated. For 0.5 kbar and an inner radius of 3.05 cm it was seen that aluminum is a better canister material to use than steel since the overriding constraint is density.

For 1.0 kbar the dominant mode of failure will be crushing and to satisfy the crushing constraint with an inner radius of 3.05 cm, a density mismatch of 1.10 is necessary. If a density mismatch of 1.25 is allowed a factor of safety of greater than two can be expected and a 6061-T6 aluminum design still looks more advantageous than steel at 1.0 kbar. However, the disadvantage of this type of aluminum is that the crushing constraint requires fairly thick canisters for pressures just slightly above 1 kbar.

Thus, although a 6061-T6 aluminum canister appears to be superior to a steel one at pressures of 1 kbar or less, the design is quite sensitive to pressures slightly above 1 kbar and yields unpractical designs. It will be seen that 7075-T6 aluminum is the obvious choice between the two aluminum types.

7075-T6 aluminum with a yield strength of $50,000 \text{ N/cm}^2$ looks very promising for pressures up to 2 kbar. Figures 3.15 through 3.18 show the design constraints for pressures of 0.5, 1.0, 1.5, and 2.0 kbar. These figures show that for pressures of 1 kbar or less, density is the overriding constraint for a 3.05 cm inner

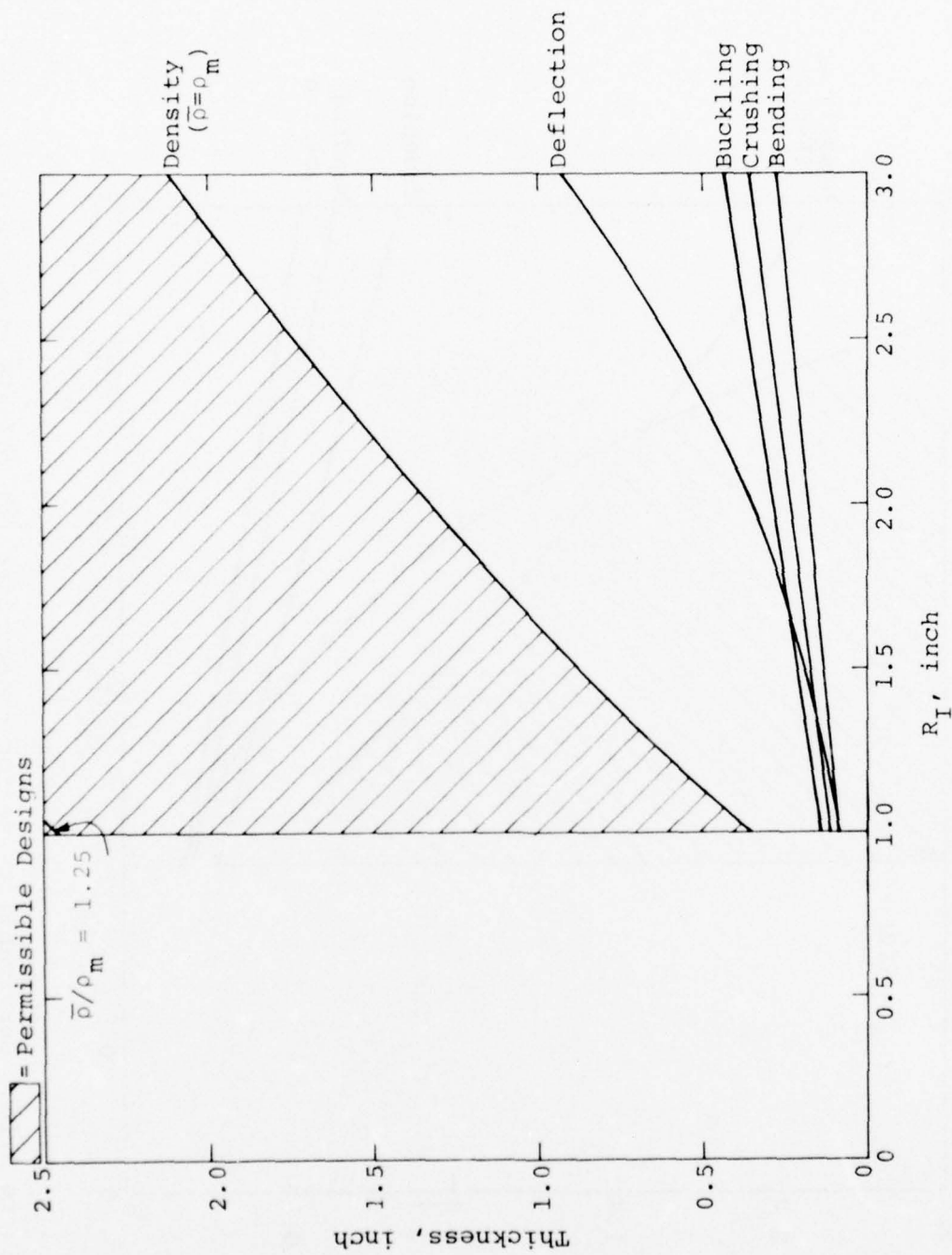


Figure 3.15. Survivability design constraints for 7075-T6 aluminum at 0.5 kbar.

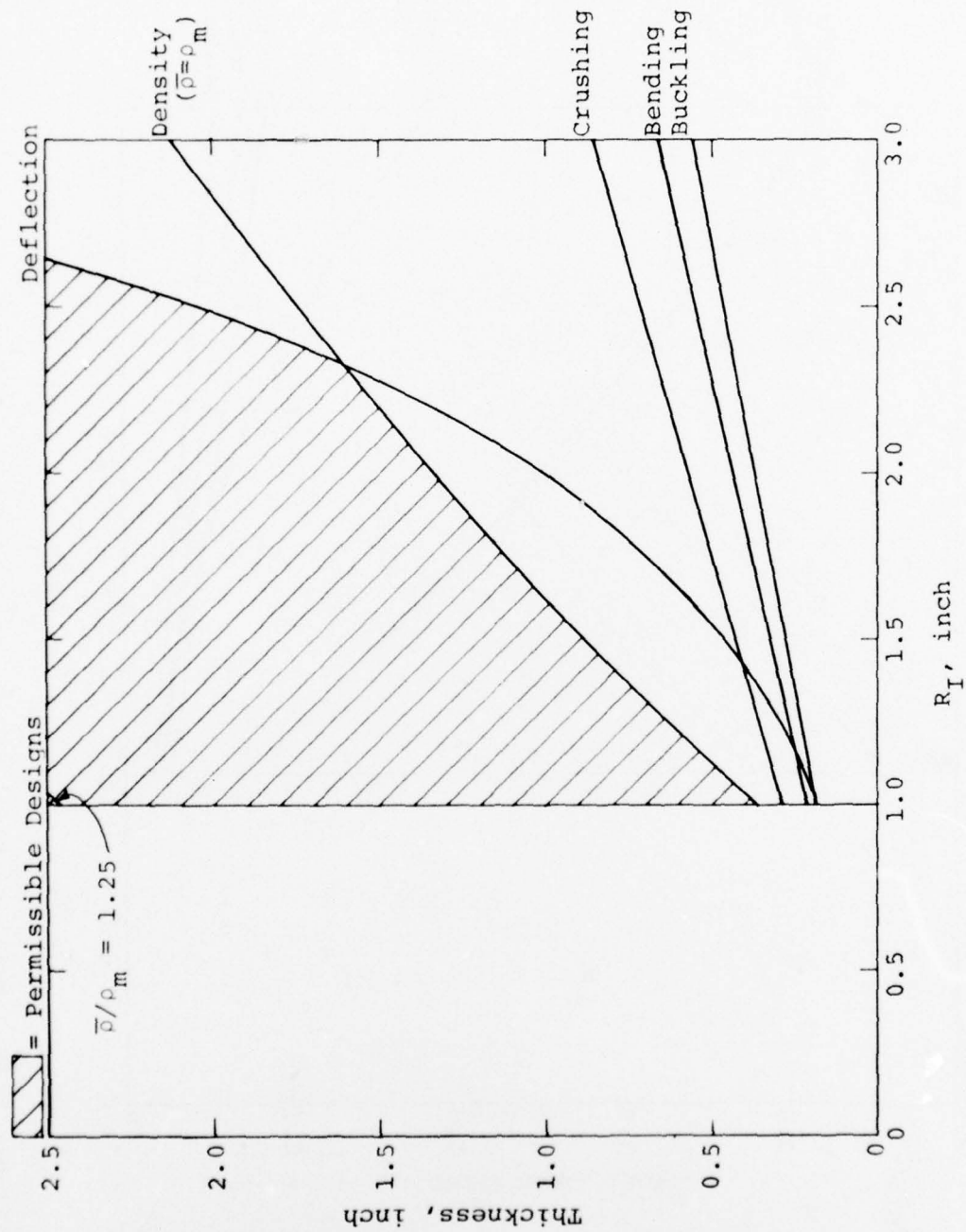


Figure 3.16. Survivability design constraints for 7075-T6 aluminum at 1 kbar.

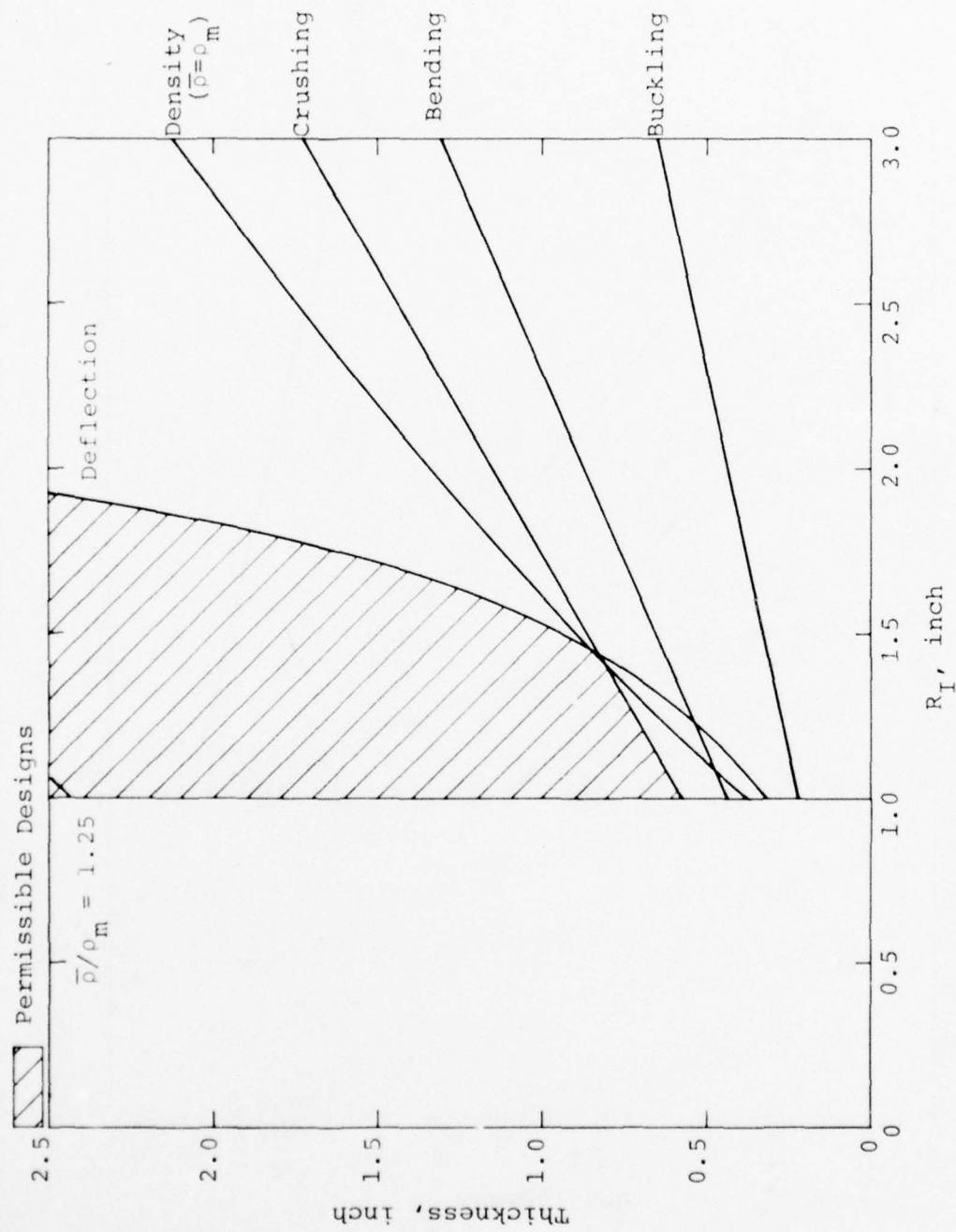


Figure 3.17. Survivability design constraints for 7075-T6 aluminum at 1.5 kbar.

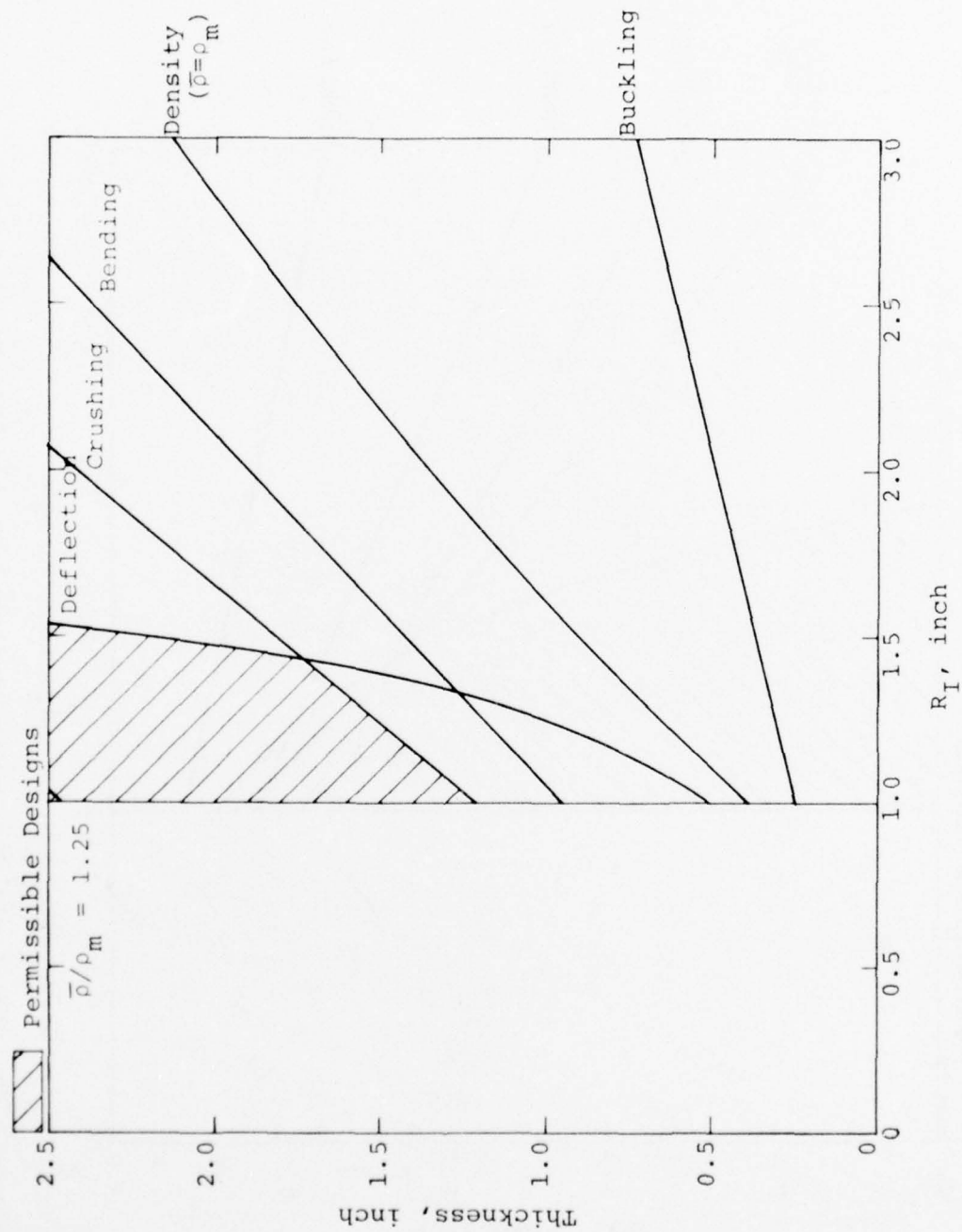


Figure 3.18. Survivability design constraints for 7075-T6 aluminum at 2 kbar.

radius EDS canister. For a 2 kbar pressure, a 3.81 cm thick canister is necessary to prevent crushing which is the dominant mode of failure. These dimensions correspond to an EDS with a density mismatch of 1.13 and a weight of about 36 kg. Allowing a density mismatch of 1.25, a safety factor of 1.86 can be obtained for 2 kbar which is quite promising. Figure 3.19 which plots minimum wall thickness versus pressure, indicates that a 3.05 cm inner radius design with a density mismatch of 1.25 (wall thickness equals 7.11 cm) would be good to 2.25 kbar.

Thus, it appears that an EDS canister made of 7075-T6 aluminum is superior either to a 4130 steel canister or a 6061-T6 aluminum canister. 7075-T6 aluminum could safely be used for pressures up to 2 kbar.

3.3 CANISTER COUPLING TO MEDIA

Much work has been done in studying the effects of emplacement of an earth motion sensor in a free-field medium, and it was beyond the scope of work for this project to duplicate such studies. Rather, some of the results of such studies were used to study the impact of grout selection upon gage emplacement.

Based upon available data (References 6, 7, and 8), a review of various grout materials was made relative to emplacement of the EDS in the Rainer Mesa, NTS, Area 12 free field.

Grout recommendations for EDS emplacement was based upon considerations of three basic parameters: (1) strength (τ), (2) density (ρ), and (3) impedance (Z).

The Rainer Mesa is composed almost entirely of tuffaceous strata of which the top consists of 10 to 50 meters of dense welded tuff overlying 600 meters of relatively soft tuff strata which in turn lies upon thick Paleozoic carbonate rock.

Tuff materials data from NTS Area 12 is presented in Reference 7. A limited amount of triaxial compression tests were

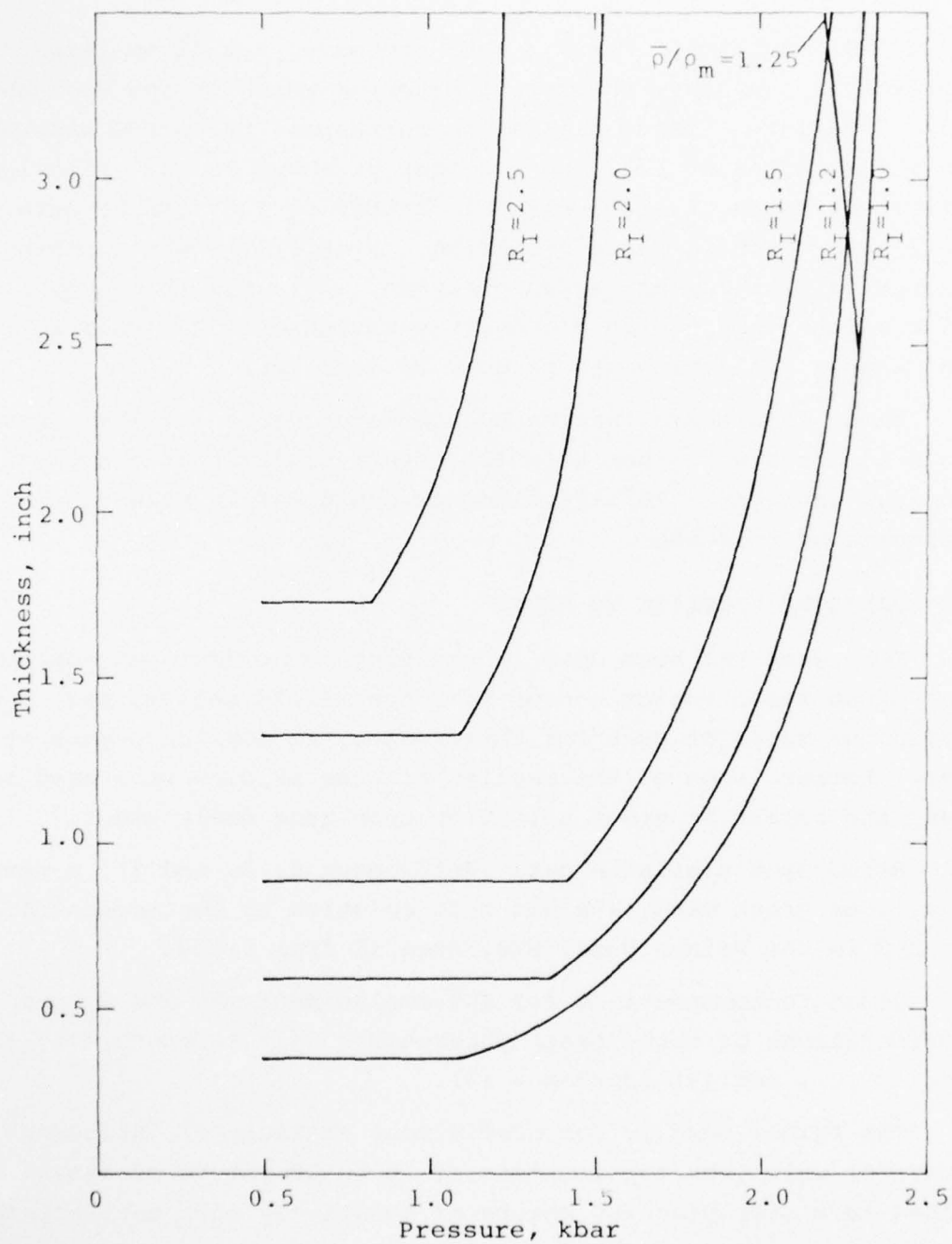


Figure 3.19. Minimum canister thickness versus pressure for 7075-T6 aluminum.

performed from which a shear strength evaluation could be made. Average data taken from five drill holes at NTS U12.07 in the area of Husky Pup UGT are presented in Table 3.2 for comparison with some NTS grouts.

Comparison of the average density of 1.99 gm/cm^3 to other measured densities at nearby sites indicates that this value should probably be considered as an upper bound; however, for this study it is used as a reasonable approximation.

Comparisons of strength, density, and impedance may be made for a limited number of grout materials based upon available grout material data (References 7 and 8). Five grouts were examined; maximum shear stress, density, and seismic impedance for three of these grouts are presented in Table 3.2.

Comparing the data in the table with the averaged values for Rainer tuff, the following observations may be made.

1. Strength. Grout No. 3 (NTS, high strength, DSHSG) is the only grout material having a shear strength equal to or greater than that of the free-field media at a 4 kbar restraining pressure. Grout No. 2 (NTS, rock matching DSRM-2) is the second best choice. Grout No. 1 (NTS, Super lean HSSL-1) has very poor shear strength.

2. Density. With the exception of Grout No. 1, all of the grouts have densities which match the free-field density within two percent.

3. Impedance. The best impedance match is obtained with the No. 2 grout which has a seismic impedance approximately nine percent less than the free-field impedance. The second best match is found for the No. 3 grout which is 25 percent high. All other grouts were 43 percent or more too low

Based upon these comparisons, the final choice would appear to be either the No. 2 or No. 3 NTS grouts. It is imperative

Table 3.2. Density, maximum shear stress, and seismic impedance for the grout candidates.

Type	ρ (gm/cc)	Impedance Z (gm sec/cm ³)	τ_{\max} at 4 kbar
1. NTS SuperLean HSSL-1	1.75	313.6	4 bar
2. NTS Rock Matching DSRM-2	2.03	504.8	90 bar
3. NTS High Strength DSHSG	1.95	697.0	500 bar
4. NTS Tuff ^a	1.99	557	245 bar

^a Average values from Reference 7.

that the grout used to emplace the EDS maintain its structural integrity during transit of the free-field stress wave. The most severe EDS emplacement was at $\sigma_1 = 0.5$ kbar (peak radial soil stress). The confining stress, σ_3 , can be estimated for the relationship arising from a plain strain, or uniaxial strain condition, i.e.,

$$\sigma_3 = \frac{\nu}{1-\nu} \sigma_1$$

For the NTS Ranier tuff a reasonable value for Poisson's ratio is $\nu = 0.33$. Therefore, $\sigma_3 = 0.5 \sigma_1 = 0.25$ kbar. Failure envelopes for these grouts (Reference 7) indicate that at $\sigma_3 = 0.28$ kbar the allowable stress difference ($\sigma_1 - \sigma_3$) for the No. 2 and No. 3 grouts are as follows:

No. 2 NTS ($\sigma_1 - \sigma_3$) = 0.13 kbar at $\sigma_3 = 0.25$ kbar

No. 3 NTS ($\sigma_1 - \sigma_3$) = 0.69 kbar at $\sigma_3 = 0.25$ kbar

or

$(\sigma_1)_{\max} = 0.38$ kbar, for Grout No. 2

$(\sigma_1)_{\max} = 0.94$ kbar, for Grout No. 3

Since the free field $\sigma_1 = 0.5$ kbar, the NTS No. 3 high strength grout (DSHSG) appears to be the optimum choice for EDS emplacement. Unfortunately, DSHSG was found to be unsuitable for pumping into the drill hole and the choice of HPNS-2 was made as an expedient decision at the time of installation. No test data was available regarding the physical properties of this relatively new grout.

CHAPTER 4

HARDWARE DESIGN

Descriptions and discussion of the EDS design have been classified in this chapter as pertaining to either the transducer or the canister. The transducer embodies that portion of the EDS which generates an output signal that is proportional and in response to the desired input stimulus. The canister serves a dual role by providing physical protection for the transducer, as well as offering a mechanism for coupling to the media to assure the EDS responds with the earth particle displacement.

4.1 THE TRANSDUCER

The EDS design is derived from an adaptation of the TRIM gage manufactured by KSC (Reference 1). The EDS and TRIM gages are similar in principle to the Linear Velocity Transducer (LVT), yet differ by virtue of a radial magnetic field and discrete coils.

4.1.1 Transduction Principle. The EDS is a self-generating transducer whose output signal is the result of an electromotive force (emf) that is induced in discretely spaced coils by relative motion of an inertial mass containing a radial field permanent magnet.

The transduction principle is described by Faraday's law of electromagnetic induction which states that the emf induced in a loop of wire conductor is proportional to the rate of change of the magnetic flux linkage. For a multiturn coil of wire in a time varying magnetic field, this law may be expressed mathematically as

$$e = -n \frac{d\phi}{dt} \quad (4.1)$$

where

e = induced emf,

n = number of coil turns,

and

$d\phi/dt$ = magnetic flux linkage time rate of change.

4.1.2 Sensor Geometry. The geometry of the transducer active sensor is illustrated in Figure 4.1. It is seen that the coil tube and inertial slug are free for relative motion along their mutual longitudinal axis. Friction provides the only coupling between the two elements for axial motion, as long as the inertial slug is within the active region of the coil tube. The inertial slug contains a toroidal permanent magnet whose field extends radially outward. Multiple coils spaced 2.54 cm apart along the length of the coil tube are connected in series.

It is now noted that if the coils are coupled to move with the earth and the coefficient of friction between the coil tube and inertial slug is low enough, axial motion of the earth will result in a changing magnetic field for the coils due to induced relative motion between the coils and magnet. The coil output voltage is proportional to the time derivative of the displacement, i.e., the relative velocity (v).

The sensitivity (S) of the EDS to relative velocity is defined as

$$S = \frac{e}{v} \quad (4.2)$$

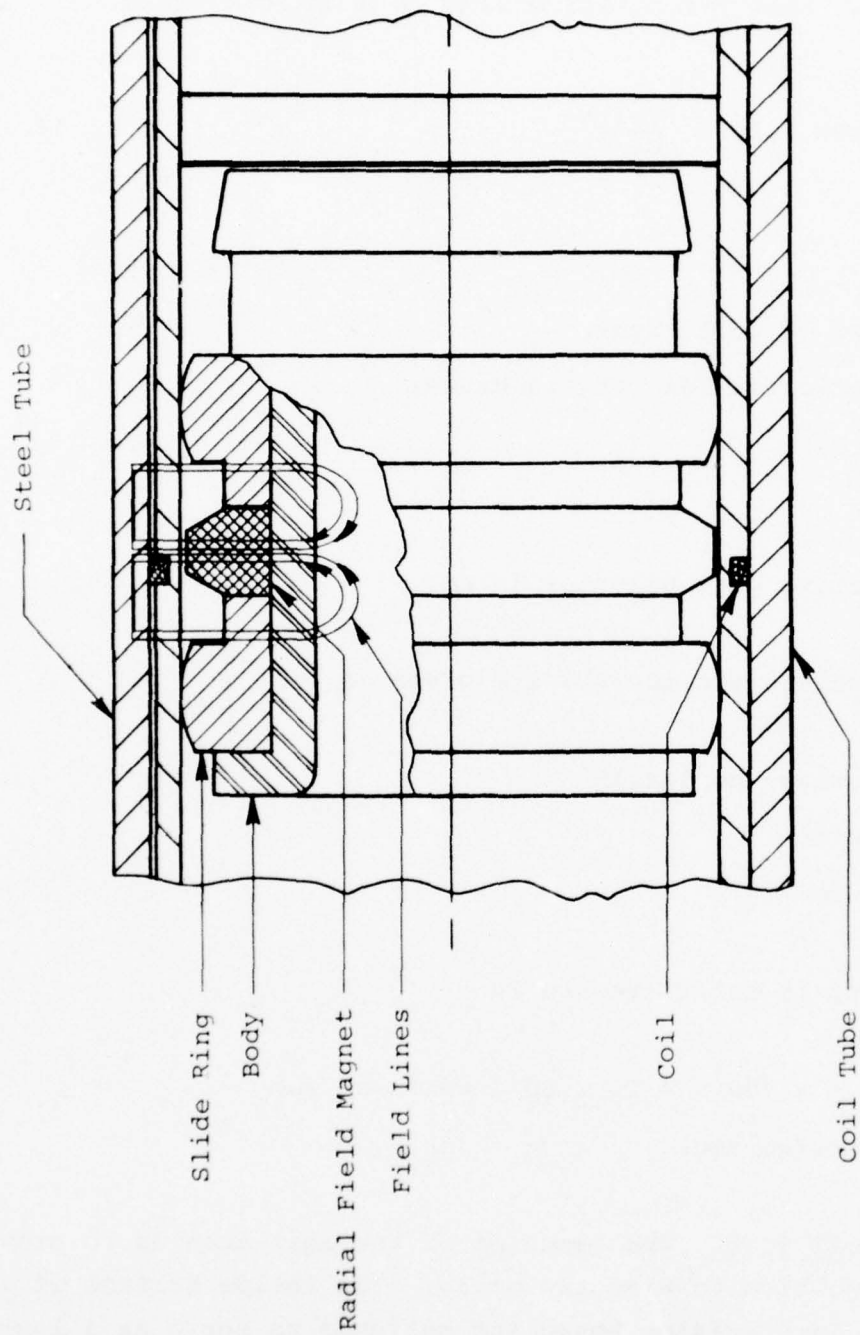


Figure 4.1. Cutaway view of EDS core geometry.

It can be shown that for a coil moving in a uniform magnetic field

$$S = n \cdot \pi B d \cdot 10^{-8} \frac{\text{volts}}{\text{cm/sec}} \quad (4.3)$$

where

n = number of coil turns,

B = magnetic flux density in gauss,

and

d = effective coil diameter in cm.

These design values for the EDS are given as

$B = 700$ gauss (nominal)

$n = 45$ turns

$d = 4.29$ cm

The sensitivity is calculated to be

$$\begin{aligned} S &= 45 \times \pi \times 700 \times 4.29 \times 10^{-8} \text{ volts/cm/sec} \\ &= 4.25 \text{ mv/cm/sec.} \end{aligned}$$

4.1.3 Coil Tube. The function of the coil tube is to provide a form on which to wind the coils. The inside surface of the coil tube is precision honed and polished to serve as a low-friction race for the sliding contact bearings of the inertial

slug. Figure 4.2 is a photograph of the coil tube during assembly.

The tube is made from 6061-T6511 aluminum and is 99 cm long with 37 coils spaced 2.54 cm on centers along the active portion of the tube. Each coil consists of 45 turns of No. 32 AWG copper magnet wire. In addition to the nylon insulation on the wire, the outer surface of the tube was electro-etched to smooth sharp corners before anodizing for extra insulation to prevent shorting to the coil form as the wire made right angle bends into the slots. The nominal coil is 4.29 cm in diameter by 0.25 cm wide. The coils are layer wound all in the same direction as one continuous winding. The effect is 37 discrete segments of series-aiding coils.

The mild steel outer tube, seen also in Figure 4.2, is then potted void free in place over the aluminum coil form with Hysol epoxy. The coil tube has been structurally weakened by the presence of the coil grooves and the primary function of the outer tube is to provide reinforcement. As an added bonus, the permeability of the steel serves to shape the magnetic field and enhance the sensitivity of the EDS.

4.1.4 Inertial Slug. Elements of the inertial slug are the magnet, bearing rings, core, and a latching ring. Figure 4.3 is a photograph of the inertial slug and the latching assembly.

A sectional view of the slug latched in position is shown in Figure 4.4. The plastic bearings are machined of solid bulk nylon that has been loaded with molybdenum disulfide. This material is manufactured by The Polymer Corporation, Reading, Pennsylvania under the trade name Nylatron. Screening experiments were conducted in the laboratory with a flat inclined plane of polished aluminum bar stock and various candidate bearing materials. The Nylatron surface was treated with Dow Corning Molykote 321 to fill the surface tool marks. With a dry film

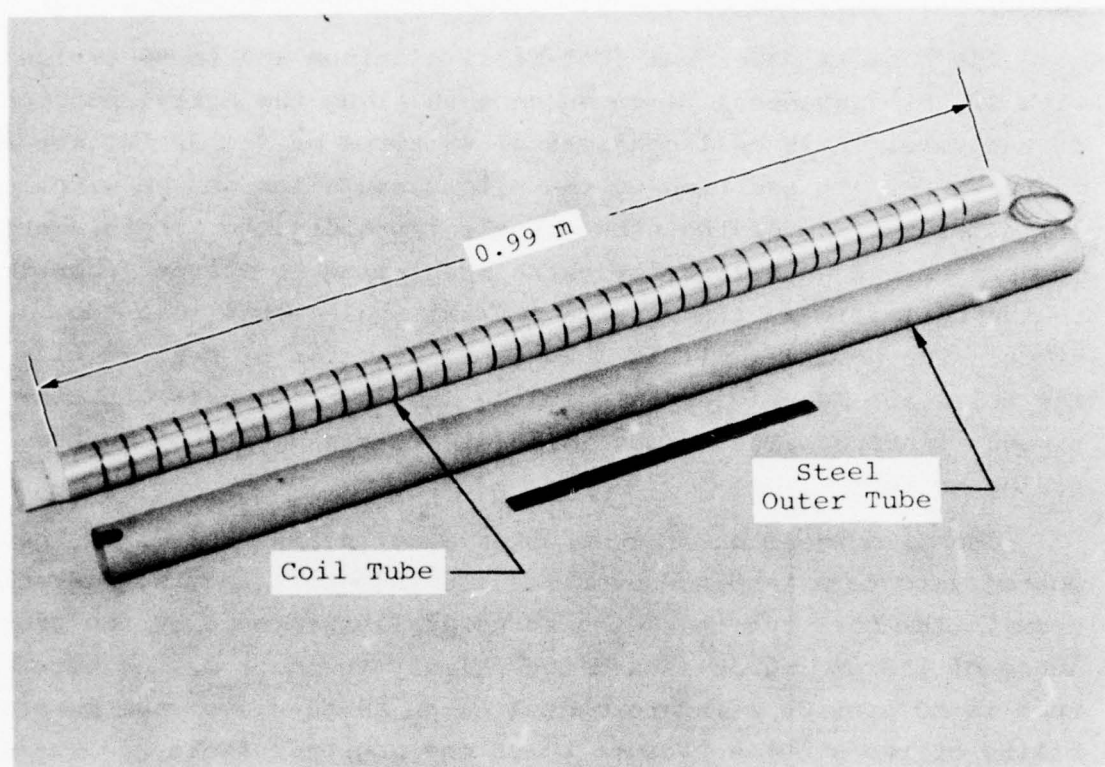


Figure 4.2. Photograph of EDS coil tube during assembly.

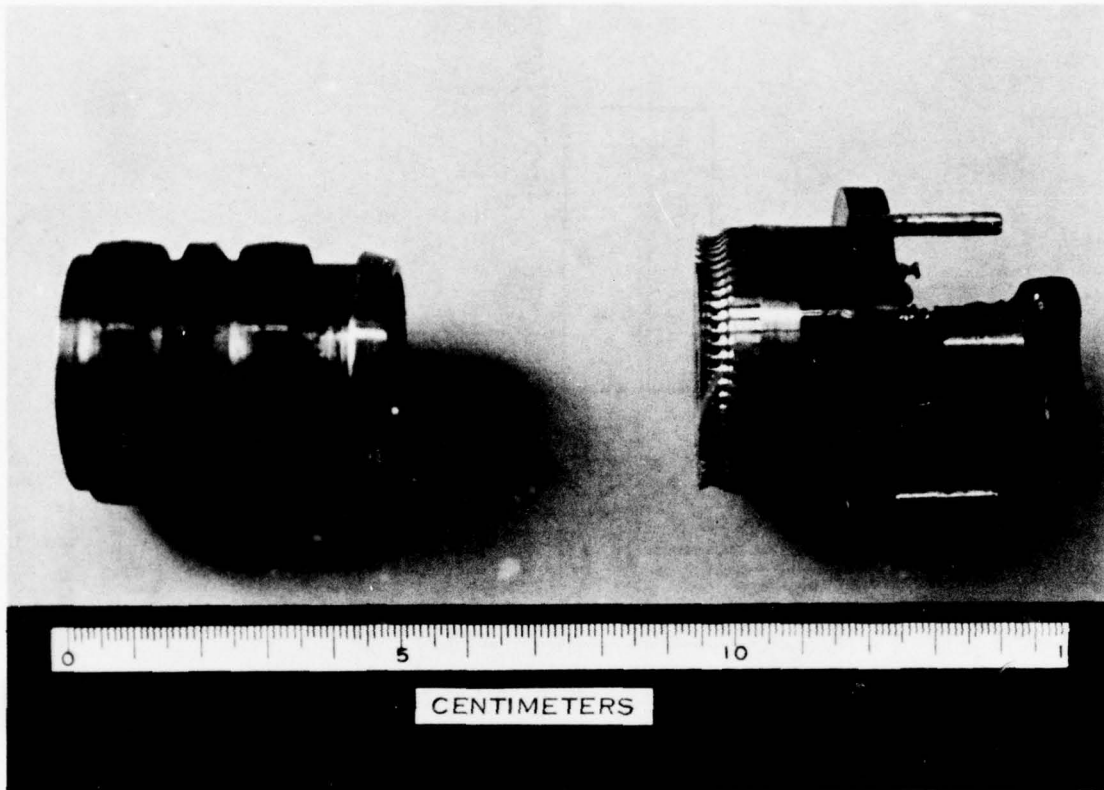


Figure 4.3. Photograph of EDS inertial slug with latching mechanism.

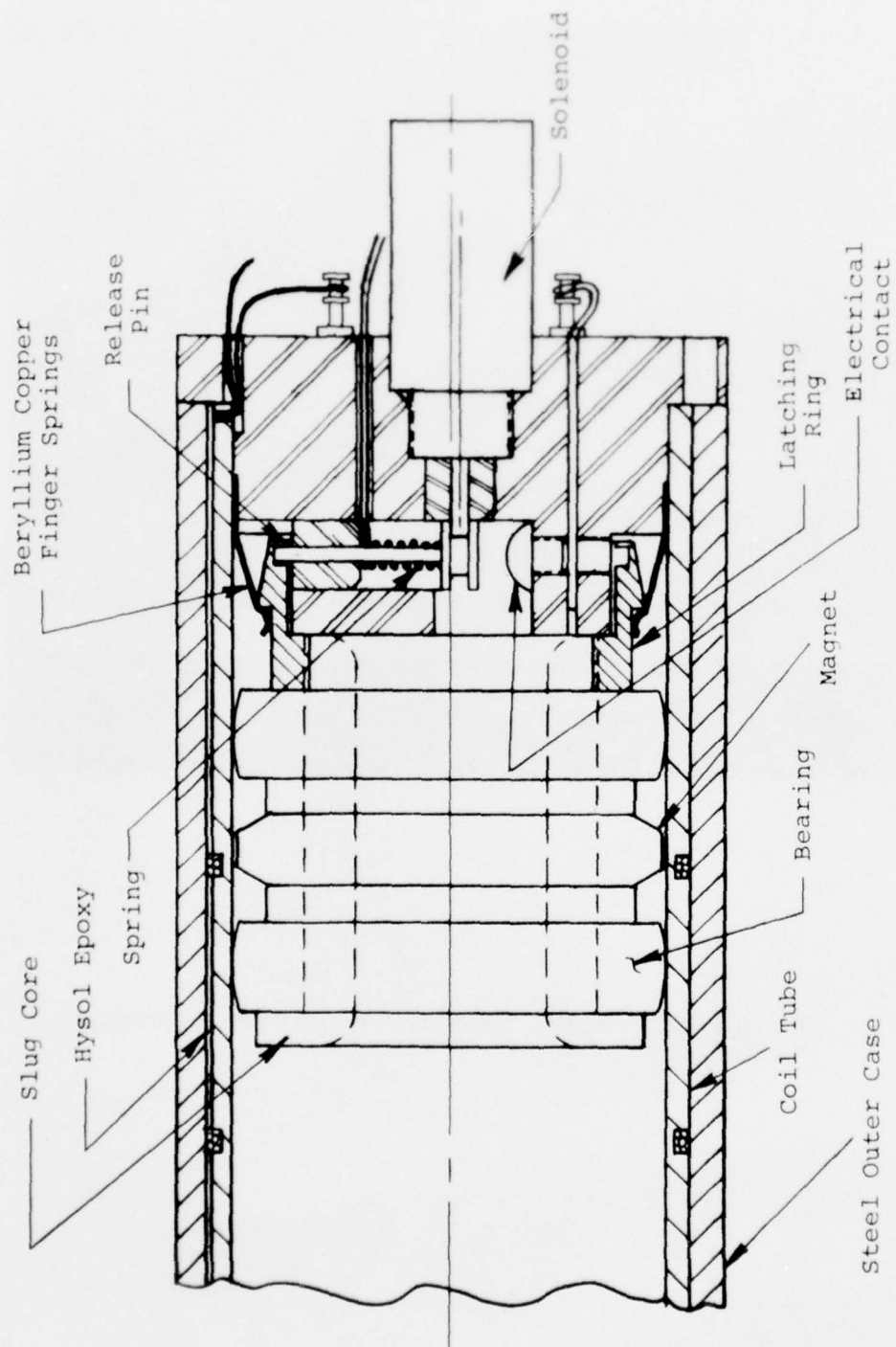


Figure 4.4. Details of solenoid latch for inertial slug.

fluorocarbon lubricant (Miller-Stephenson MS-122) on the aluminum surface, the coefficient of friction for breakaway was measured at 0.084 with a dynamic value of 0.052. Analysis has shown that with these values the frictional effects would be acceptable. The nominal radial clearance between bearings and tube is 0.14 mm.

The magnet consists of three 120 degree segments of barium ferrite ceramic manufactured by Indiana General under the trade name Indox-1. The field is radially outward and the corners are chamfered to shape the magnetic field. The segments are magnetized to saturation which gives a flux density in the air gap from 600 to 800 gauss. The segments are assembled to the slug core with epoxy.

The latching ring is threaded to the slug core and serves as a retainer for the second bearing. Features of the latching mechanism are given in Section 4.1.5 which follows.

4.1.5 Latching Mechanism. The latching mechanism is required to insure that the inertial slug remains in place during shipment and installation as no provisions exist for "cocking" or returning the slug to its seated position prior to measurement. Details of the latch are seen in Figures 4.3 and 4.4.

A solenoid actuated latch pin provides a positive lock during handling. After the EDS installation is completed, the solenoid may be actuated prior to the measurement time. This retracts the pin and enables relative motion between the slug and the coil tube. When the pin is retracted, an electrical contact is closed for purposes of monitoring the status of the lock.

A provision to lightly restrain the slug prevents it from coasting away from the seated position in the event the EDS is tilted downward. These beryllium copper finger springs require approximately 1 g additional to release the slug. This could introduce a significant error if the initial acceleration buildup

was slow. Due to the shock nature of the environment for which the EDS is designed, this breakaway error is negligible.

4.1.6 Electrical Circuit. The EDS electrical circuitry is shown in Figure 4.5. The signal generating coils are connected in series-aiding. The output signal is developed in only one coil at a time, neglecting fringe effects on adjacent coils. The total measured resistance is 126 ohms with 9 millihenries of inductance.

Two monitoring circuits are provided to remotely determine the status of the EDS. The first consists of a resistor that is switched in parallel with the latching solenoid when the pin is properly retracted after the solenoid has been energized. The resistor value approximately matches the solenoid resistance providing an unambiguous change in resistance between the two states. The second resistor matches the value of the EDS coil and is switched in parallel with the EDS until the slug breaks away from the seated position, again providing an indication of the slug position by the resistance reading.

4.2 THE CANISTER

The coils and inertial slug obviously require physical protection from the environment along with a mechanism to couple the coils to the media. The canister serves to provide both of these functions. It consists of the outer case with coupling rings and a cable transition.

4.2.1 Outer Case. The structural strength, rigidity, and protection for the transducer is provided by a pipe made of 4130 heat treated steel. The canister is shown in the assembly photograph which is Figure 4.6. The steel rings serve primarily to couple the pipe to the grout. Additional stiffening they provide may be offset by the weakening caused by welding. This is a

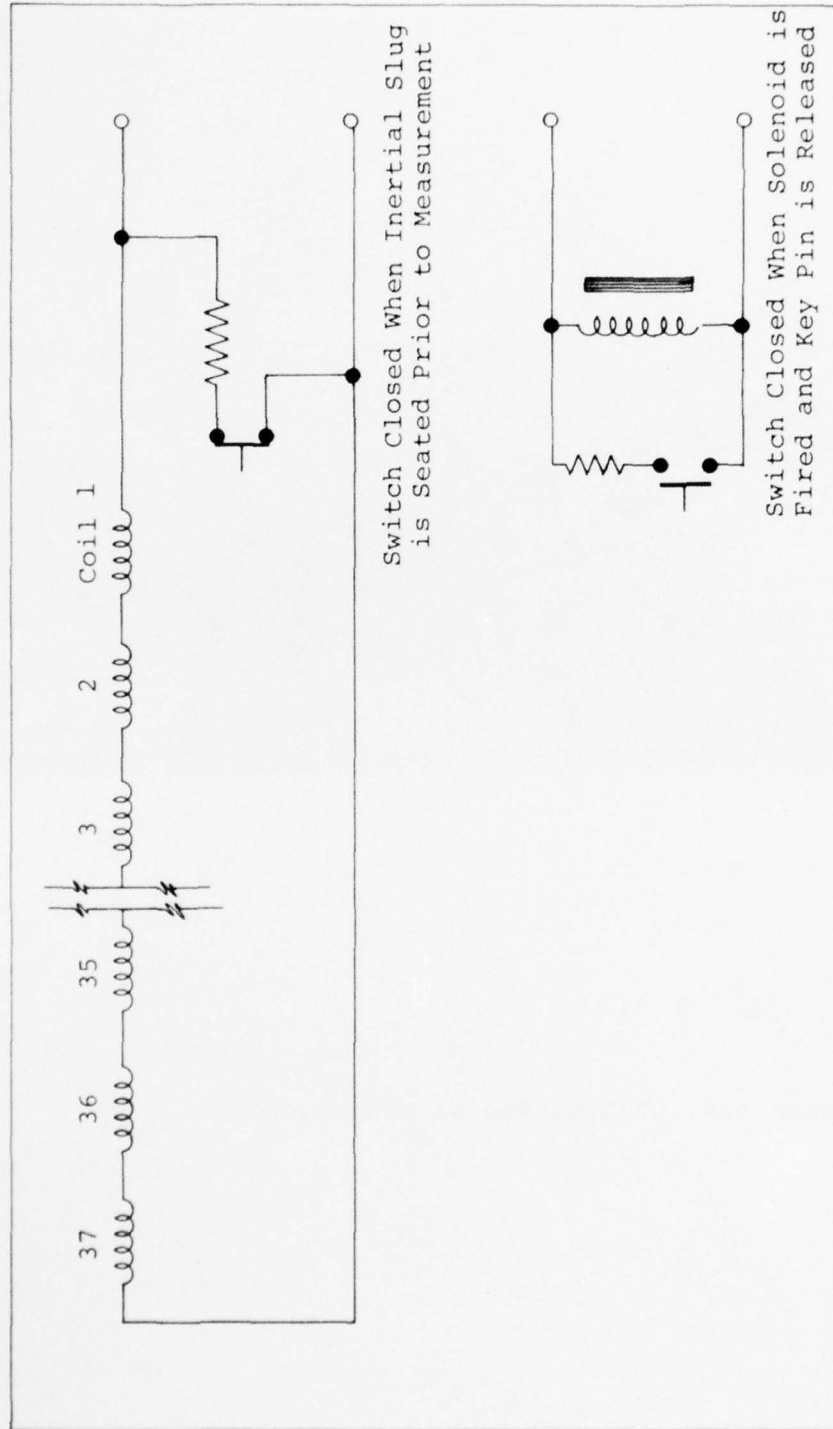


Figure 4.5. EDS circuit diagram.

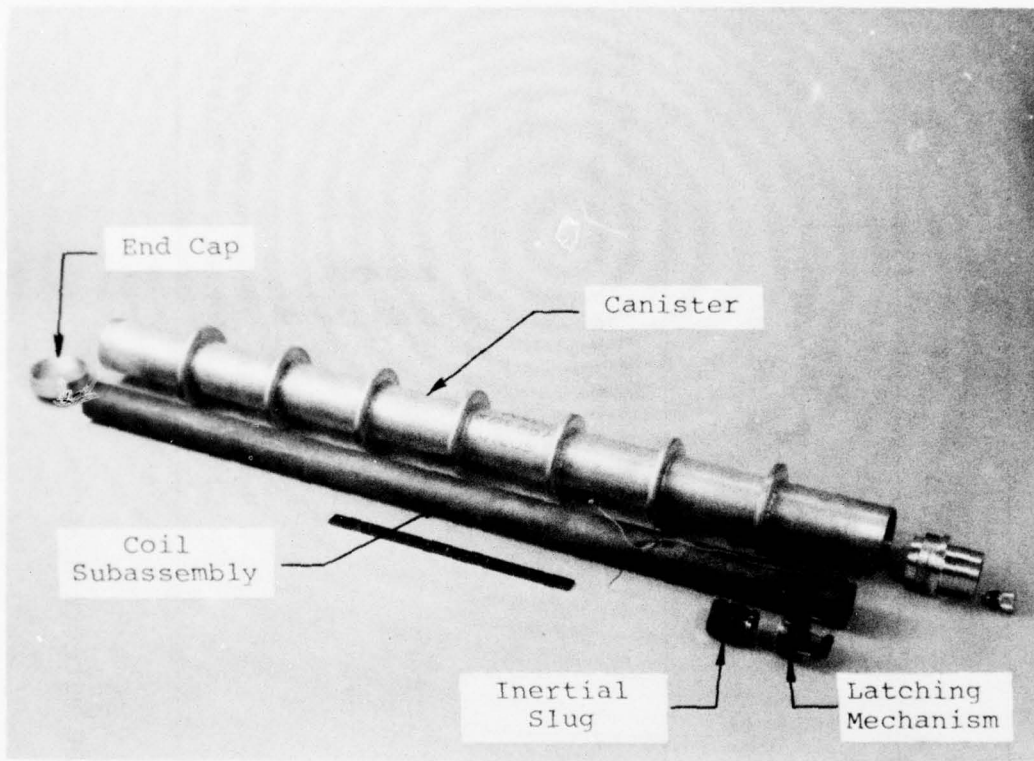


Figure 4.6. Photograph at EDS assembly.

complex analysis problem that was not specifically solved. Figure 4.7 is a drawing of the outer case and coupling rings.

The transducer is installed in the tube with no allowance for axial movement. However, limited radial movement is permitted. Silicone rubber is poured around the EDS sensor to fill the void. General Electric RTV 602 was selected on the basis of modulus, density, and availability. This filler provides damping for any shock induced vibrations in the coil tube while at the same time it decouples the tube from canister distortion.

Using the survival criteria established in Chapter 3, it is estimated that the failure mode for the canister is most probably one of excessive buckling deformation above 1.4 kbar static pressure level. This failure is not necessarily one of catastrophic unrestrained yielding because of the conservative design approach taken, along with the recognition that the dynamic loading is not as severe as the static condition used in the design analysis.

4.2.2 Cable Transition. Cable survival is essential to the successful measurement and is an important facet of the total design. The most vulnerable location for cable damage is the point of exit from the canister. Several protection methods were considered and evaluated for application to the EDS.

The final design consists of a graded strength transition of aluminum that is faired from the diameter of the EDS canister tail piece to tangentially approach the diameter of an aluminum tube that extends beyond the transition for 75 cm. The 0.79 cm (5/16-inch) aluminum refrigeration tubing is attached to the cable transition with a flared end that also serves as the connection point for the braided cable shield.

The principle of this design is to provide a gradual mechanical impedance transition from the rigid canister to the flexible cable. An abrupt cable exit would certainly invite cable failure in the face of any shear environment.

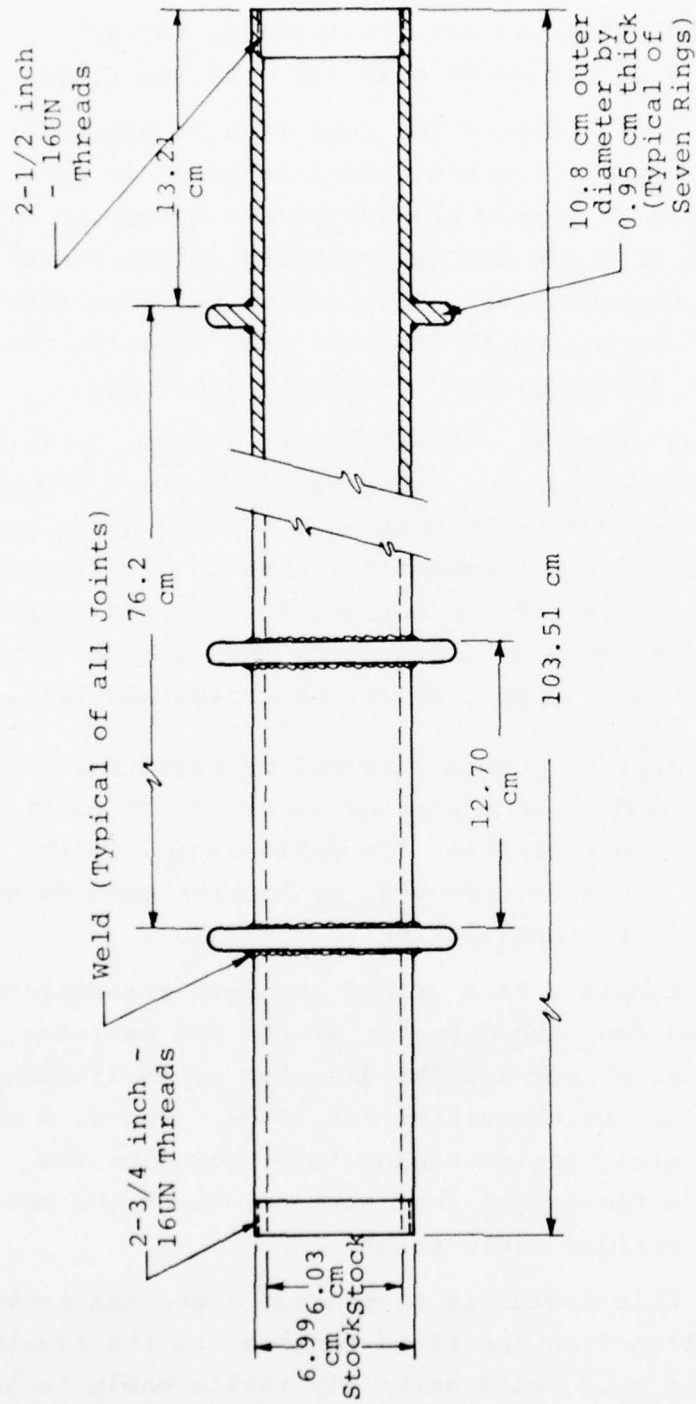


Figure 4.7. Drawing of EDS canister.

Initial motion of the EDS canister can be expected to ram the tube into the cable due to the length of the canister and its orientation with respect to the shock wave. This potential hazard for the cable is dealt with by providing a length of aluminum tubing over the cable that is formed into several spiral convolutions. In addition to the physical protection this affords, the stiffness of the tubing permits the preforming of the spirals as seen in Figure 1.1 before installation.

A serious deficiency in the EDS design is that a potential pressure leak exists via the cable vinyl outer protective jacket. Sealant between the cable and the aluminum tubing prevents pressure leaks around the outside of the cable. However, any penetration through the cable jacket would result in a direct pipe line into the interior of the EDS. This type of damage could easily happen by abrasion during installation. An improved design would implement a pressure tight feedthrough or connector inside of the rear plug.

Details of this design are seen in the assembly drawing of the EDS seen in Figure 4.8.

4.3 THE EDS

The effective density of the EDS is calculated by including the volume and weight of grout included in the space between the coupling rings. The density thus calculated is 2.5 gm/cc which is 25 percent above the average for NTS tuff in which the EDS is installed.

This density match compared favorably with that of the SCEMS package fielded by Sandia at the Dido Queen High Fluence Recovery (HFR) station. Excellent long-time stress and acceleration records were reported with a 2 kbar peak pressure level for this event. The SCEMS canister dimensions are approximately 1 meter long by 30 cm diameter with coupling rings extending the effective diameter to approximately 66 cm (Reference 3).

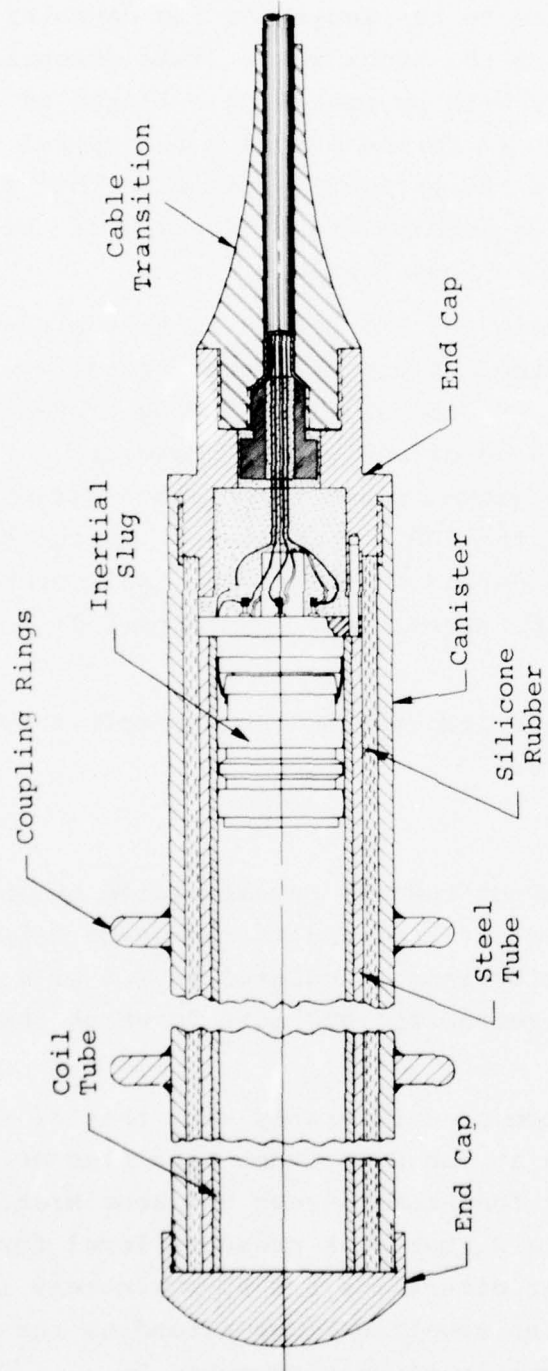


Figure 4.8. Cross-sectional drawing of EDS.

As the measurement is moved closer toward the source, the EDS must be longer, since it must necessarily be longer than the maximum displacement to be measured. This is in opposition to other requirements because the field gradients are greater closer in and the design objective is toward a shorter instrument that can respond with the earth particles. Thus, the length dictated by a direct measurement of earth displacement presents a limitation in the higher stress levels. The very large displacements associated with the 1 or 2 kbar region suggest that some degree of viscous damping might be required to reduce the length.

The question of viscous damping has been addressed in a very cursory manner and serious consideration awaits the successful development of an undamped version of the EDS. The preliminary analysis dealing with damping that has been done is included as Appendix A.

CHAPTER 5

PERFORMANCE TESTS

The EDS was calibrated in the laboratory at KSC in two ways. Free-fall tests in which the inertial slug was permitted to pass through the coil tube under the acceleration of gravity provided one type of calibration. Another method used was to drive the magnet through the coils at a measured velocity using a reciprocating crankshaft drive. Each of the methods are described in the following paragraphs along with test results.

The EDS was also tested at Sandia Laboratories in Albuquerque (SLA) on a vertical drop test machine that simulated the shock pulse predicted for the free field installation. Tests were conducted with three different orientations of the EDS axis with respect to the vertical. The worst case tests were at a 45 degree angle and a nominal 150 percent of the predicted peak axial acceleration.

Two series of tests were run at SLA, the first on 4 June 1975 with the principle objective of proof testing the mechanical design of the EDS against failure in the extreme shock environment. These first tests used the prototype EDS that was made with a polycarbonate plastic coil tube. The coefficient of friction was measured to range between 0.2 to 0.3. Since this value was recognized as being unacceptably high, no serious effort was made to characterize the gage response using results from the first test series.

The second series of tests was conducted on 30 July 1975 using one of the EDS models scheduled for field tests at a later date. Analysis of the test results from this series are included in this chapter. The Crescent gage was tested simultaneously with the EDS and these data are also presented.

5.1 BENCH TESTS

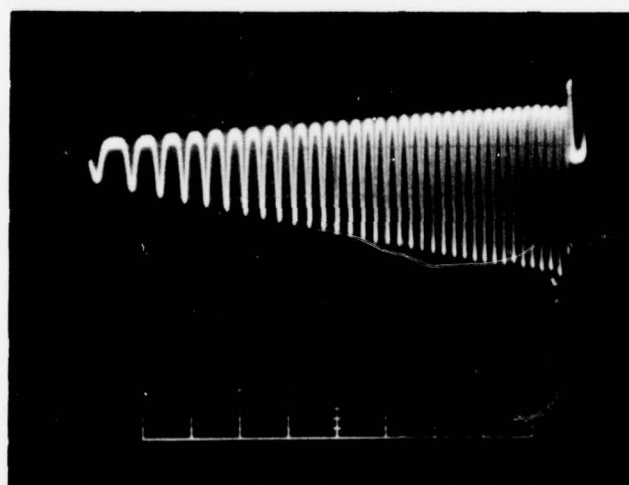
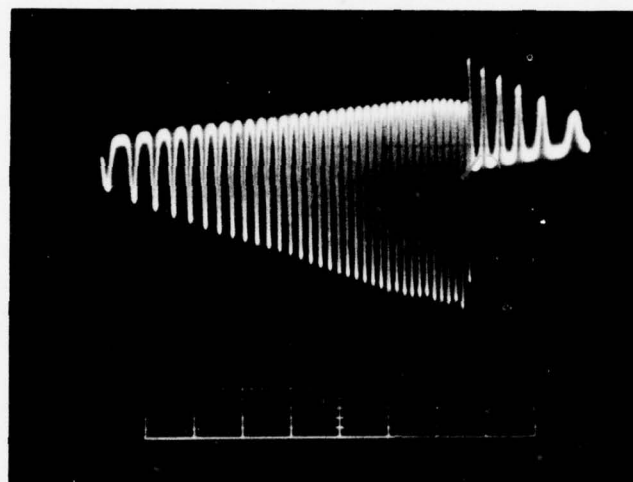
5.1.1 Gravity Fall-Through. Upon completion of the EDS transducer assembly, the output signal was monitored on an oscilloscope while the inertial slug was dropped through the tube. These tests were conducted with the EDS axis oriented at both zero and 45 degrees from the vertical.

Analysis of these data would show any serious problems with slip-stick motion along the tube length. At any given velocity the analog peak amplitudes are a function of the magnet strength and coil geometry, while the digital pulse rate depends on the spacing between the coils. The independent nature of these two signal characteristics allows a self-calibration of the EDS.

Figure 5.1 shows oscilloscope traces from the prototype model EDS taken at zero and 45 degrees. The results of these tests are presented as an illustration of the data reduction techniques and information in the signals.

The graphic data traces were first digitized to yield a time and voltage amplitude measurement for each of the peaks. An average digital velocity between peaks was easily calculated using the delta times and knowledge of the coil spacing. The average analog peak amplitude corresponding to the average velocity was calculated and the data are plotted as shown in Figure 5.2. Linear regression by the method of least squares was used to calculate the slope of this data plot which gives the sensitivity of the EDS as 4.42 mv/cm/sec.

Using this calibration data, the magnet velocity was calculated for each amplitude peak and is shown plotted in Figure 5.3. The theoretical free fall velocity is also shown on the plot for reference. Note that even at zero degrees, the effects of frictional drag are evident as the bearings contact the tube wall in passage. The prototype EDS model used for this test was made with polycarbonate coil tube that was fabricated from four



EDS at 45 degrees

Vertical gain = 500 mv/division
Time base = 50 ms/division

Figure 5.1. Oscilloscope traces for gravity fall-through tests.

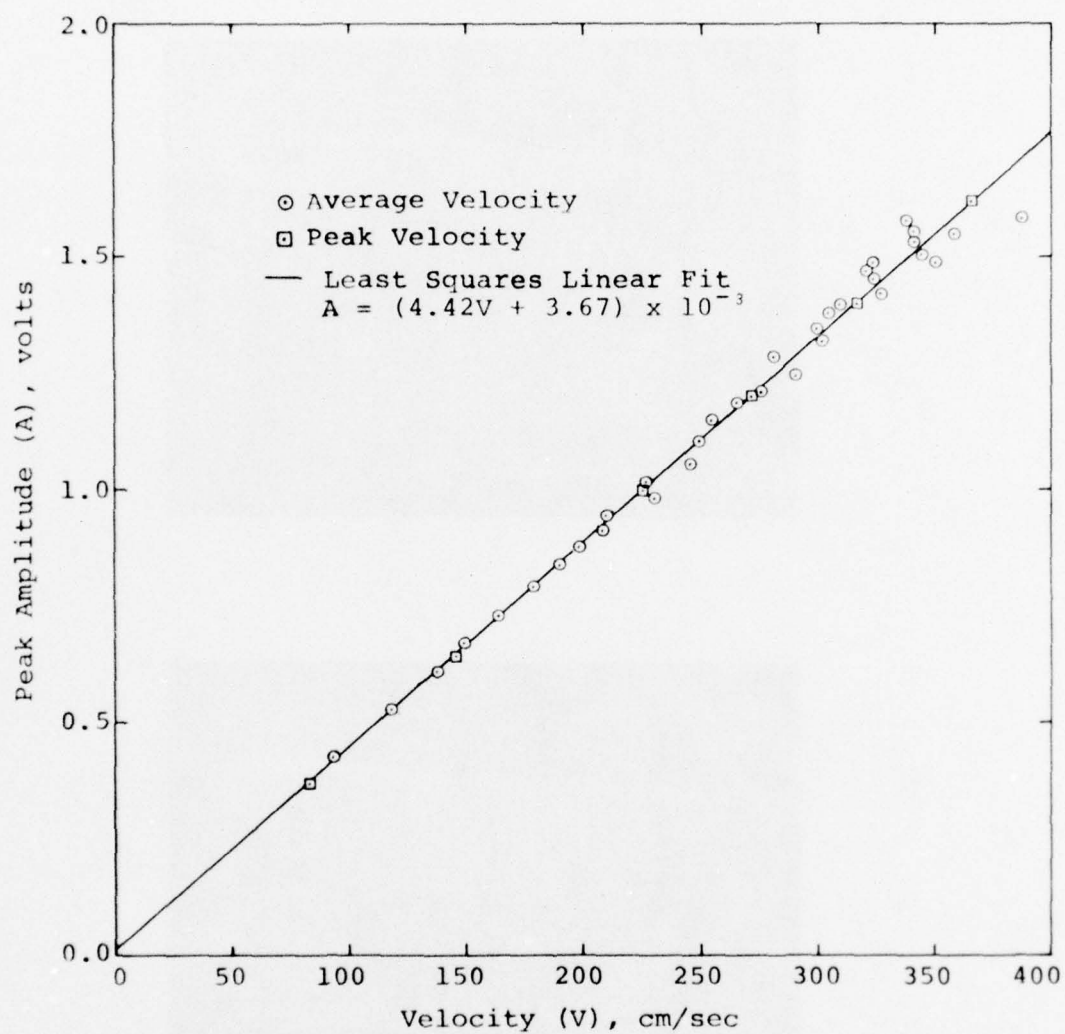


Figure 5.2. Calibration of EDS from gravity fall-through test data.

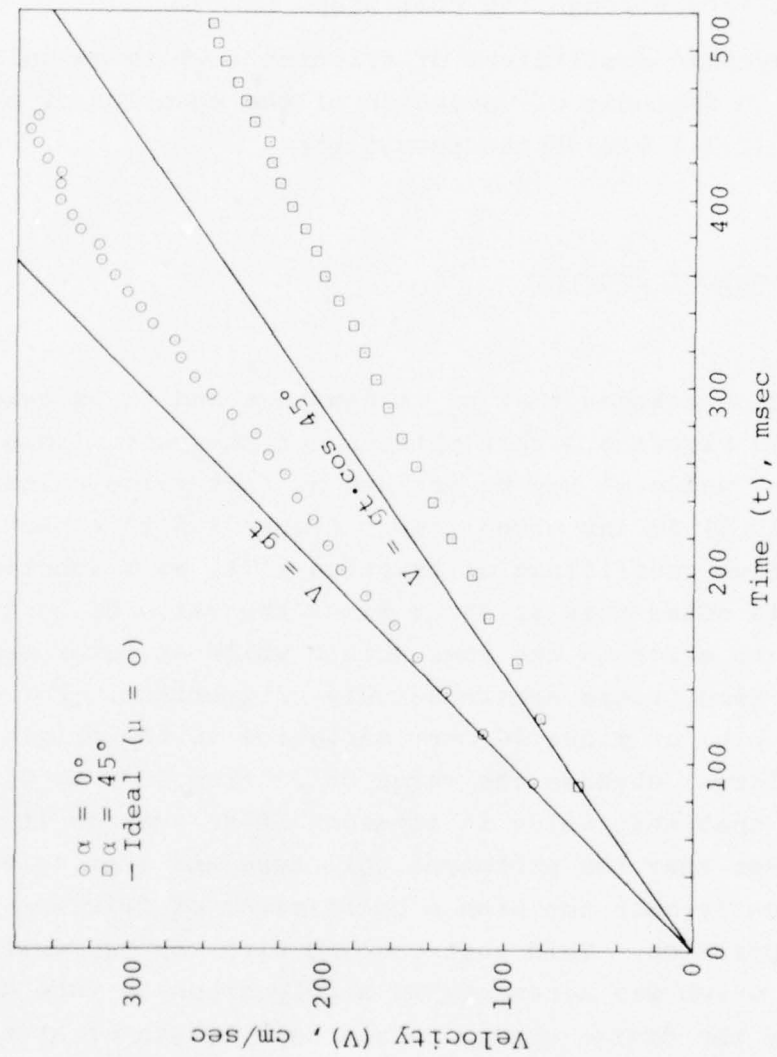


Figure 5.3. Velocity versus time for EDS slug in free fall.

segments. The figure clearly shows the effect of the increased drag as the inertial slug moves through each joint.

Displacement data from these fall-through tests are plotted in Figure 5.4. As with the velocity plots, the ideal calculated values are shown assuming the coefficient of friction is zero as the slug slides through the coil tube.

The dynamic coefficient of friction (μ_2) is calculated from relations in Appendix C. Solution of the equation of motion (Equation (C.1)) yields the result that

$$\mu_2 = \frac{1}{\tan \alpha} - \frac{\dot{x}}{gt \cdot \sin \alpha} \quad (5.1)$$

This equation assumes that μ_2 is constant and it is evident from the data in Figure 5.3 that this is not the case. However, an "effective" value μ' may be defined as that value calculated from Equation (5.1) at any given time. Figure 5.5 is a plot showing the effective coefficient of friction $\mu'(t)$ as a function of time (t). It is noted that at early times the value of μ' is extremely sensitive to error in the time origin while at later times small errors in time origin are relatively unimportant. For example at 500 msec, plus or minus 20 msec variation in the origin (which is absurdly large) changes the value of μ' from 0.22 to 0.28. Remembering that this value is somewhat of an average it was clearly seen that the prototype coil tube and bearing combination had inherently much too high a coefficient of friction for satisfactory operation. This fact coupled with the segmented construction which was necessary in a polycarbonate tube design encouraged the design change to a single length of highly polished aluminum coil tube for the final EDS model.

The EDS field models were also tested using gravity fall-through methods but the data were never digitized since the

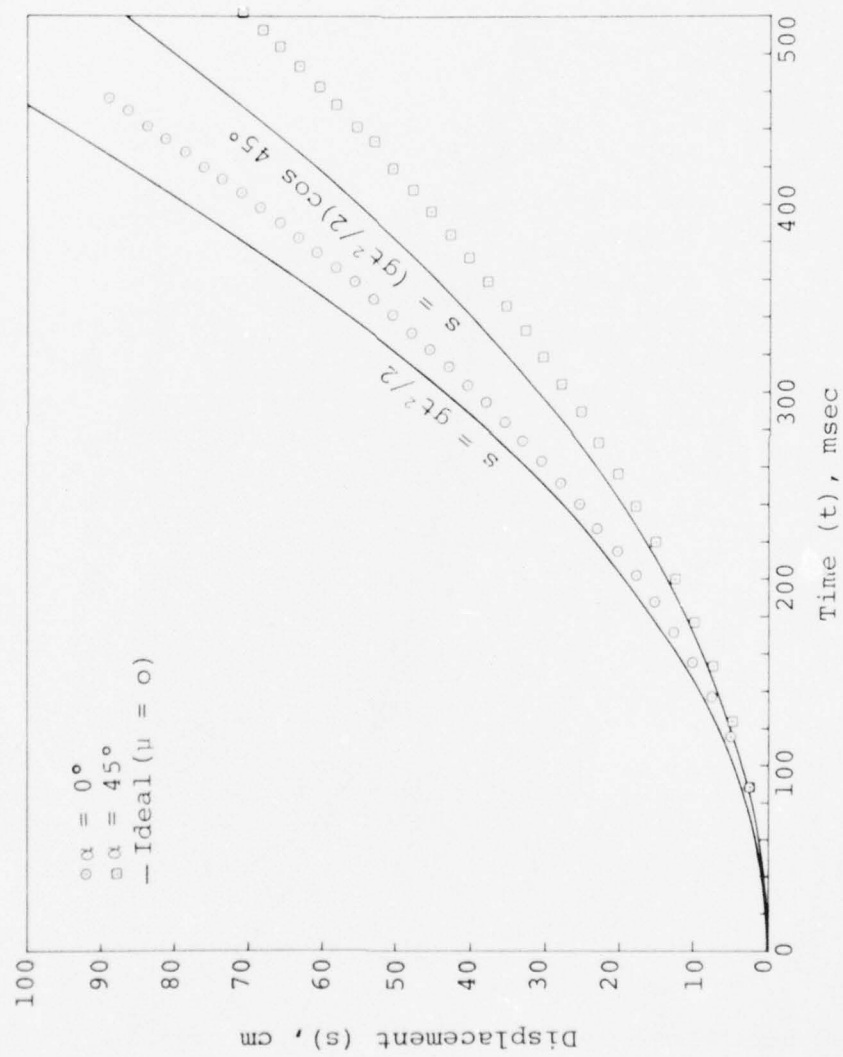


Figure 5.4. Displacement versus time for EDS slug in free fall.

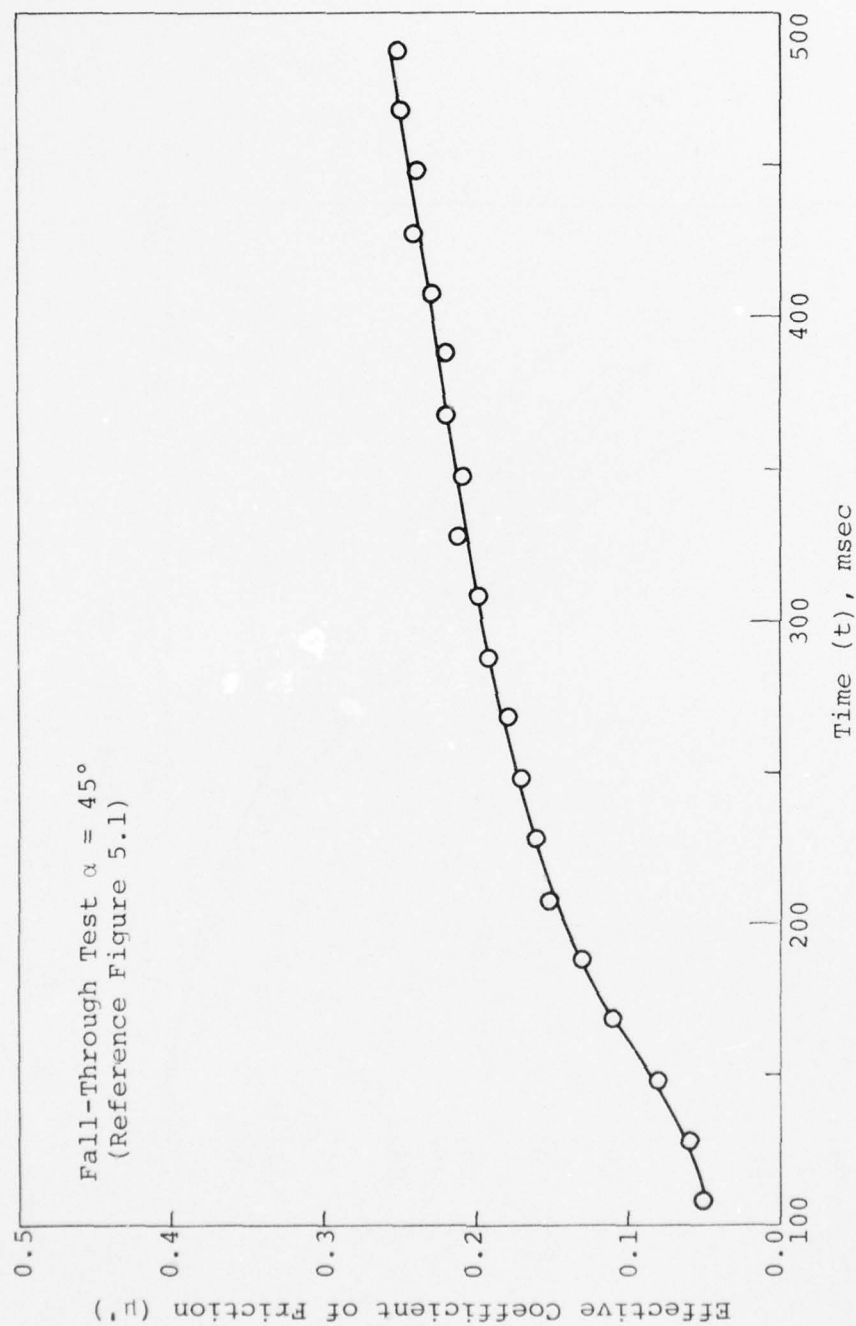


Figure 5.5. Effective coefficient of friction for prototype EDS.

exercise was academic in view of the failure in the field to record any data. The drop test data in Section 5.2 shows that further analysis of the field models would be pointless.

5.1.2 Sinusoidal Calibration. A reciprocating crankshaft drive attached to the EDS magnet was also used to measure the sensitivity of each coil. This method allows for forcing the magnet through each coil at a known velocity without concern for frictional drag on the bearings.

A connecting rod attached to a flywheel at radius (R) was used to furnish a reciprocating motion of the magnet. The velocity of the magnet may be given as

$$v = 2\pi f R \cos(2\pi ft)$$

where f is the rotational speed in revolutions per second. When the geometry is adjusted so that maximum velocity occurs as the magnet crosses the coil center, then it can be shown that the coil sensitivity (S_c) is

$$S_c = V_p / (2\pi f R)$$

where V_p is the measured peak voltage.

Using this method of calibration the individual coil sensitivities may be compared for differences which might arise from manufacturing tolerances or coil winding errors. Individual differences may be readily taken into account in the data reduction process to improve the accuracy of calibration if needed. The open circuit sensitivity of both EDS field units was measured at 4.79 mv/cm/sec using this method of calibration at a velocity of 142 cm/sec.

This sensitivity is slightly different from the prototype because of dimensional changes in the coil design. A last minute change in calibration was caused by overheating the magnets during final assembly. A heat-curing epoxy was used and malfunction of an oven temperature controller caused the magnets to be heated to an estimated 500°C which resulted in a 20 percent loss of sensitivity. Time schedules did not permit recalibration with the reciprocating drive and the EDS final calibration was determined by the self calibrating method described in Section 5.1.1.

5.2 SHOCK TESTS

The objective of the drop test effort was to evaluate the EDS system when subjected to laboratory controlled shock environments which provided a simulation of the free-field environments in which the EDS was expected to operate.

As in most simulation test programs, it was virtually impossible to reproduce all aspects of the EDS free-field environment. However, due to the strong dependence of EDS response on coulomb frictional coupling it seemed reasonable to reproduce the acceleration time histories expected in the free field. This was accomplished with a drop test experiment in which the test mass (m_v), which includes EDS, fixturing, and drop table, impacted a linear receiver spring at a predetermined velocity level (\dot{x}_v) (see Figure 5.6). For a linear system, where the EDS slug mass is negligible compared to the overall test mass, the resultant deceleration pulse may be approximated as a half sine wave. By proper choice of the receiver pad and impact velocity the magnitude and duration of this half sine pulse was tailored to match the magnitude and duration of the initial (and most significant) free-field radial acceleration pulse.

In order to simulate correct pulse durations for these two free-field conditions, the frequency (f) of the total mass and receiver-spring system must satisfy the relation:

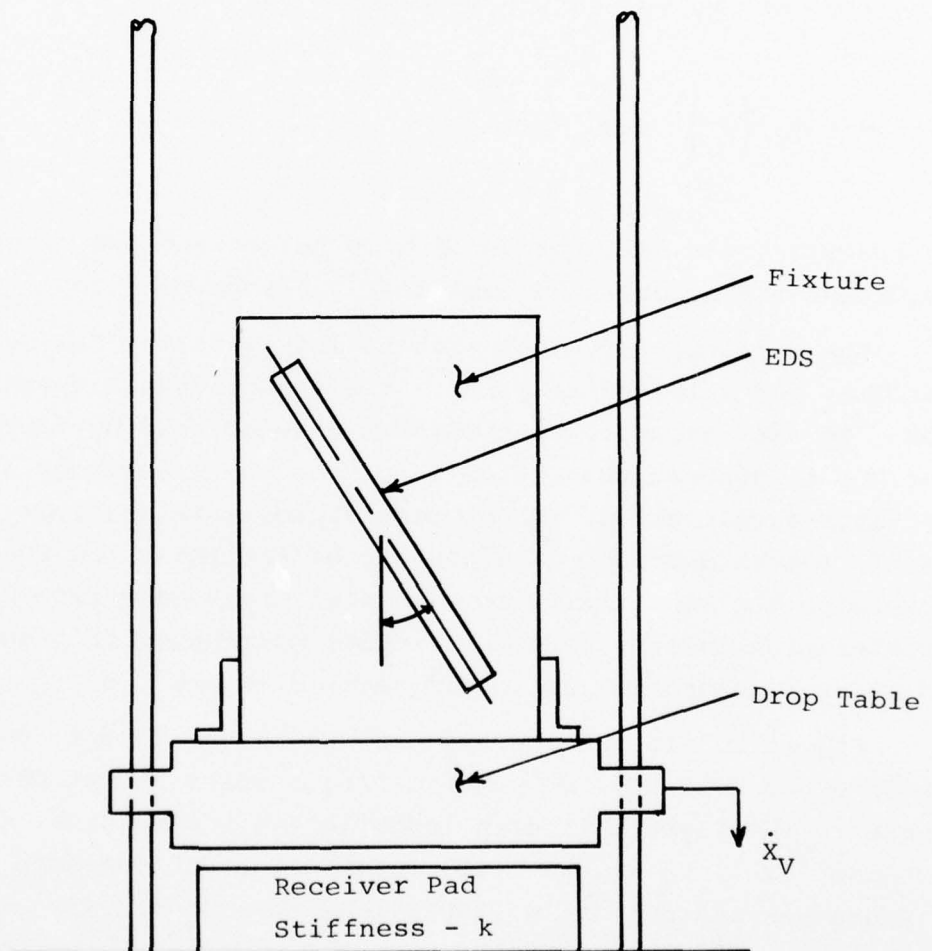


Figure 5.6. EDS drop test geometry.

$$t_g = \frac{1}{2f}$$

Given the total test mass, (m_V), the required spring rate (k) of the receiver may be readily determined as:

$$k = m_V \left(\frac{\pi}{t_g} \right)^2 .$$

In practice, the combination of drop height and pad material and thickness are established empirically before each test.

The vertical drop test machine (DT-1) at the SLA Shock Test Facility was selected to perform the environmental tests of the EDS. It was necessary to provide a massive holding fixture for the EDS to support the entire length of the transducer during off-axis acceleration. Three test angles were desired: zero, 26.57, and 45 degrees. The purpose of inclining the EDS was to determine its sensitivity to simulated transverse free-field acceleration pulses. The test angles correspond to transverse-to-axial acceleration ratios of zero, 0.5, and 1.0.

Figure 5.7 is an assembly drawing of the fixture that was designed to hold the EDS and facilitate tests at the desired angles. The fixture is seen installed in the vertical drop test machine (DT-1) in Figure 5.8. Total weight of the drop table and fixture was approximately 1200 kilograms. To minimize the drop height required, bungee cords are used to accelerate the table, providing initial acceleration values of up to 15 g. These rubber band cords may be seen in Figure 5.8 with three attached to each corner of the table.

5.2.1 Series I Drop Tests. Two test series were conducted at the SLA Shock Test Facility: the first series (4 June 1975)

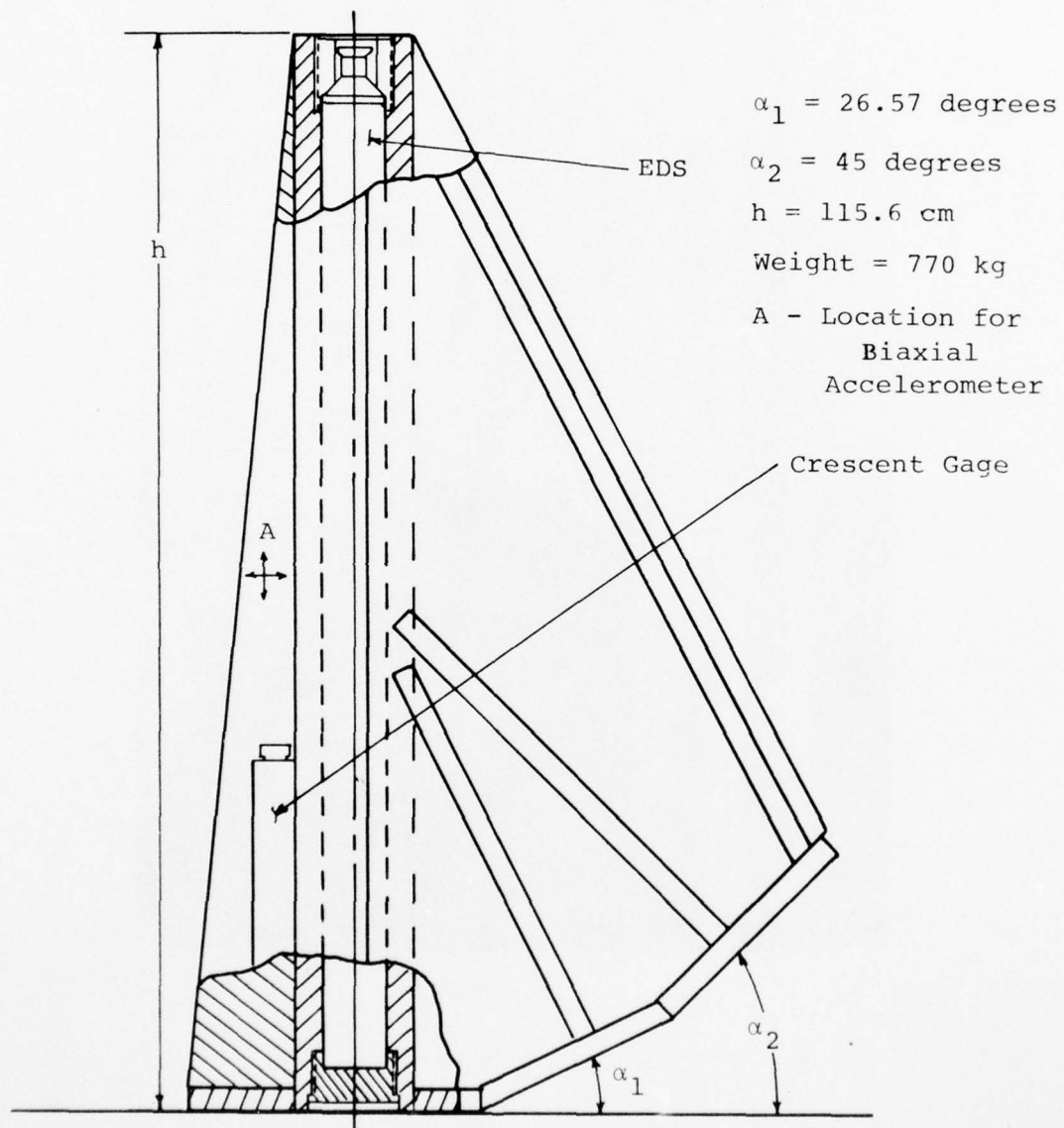


Figure 5.7. EDS drop test fixture.

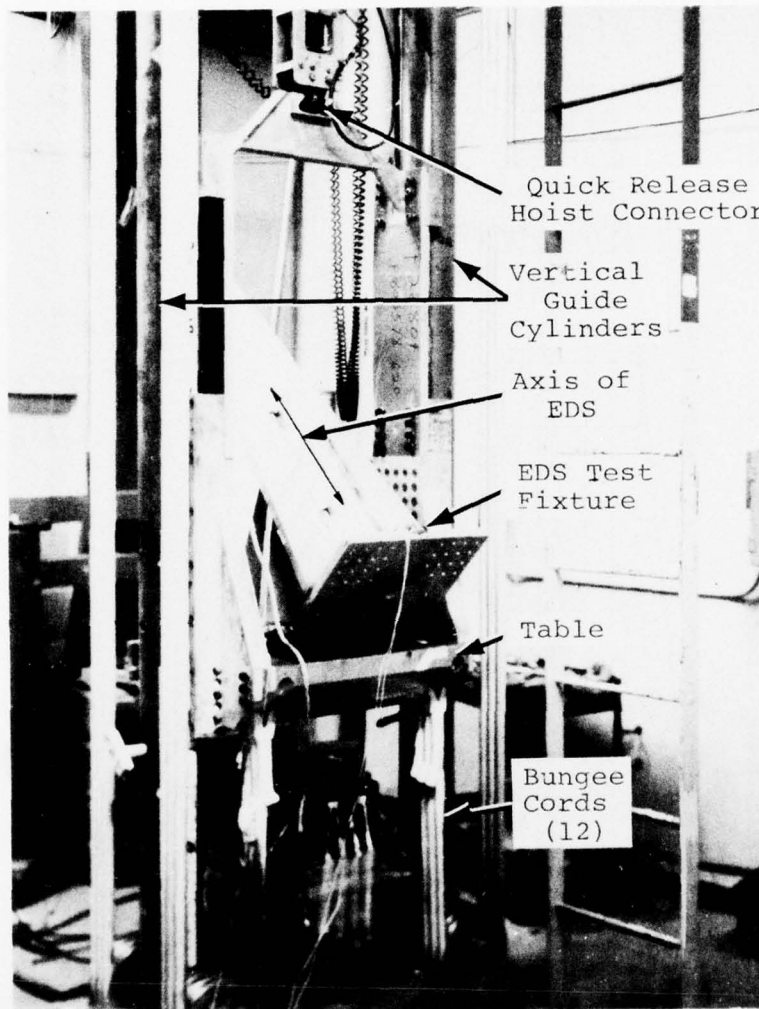


Figure 5.8. SLA vertical drop tester (DT-1) 45 degree test configuration for EDS.

serving as a shakedown to check out test procedures and instrumentation. Also, the rigidity and shock survivability of the EDS canister and drop test fixture were proof tested.

The test was instrumented with three accelerometers and a pre-impact table velocity system for diagnostic measurements of the input stimulus to the EDS. Two hand-picked accelerometers furnished by the transducer evaluation laboratory at SLA were quartz piezoelectric types (Kistler 805) that had a known history of stability and reliability. These select transducers were mounted biaxially on the EDS test fixture to measure the axial and transverse accelerations. The third transducer mounted to the drop table for measurement of the vertical acceleration pulse was a ceramic piezoelectric type (Endevco 2225). Overall calibration accuracy for the table acceleration measurement system was within 15 percent while the two specially selected units improved this number to five percent measurement accuracy.

The table velocity measurement was made with a photo-optical light beam system with an interrupter bar mounted on the drop table. An electronic circuit provided a pulse output for each time the light beam was interrupted by the plastic bar with an opaque pattern photo-chemically etched on its surface. The length of this plastic interrupter was limited to around 15 cm because the severe shock environment would tend to snap the ends from longer sections. Thus, this system provided just a few pulses suitable only for measurement of table pre-impact velocity.

The prototype EDS used for Series I was known to have an unacceptably large coefficient of friction (0.3) hence, only quick look evaluation of the data was pursued. None of the test is presented in this report since Series II has superseded the earlier tests. Test environments ranged from a minimum of 80 g up to 400 g peak at the highest test level. Test angles of zero, 26.57, and 45 degrees were used with a total of six successful drops.

Procedures and methods developed during Series I were invaluable to the success of Series II which was to follow. Perhaps the most important lesson learned was that the accelerometer data was contaminated with shock induced cable noise that precluded long term integration of the records to determine table velocity and displacement time histories. Since the EDS was designed to measure these parameters, this left us with no record of the input stimulus to correlate with the EDS indicated measurement. The method used to measure the velocity and displacement in Series II is described in Section 5.2.2.

In addition to the above, the shock survivability of both the EDS and the test fixture was proven. These were not of trivial importance because any mechanical design defects of a structural nature could have been corrected in the field models whose fabrication had been delayed to await results of the shock tests. Also, the design of the drop test fixture could have given rise to mechanical resonances or structural failure that would require an alternate design or modification to enable a meaningful test.

5.2.2 Series II Drop Tests. The second series of tests was conducted on 30 July 1975 using one of the EDS models scheduled for field installation later. The coefficient of friction using an aluminum coil tube, still not improved as much as expected, measured between 0.10 and 0.16.

Two significant changes in the test plan were implemented for the second series of drop tests: a direct measurement of the drop table displacement was made and a Crescent velocity gage was tested simultaneously with the EDS.

The table displacement was measured directly because it was found during the first series that double integration of the table accelerometer was unsatisfactory for computing table displacements at late times.

The Crescent gage has a history of questionable performance on some past field tests. It was therefore included in the second series of drop tests in an effort to duplicate the intermittent characteristic experienced in the past. Descriptions of the Crescent gage and drop tests are presented along with test procedures, results, and analysis in Section 5.2.4 which follows later in this chapter.

The decision to test the Crescent velocity gage in parallel with the EDS necessitated a modification to the drop test fixture. An adapter for holding the Crescent gage was fabricated and welded along a gusset of the test fixture as indicated in Figure 5.7. This location displaced the Crescent gage axis about 7 cm from that of the EDS. Owing to the small size of the Crescent gage and the massive proportions of the test fixture, this unbalance did not cause any problems.

The test matrix for Series II as it was executed is shown in Table 5.1. \ddot{X} is the nominal axial component of acceleration. Four drops have been selected for discussion and analysis in this chapter; the EDS data from 100 g tests at zero and 45 degrees and the Crescent gage data from 300 g tests at the same angles. The raw data for the 300 g drops are indexed in Table 5.2 and presented in Figures 5.9 through 5.18. Results and analysis of these data are given in Sections 5.2.3 (EDS) and 5.2.4 (Crescent).

An optical system using a light beam interrupter was described earlier which provided a measure of pre-impact table velocity for Series I. To measure total table displacement in Series II, it was decided to extend the length of the light chopper bar to cover the total excursion of the table during the relevant test interval. This was accomplished by replacement of the shock-vulnerable brittle plastic in use with an aluminum bar that had slots accurately milled through to provide windows for the light beam. The active length of the bar was 46 cm. Another

Table 5.1. EDS test matrix - Series II.

Test Angle (α) (degrees)	<u>Peak Acceleration (\ddot{X})</u>		
	100	150	300
0	E,C	---	E,C
26.57	E	---	E
45	E,C	E	E,C

E = EDS

C = Crescent

Table 5.2. Test data index.

Figure No.	Gage Identification ^a	Peak (g)	Angle (α) (degrees)
5.9	EDS	300	0
5.10	Crescent	300	0
5.11	A-1	300	0
5.12	A-2	300	0
5.13	A-3	300	0
5.14	EDS	300	45
5.15	Crescent	300	45
5.16	A-1	300	45
5.17	A-2	300	45
5.18	A-3	300	45

^a A-1 - Table accelerometer
A-2 - Axial accelerometer
A-3 - Transverse accelerometer

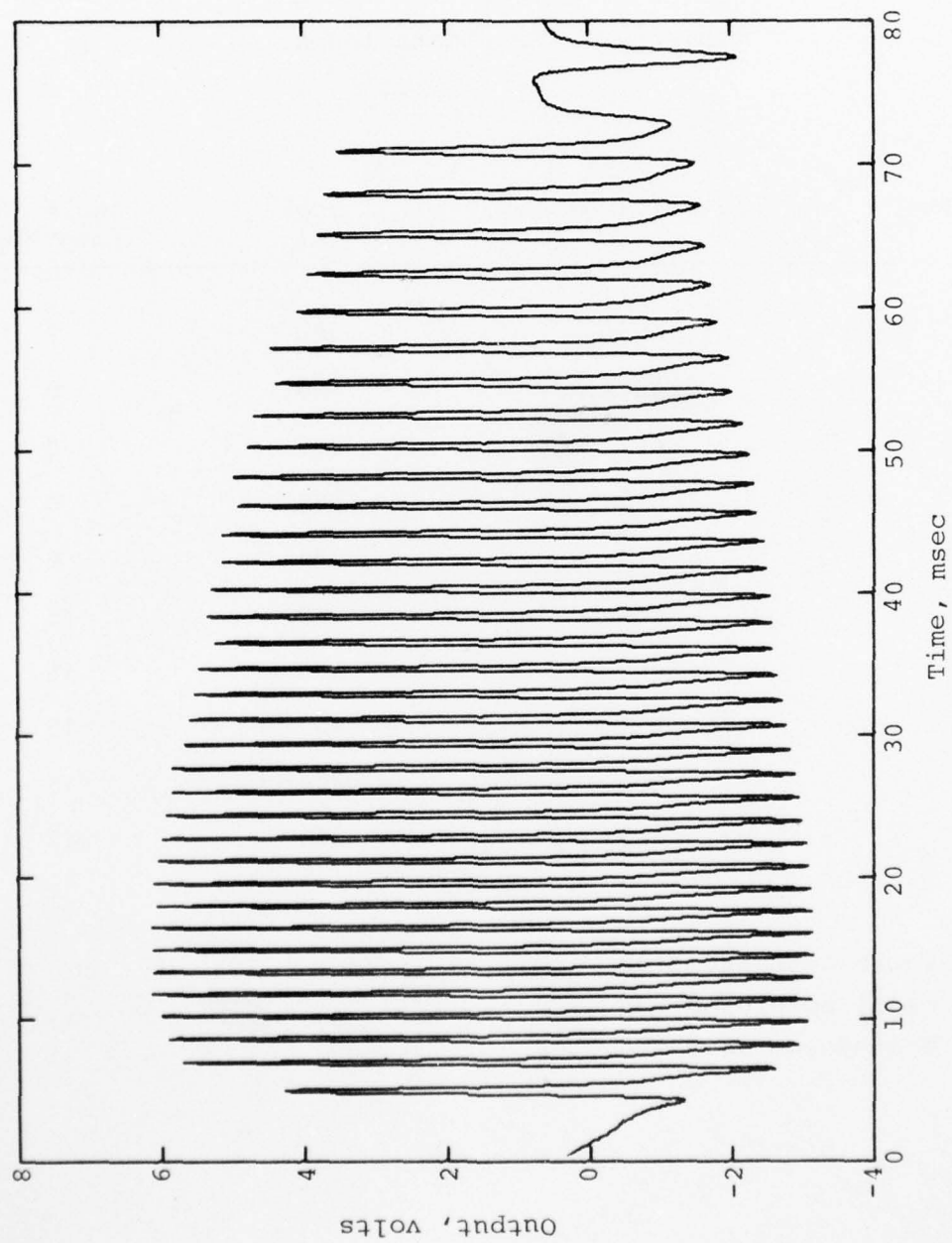


Figure 5.9. EDS signal, 300 g at zero degrees.

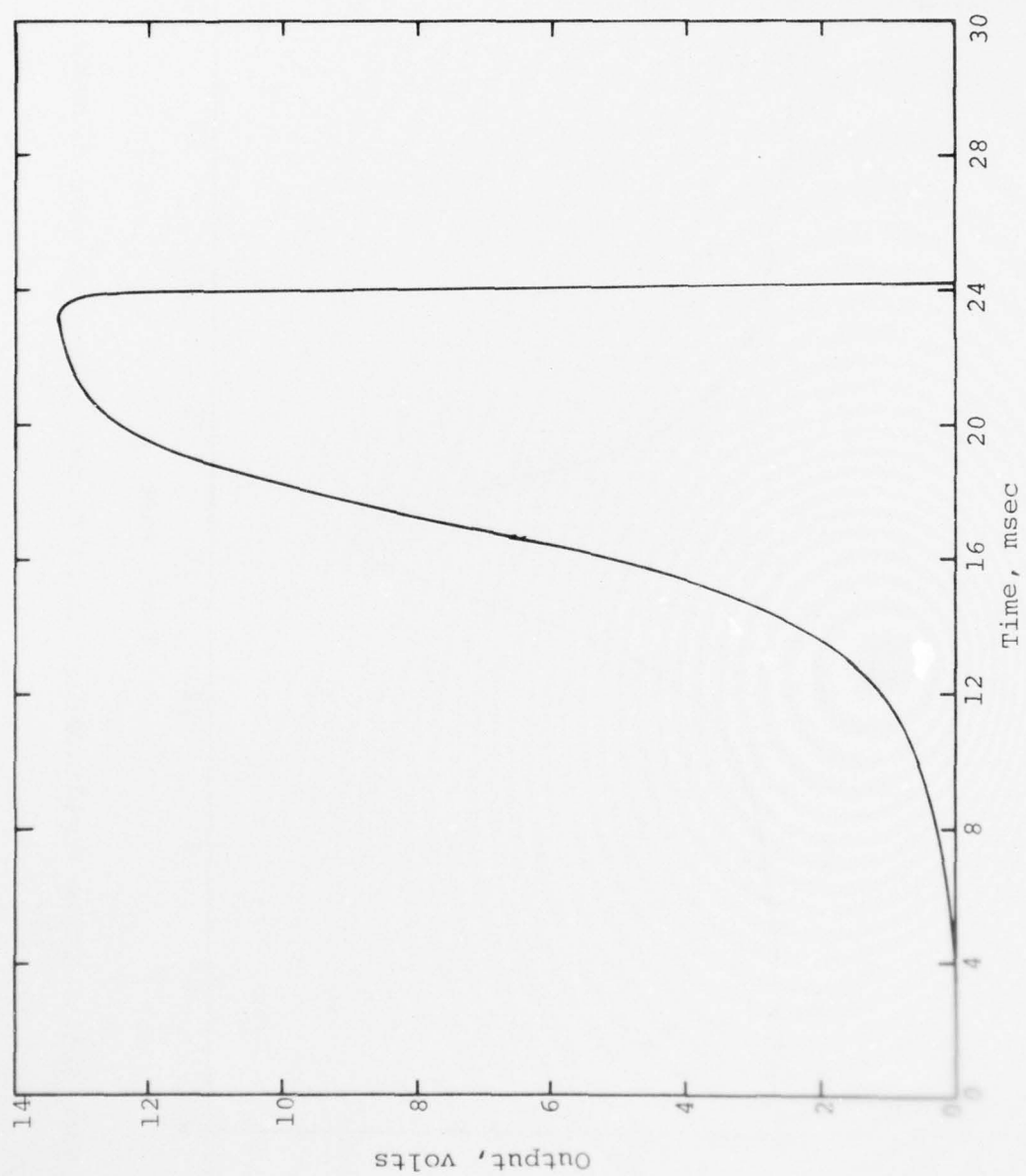


Figure 5.10. Crescent signal, 300 g at zero degrees.

AD-A047 374

KAMAN SCIENCES CORP COLORADO SPRINGS COLO
HUSSAR SWORD SERIES. HUSKY PUP EVENT. DEVELOPMENT AND TESTING 0--ETC(U)
SEP 76 H HOLLISTER, E L COLE, M A LEW
K-76-112U(R) DNA-4114F

F/8 19/4

DNA001-75-C-0277

NL

UNCLASSIFIED

2 OF 2

AD
A047374



END
DATE
FILMED

1-78

DDC

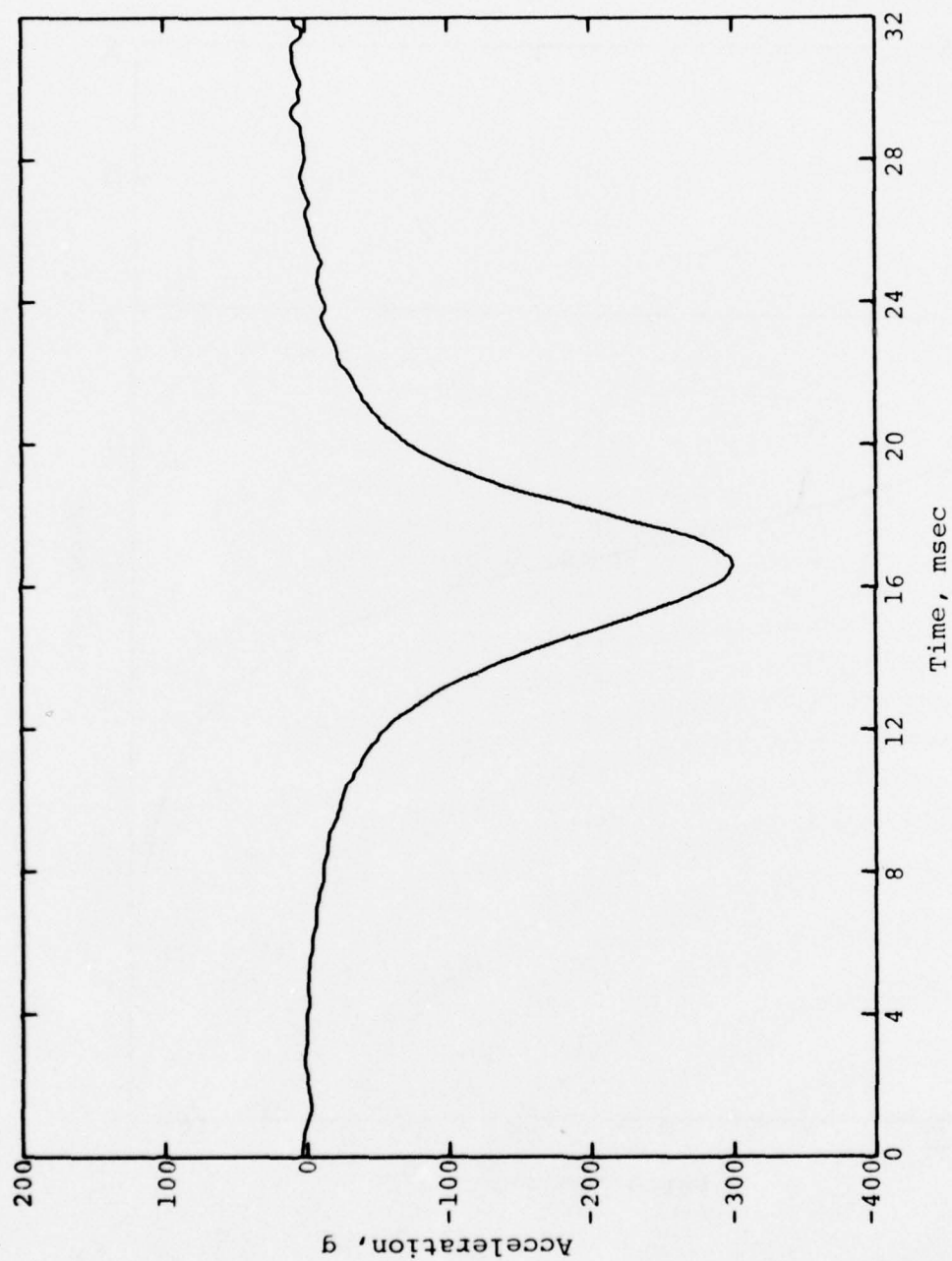


Figure 5.11. Table accelerometer (A-1) signal, 300 g at zero degrees.

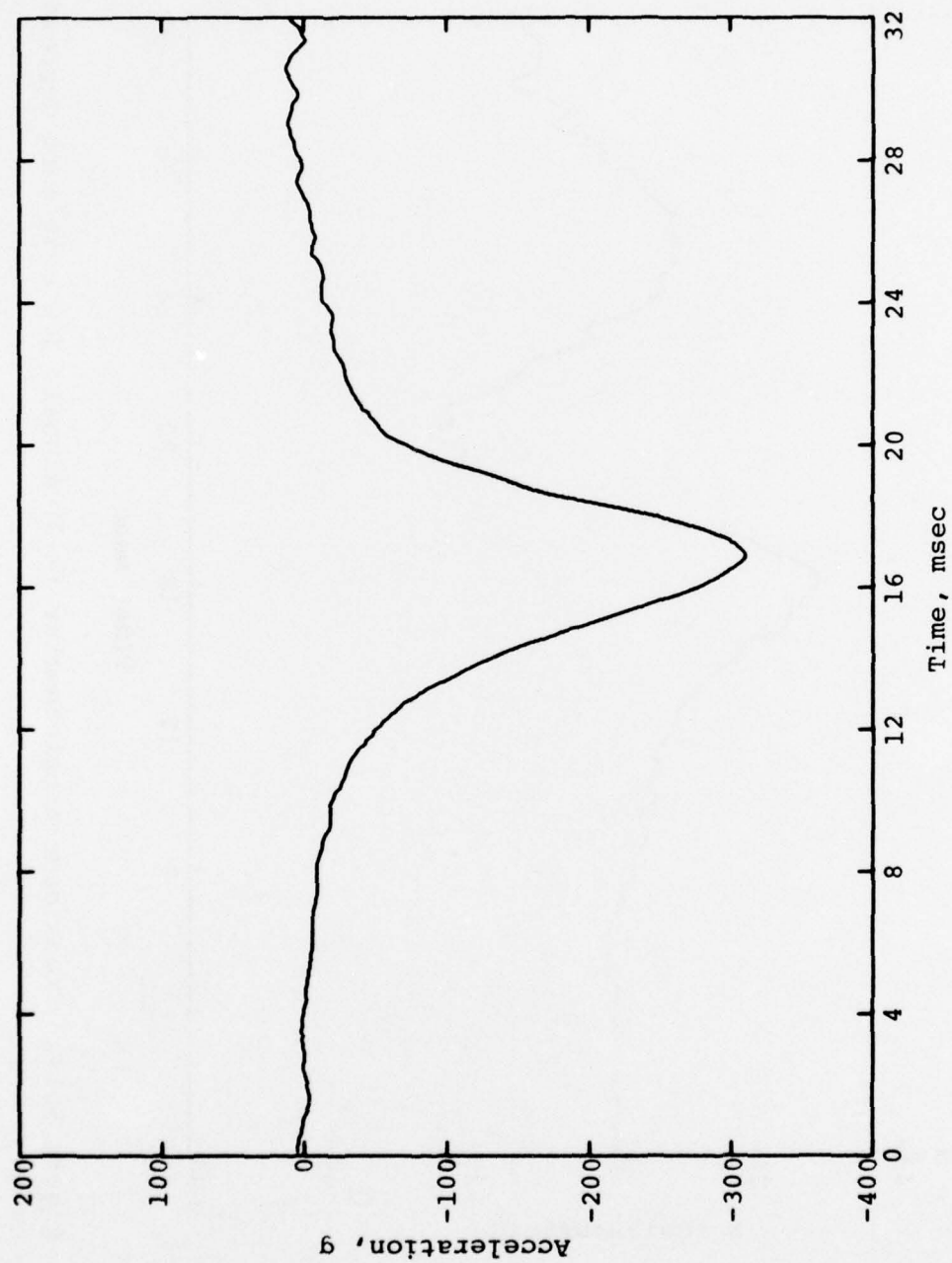


Figure 5.12. Axial accelerometer (A-2) signal, 300 g at zero degrees.

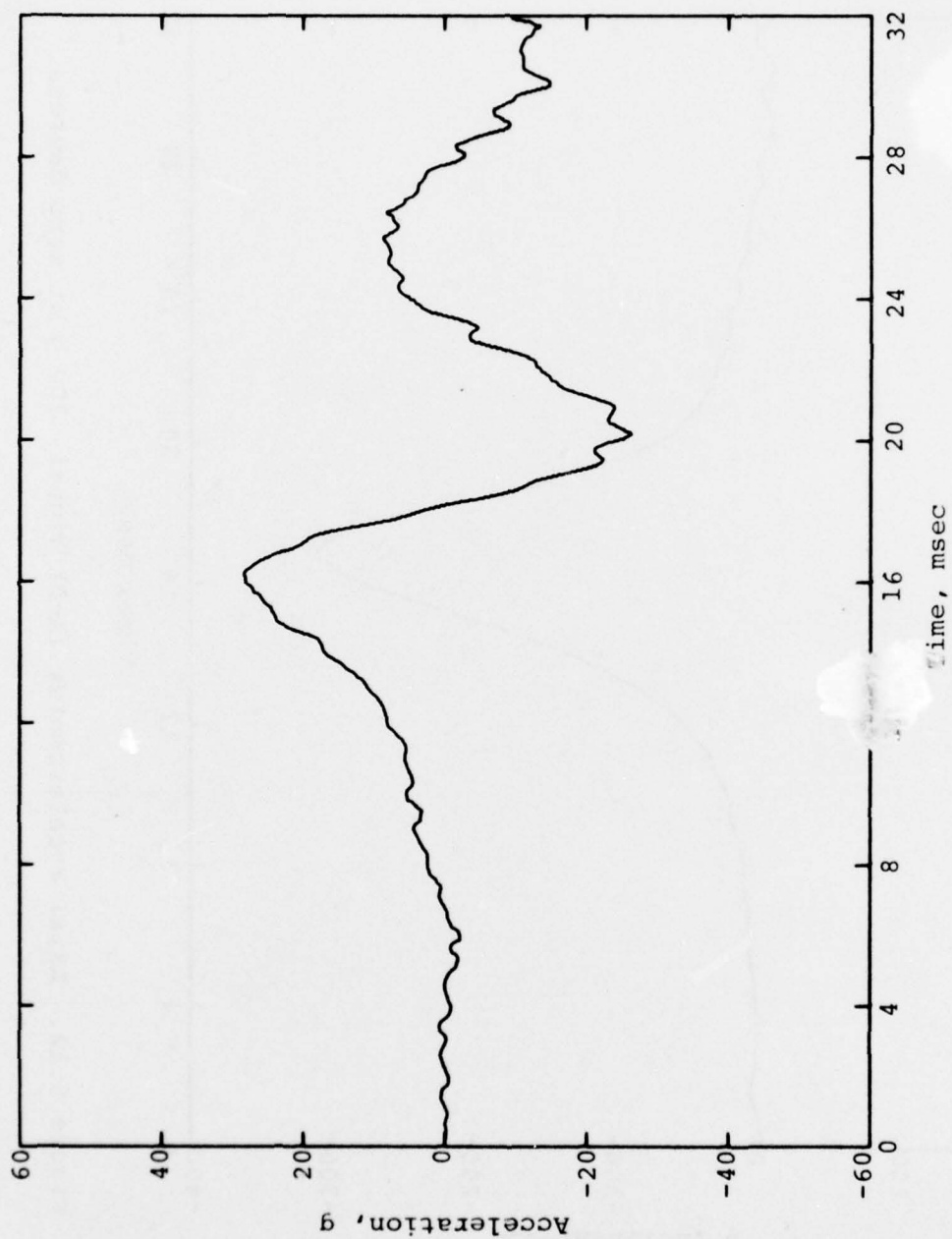


Figure 5.13. Transverse accelerometer (A-3) signal, 300 g at zero degrees.

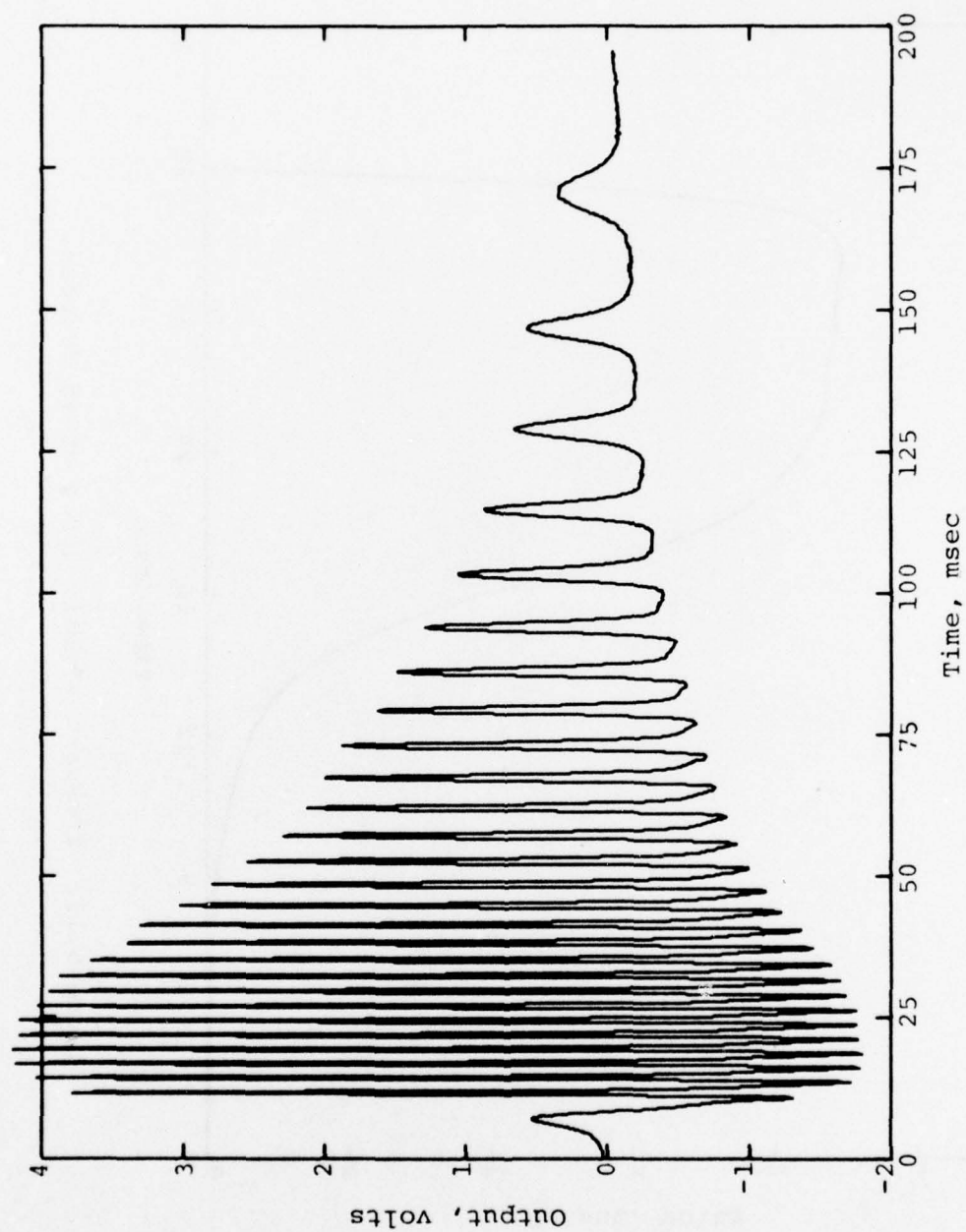


Figure 5.14. EDS signal, 300 g at 45 degrees.

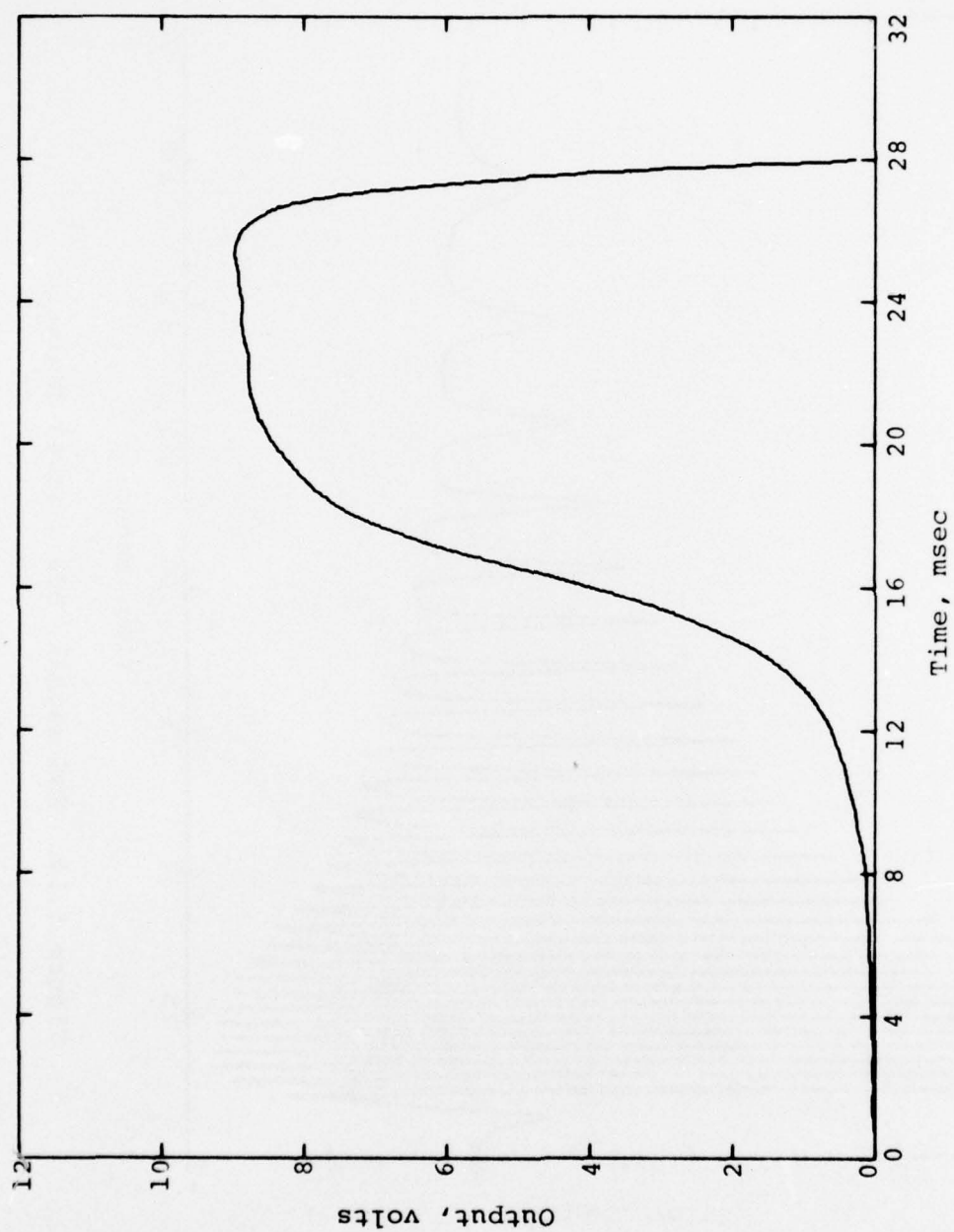


Figure 5.15. Crescent signal, 300 g at 45 degrees.

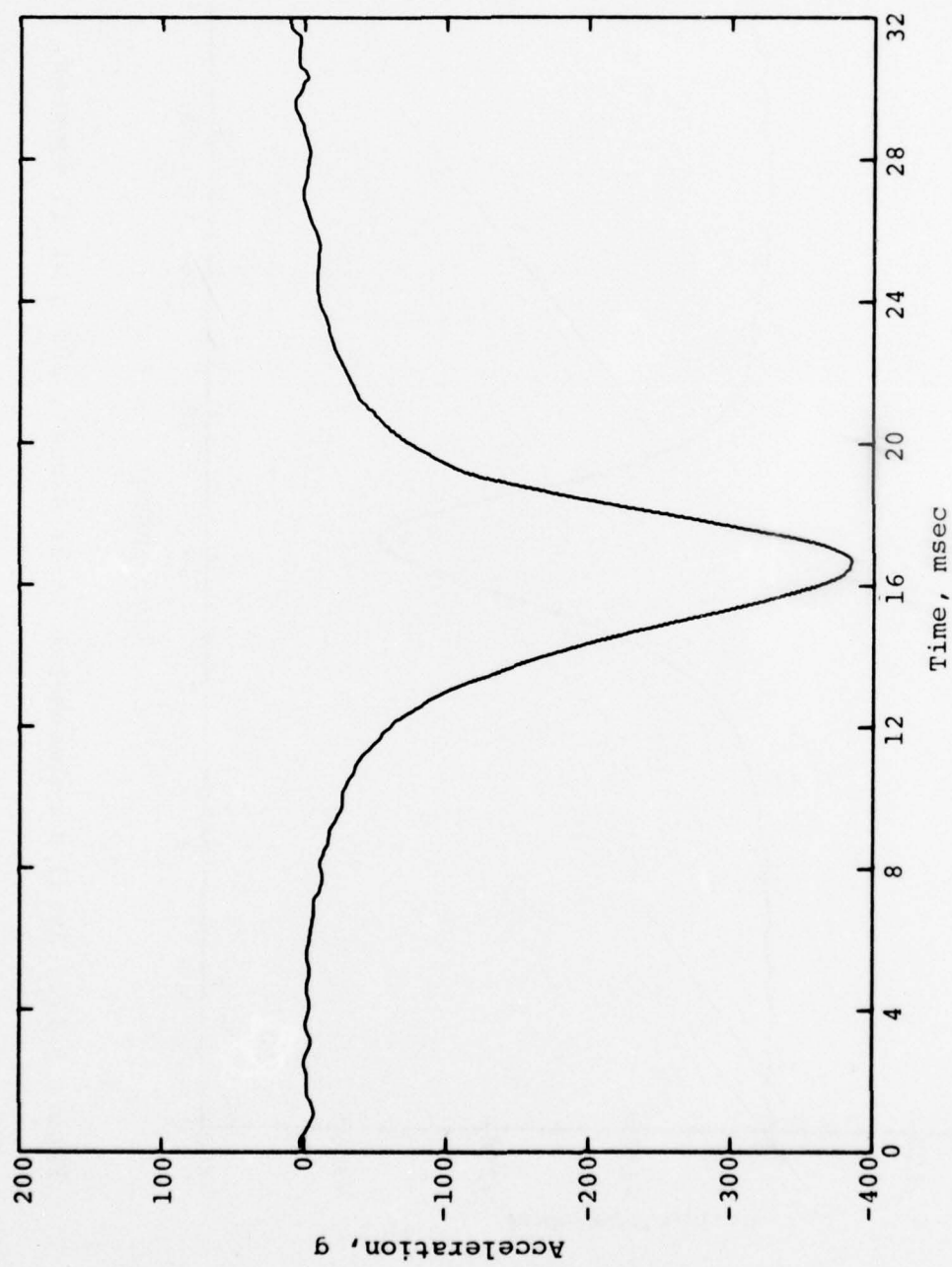


Figure 5.16. Table accelerometer (A-1) signal, 300 g at 45 degrees.

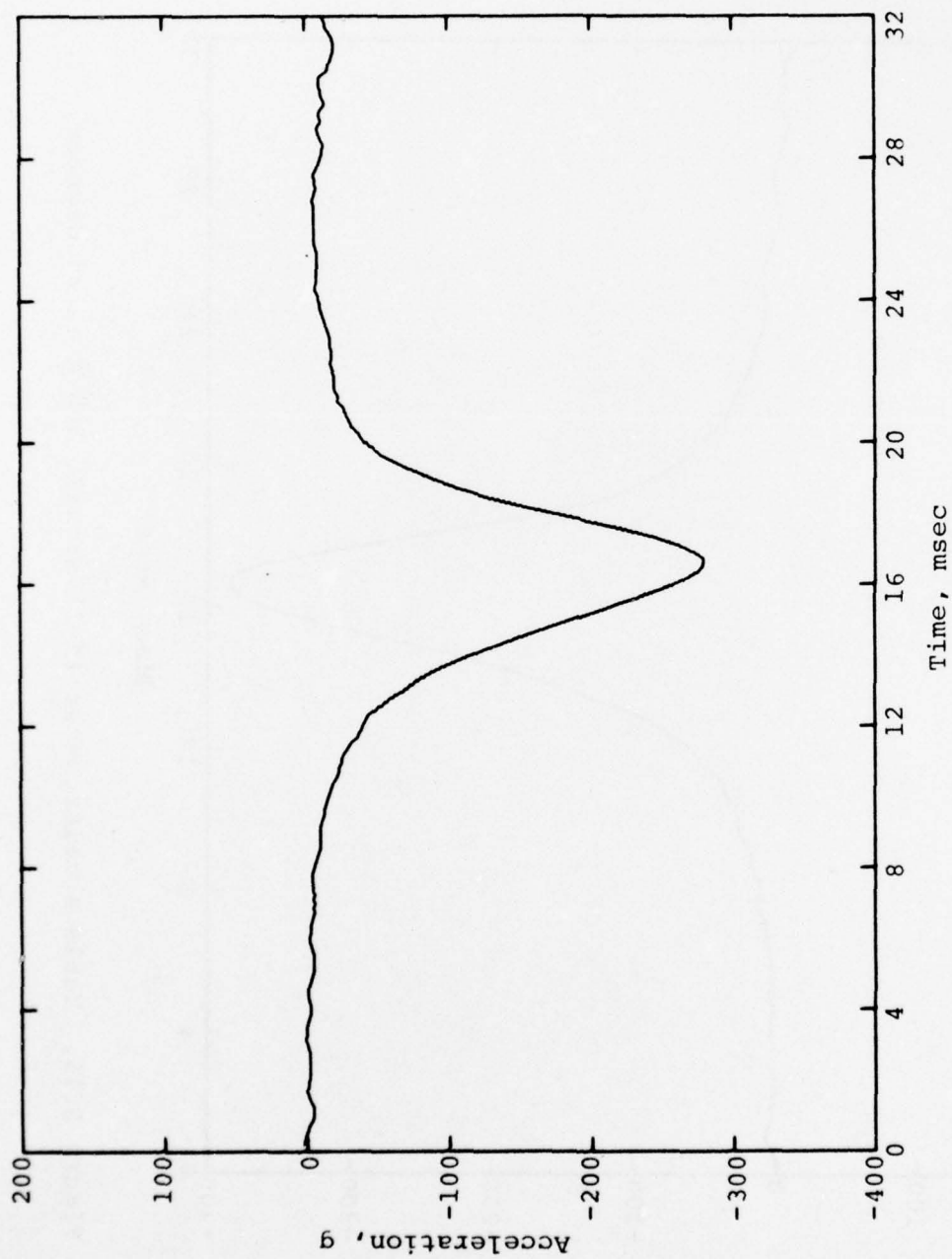


Figure 5.17. Axial accelerometer (A-2) signal, 300 g at 45 degrees.

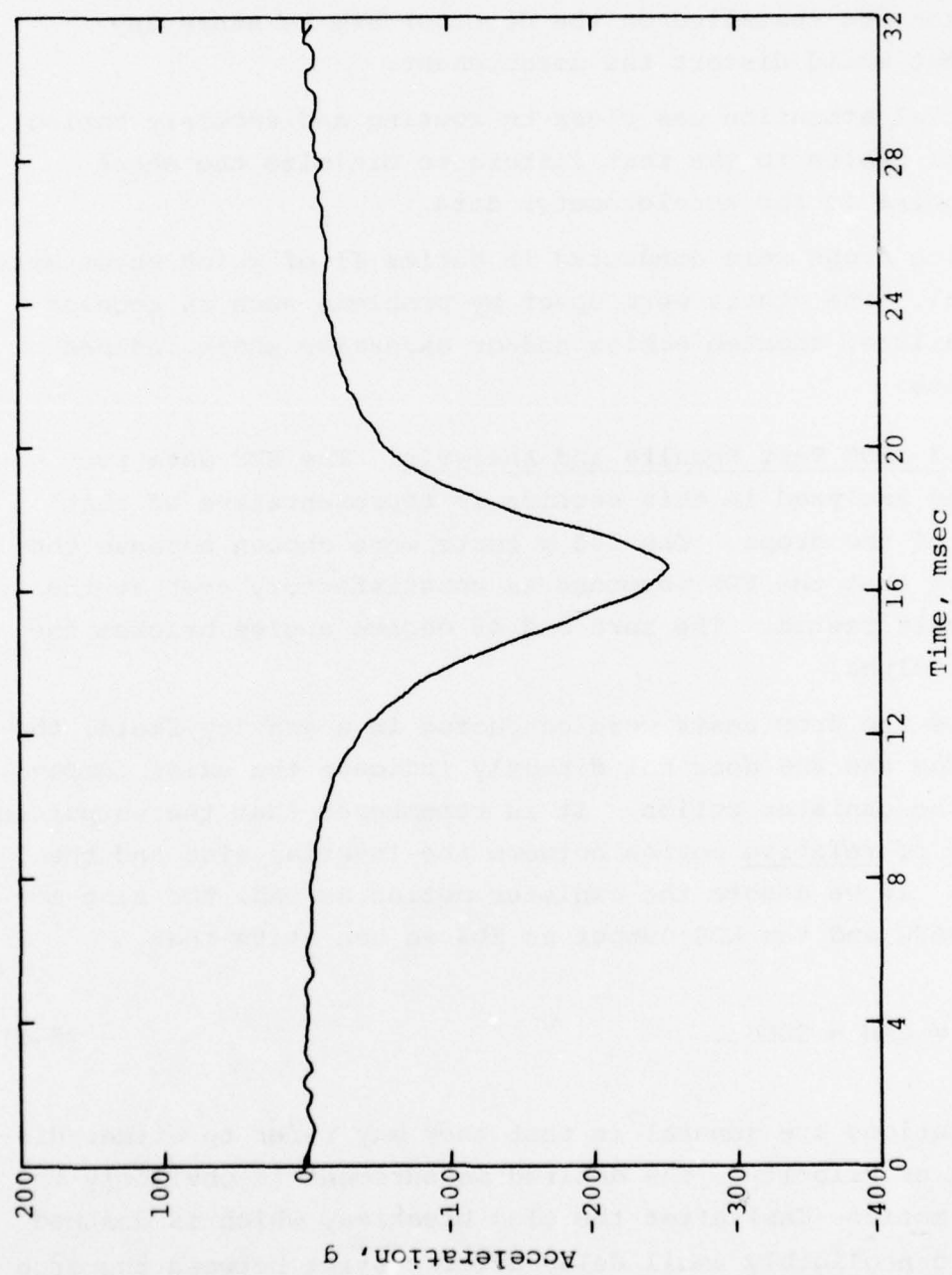


Figure 5.18. Transverse accelerometer (A-3) signal, 300 g at 45 degrees.

modification to the velocity measuring system was the shock isolation of the photo-optical sensor head and electronics. An accelerometer was installed on the detector arm to sense any motion that would distort the measurement.

Special attention was given to routing and securely taping the signal cables to the test fixture to minimize the shock induced noise in the accelerometer data.

Twelve drops were conducted in Series II of which seven were successful. The others were upset by problems such as accelerometer failure, shorted cables and/or excessive shock induced cable noise.

5.2.3 EDS Test Results and Analysis. The EDS data presented and analyzed in this section is representative of that from any of the drops. The 100 g tests were chosen because the data shows that the EDS response is unsatisfactory even at the lower levels tested. The zero and 45 degree angles bracket the range for alpha.

Since the drop tests were conducted in a gravity field, the output from the EDS does not directly indicate the axial component of the canister motion. It is remembered that the output is a measure of relative motion between the inertial slug and the canister. If we denote the canister motion as CAN, the slug motion as SLUG and the EDS output as EDS we can state that

$$\text{EDS} = \text{CAN} - \text{SLUG} . \quad (5.2)$$

These notations are general in that they may refer to either displacement or velocity. The desired measurement is obviously the canister motion (CAN) after the slug breakaway which is assumed to occur a negligibly small delay after contact between the drop table and the receiver pad.

Neglecting the effects of friction for a moment, after breakaway of the slug from the canister restraining clip, the slug motion is described by

$$v_s = (v_o + gt) \cos\alpha: \text{ velocity} \quad (5.3)$$

$$d_s = (d_o + gt^2/2) \cos\alpha: \text{ displacement} \quad (5.4)$$

where v_o and d_o refer to initial conditions at breakaway.

For analysis of the drop test data a frame of reference was chosen such that v_o is the table contact velocity zero table displacement occurs at contact (d_o equals zero). The canister motion is synonymous with table motion which was measured with an optical chopper. Reduction of the digitized EDS measurements was accomplished by solution of the equations derived from solving Equation (5.2) for CAN and substitution of Equations (5.3) and (5.4) for SLUG. For a detailed definition of the procedure used, accounting for frictional effects and slug breakaway, the reader is directed to Appendix C.

The photo-optical table velocity/displacement system (chopper) served the purpose very well giving excellent data as seen in Figures 5.19 and 5.20. The table accelerometer (A-1) was satisfactorily integrated and is plotted along with the chopper data on the graphs. As an aside, the accelerometers A-2 and A-3 were only marginally useful for integration due to shock induced cable noise and zero shifts. At 300 g, none of the accelerometer records were suitable for integration over the duration of the test. However, it will be seen in Section 5.2.4 that excellent agreement was obtained by integration of A-1 for times less than 20 to 30 milliseconds after impact. Large zero shifts on the order of perhaps 25 percent were common on the high level tests.

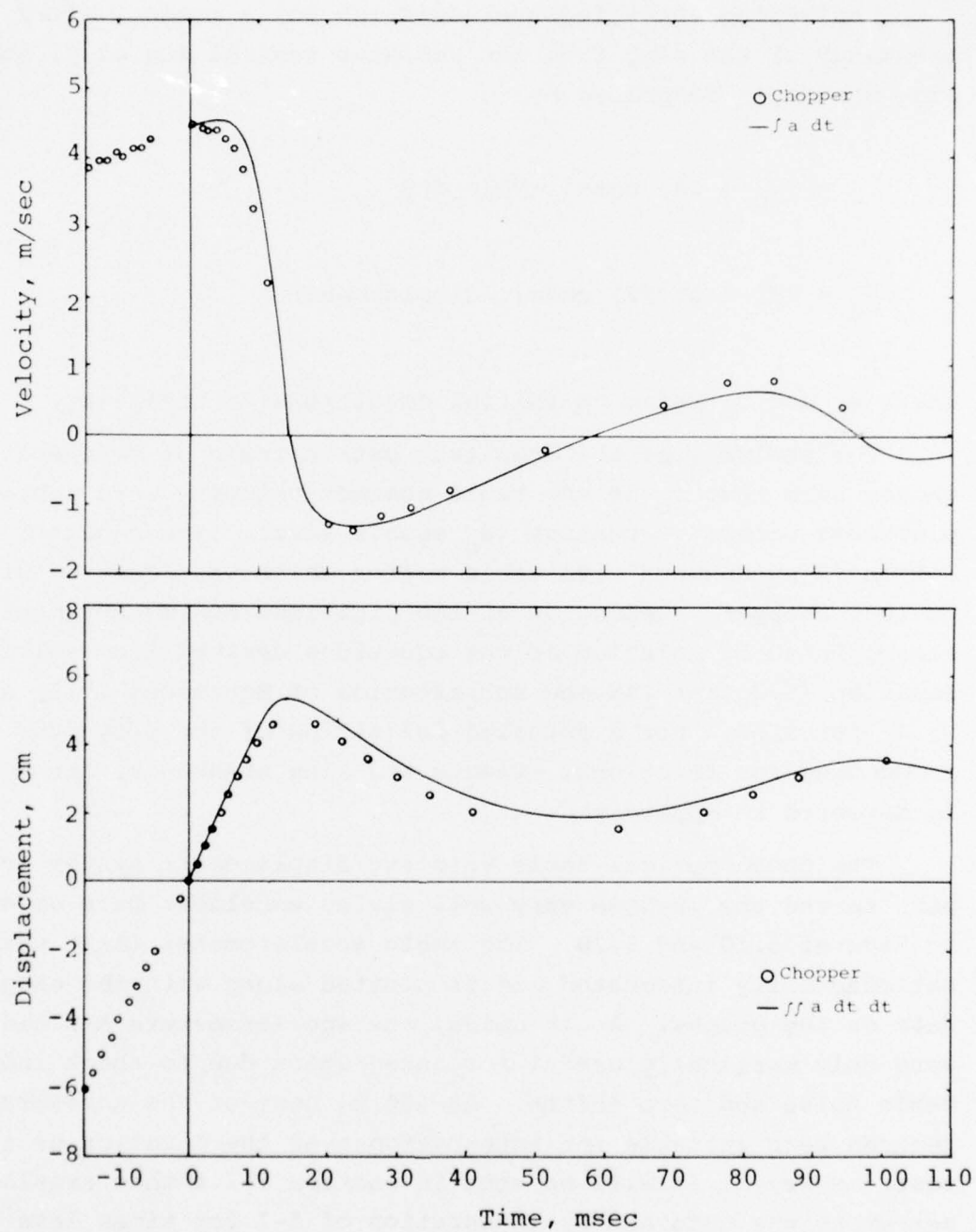


Figure 5.19. Table velocity and displacement for the zero degree, 100 g drop test.

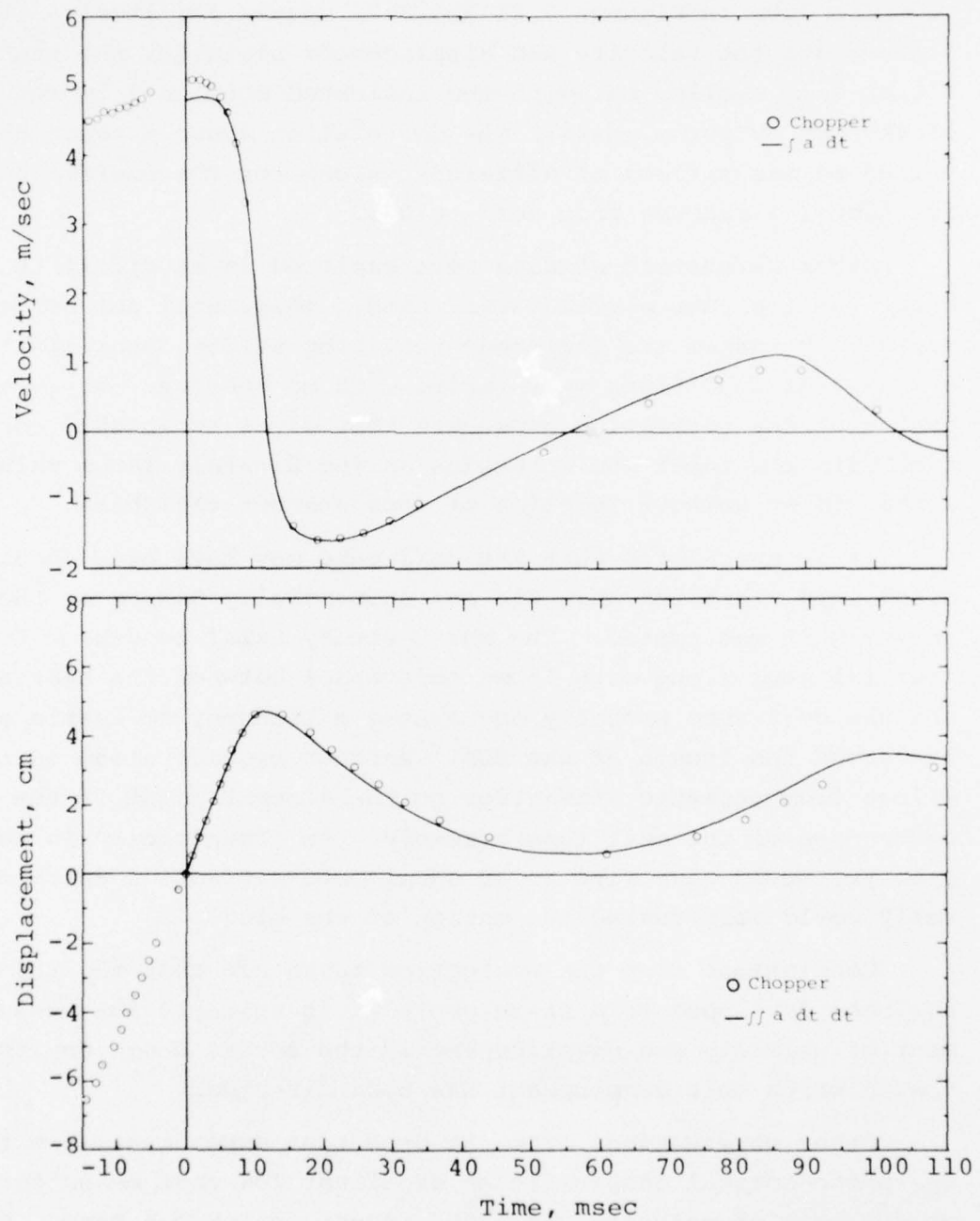


Figure 5.20. Table velocity and displacement for the 45 degree, 100 g drop test.

The data in Figures 5.21 and 5.22 speaks for itself. These figures are the velocity and displacement plots for the table motion seen earlier but with the indicated motions from reduction of the EDS output signals. The correlation shows answers obtained by assumptions of different values for the coefficient of friction (μ) ranging from zero to 0.5.

Other parametric studies were explored in an effort to account for the poor correlations noted. These will not be presented but rather the statement that time shifts, sensitivities, and initial conditions were varied with no success. It is evident that any correction procedure that gives acceptable correlation with the input would require an inordinately large value of μ that is an unknown function of some unknown variables.

It is speculated that the coil tube may have been shock excited into vibration that was not successfully damped by the RTV in which it was potted. The short stubby axial length of the inertial slug along with loose tolerances between the bearings and the coil tube probably aggravated a tendency to rattle as it traversed the length of the EDS. Another consideration is the effect from magnetic attraction to the closest point of the steel outer case of the coil tube assembly. An eccentricity in the geometry would give rise to an unbalanced attraction which naturally could vary during the motion of the slug.

Conclusions from the evaluation tests are that the EDS has not been developed to a state where it is suitable for measurement of velocity and displacement in the severe shock environment toward which this development has been directed.

Other observations from the drop test experiments are that the photo-optical chopper is an excellent low cost means for measurement of velocity and displacement for such a test. Experience with the accelerometers seems to indicate that high impedance cables should be protected from shock during the

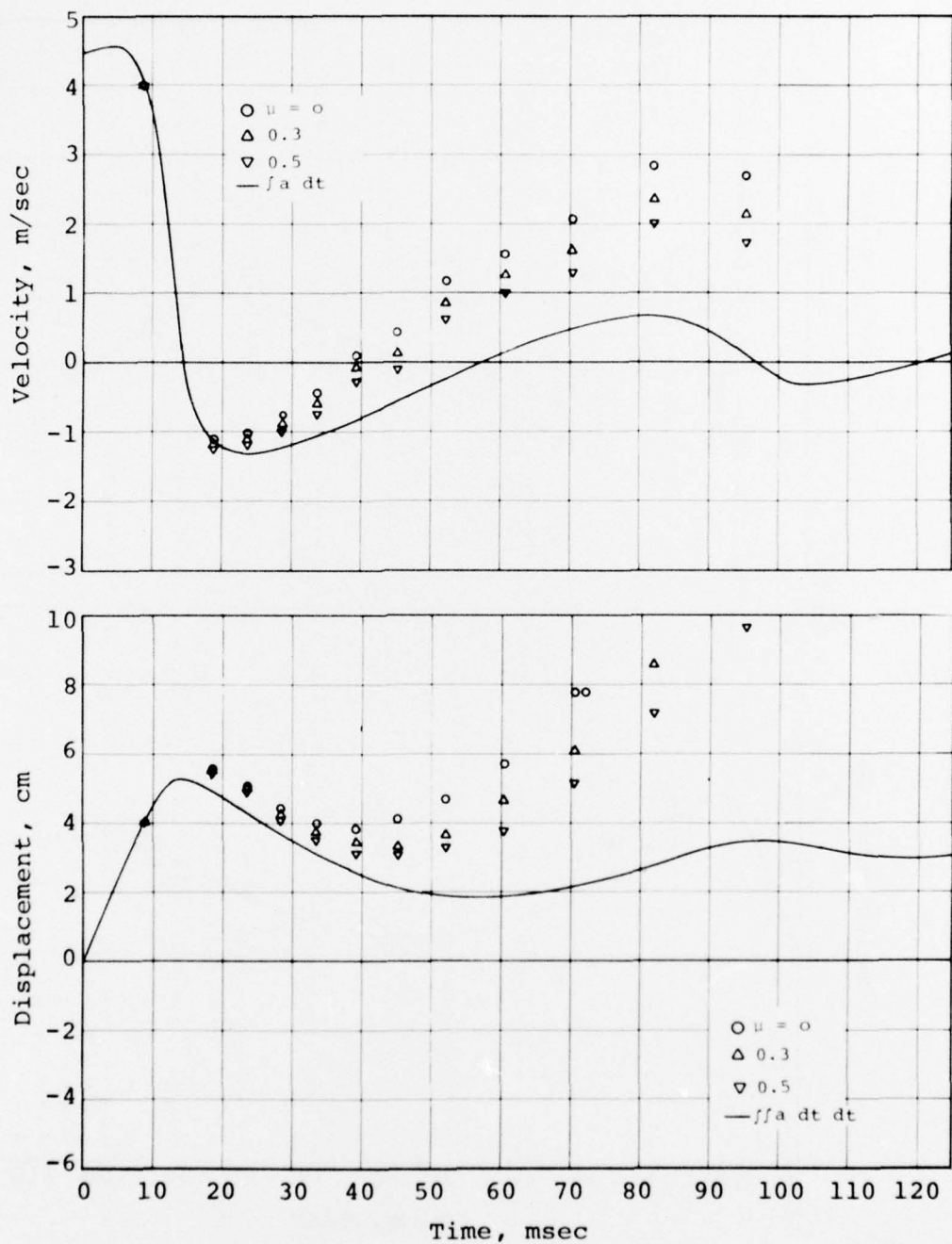


Figure 5.21. EDS output for the zero degree, 100 g drop test.

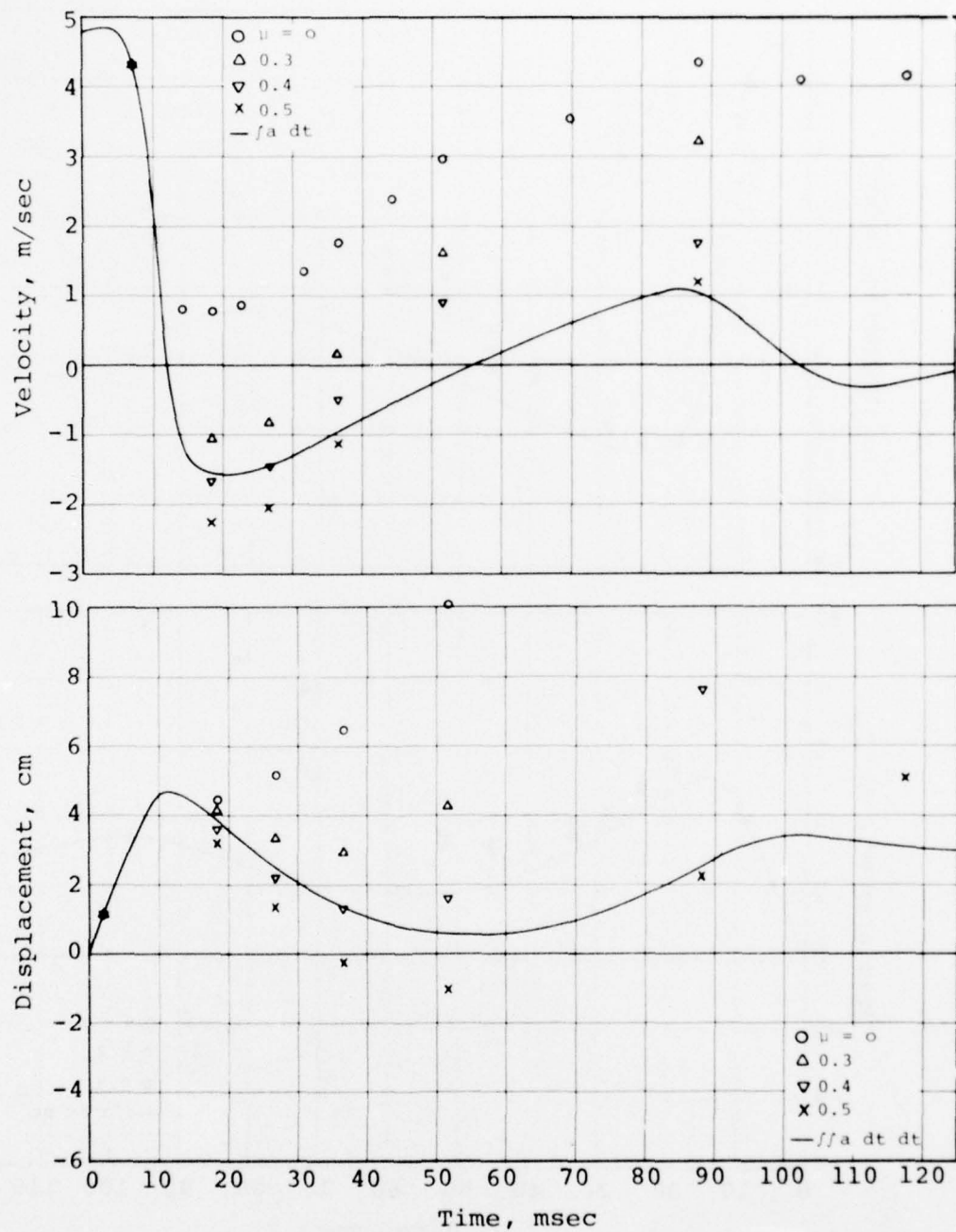


Figure 5.22. EDS output for the 45 degree, 100 g drop test.

measurement period. Although this was not tested, it is expected that the situation would have improved if accelerometers with integral impedance converters (source followers) had been used. The lower impedance level would make the triboelectric noise signals from the cable insignificant.

5.2.4 Crescent Gage Tests and Analysis. The Crescent velocity gage has been utilized frequently in the last several years for measurements of ground motion on numerous DNA sponsored experiments. The past experience has been that sometimes it apparently performed satisfactorily while at other times it would exhibit an unexpected intermittent slip-stick action.

This transducer was manufactured by Crescent Technology of Newport Beach, California for and to the specifications of Physics International Company of San Leandro, California. A detailed description of the Crescent gage is given in References 9, 10, and 11 along with records of data taken on various experiments. A photograph of the test gage is seen in Figure 5.23.

Reference 11, "Ground Motion Measurements", Operation Diamond Dust is particularly interesting in the context of this report because in addition to an excellent description of the gage, the records are seen to appear distorted by the slip-stick action mentioned earlier. Figure 5.24 is given here as a typical example of the questionable data.

In an effort to better understand the cause of this type of response, the Crescent gage was incorporated into the Series II drop tests at SLA. It was expected that sticking could be induced and further studied to learn how to eliminate it for future use. In this context, it can be stated that the drop tests were inconclusive with regard to the Crescent gage.

The gage was tested with no lubrication of any kind on the magnet slug, planning to later use molybdenum disulfide dri-film

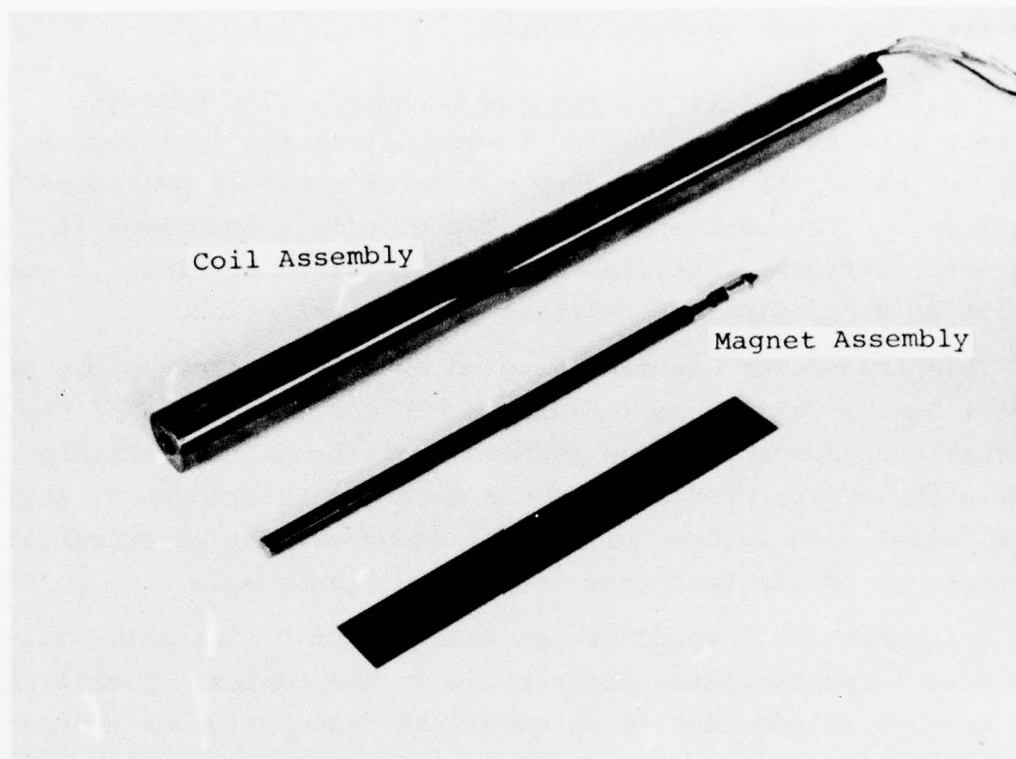


Figure 5.23. Photograph of Crescent velocity gage.

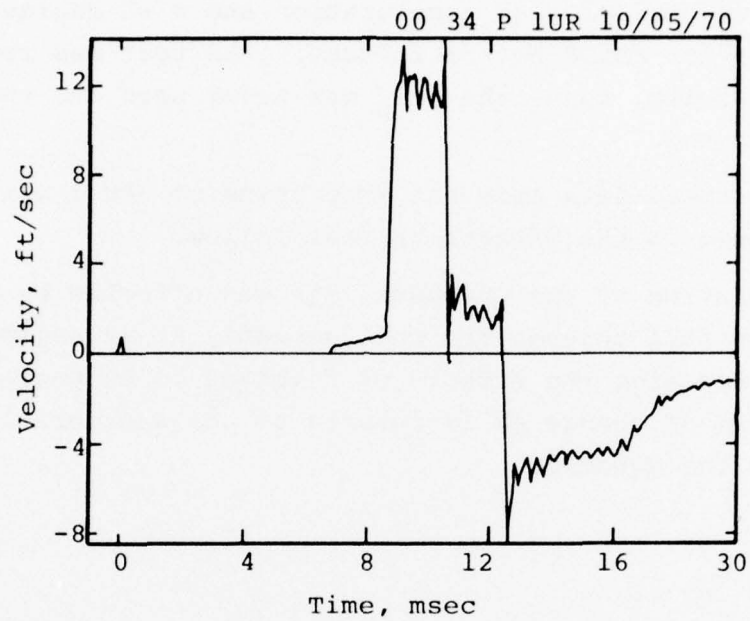


Figure 5.24. Crescent gage output signal from Operation Diamond Dust (Reference 11, Figure A.21).

lubricant after sticking had been induced. At the highest test level, the axial peak acceleration and a 45 degree test angle the sticking could not be induced. The test was repeated with still higher levels, thus, the MoS₂ was never used and the Crescent tests abandoned.

The reduced data from the drop tests at 300 g are presented and discussed in the paragraphs that follow.

Calibration of the Crescent gage was effected by permitting the slug to fall through the coil assembly at an angle of zero degrees. Assuming the effects of friction to be negligible, the voltage rate of change ΔV is related to the acceleration due to gravity by the equation

$$\frac{\Delta V}{\Delta t} = g \cdot S$$

where S is the sensitivity of the gage.

Using this method, S was measured as 7.4 mv/cm/sec at KSC prior to the SLA drop tests.

Since the Alnico rod magnetized to its ultimate level is sensitive to shock, the calibration was repeated before and after each drop test for evidence of desensitization of the magnet. Study of these freefall tests showed that if any changes did occur, they were not perceptible above the noise in the recorded data.

The output signals seen in Figures 5.10 and 5.15 were integrated and are seen in Figure 5.25. As a check on the calibration the sensitivity was also calculated for this integration with a knowledge that the stroke of the slug was 13 cm. This distance yields a value of S equals 7.68 mv/cm/sec which is the

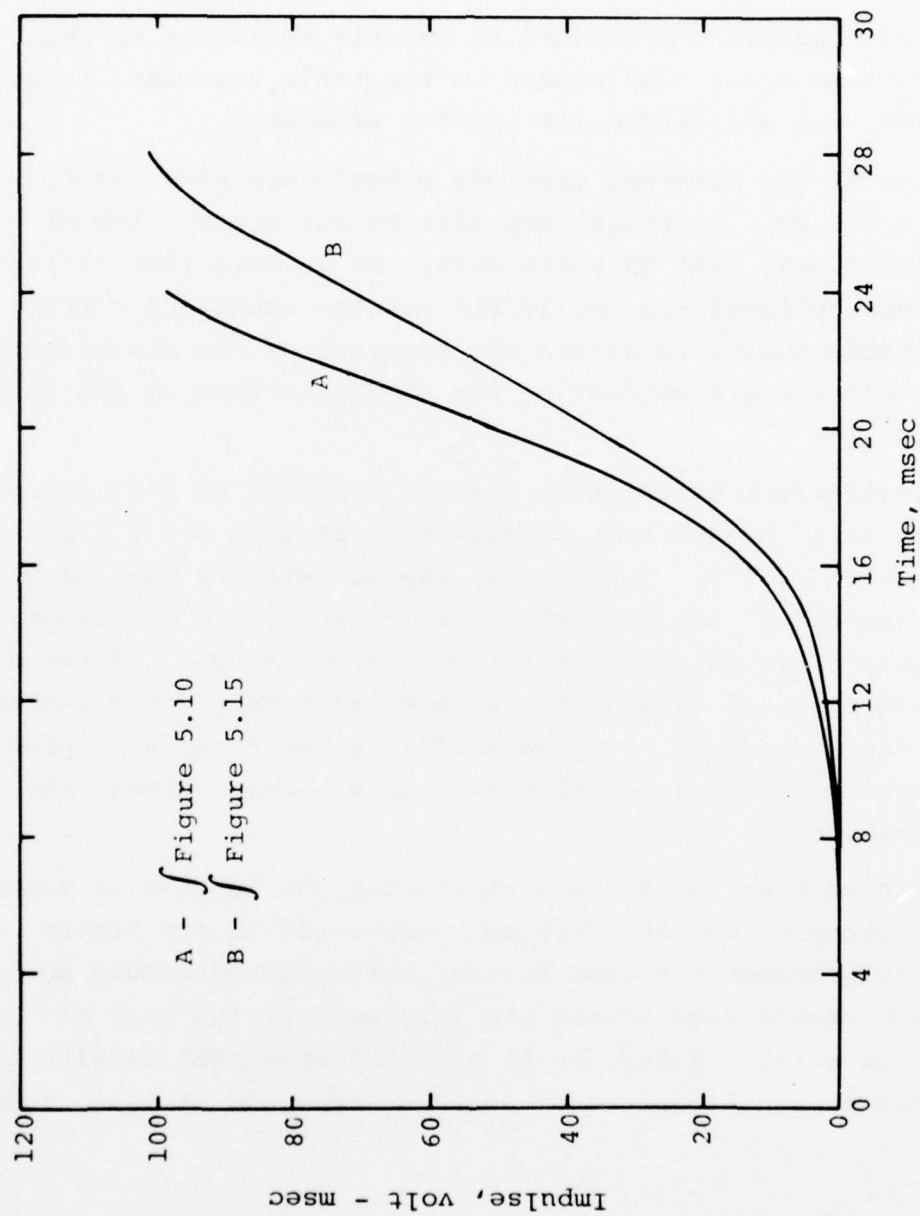


Figure 5.25. Integrated Crescent gage output signals, 300 g at zero and 45 degrees.

value used in this data reduction as it is felt to be the more correct number.

The data reduction procedure is exactly analogous to that given in Section 5.2.3 with regard to the table velocity, frame of reference, and accounting for gravity effects.

Results of the Crescent gage 300 g tests are shown in Figures 5.26 and 5.27. No effort was made to correct for the effects of frictional drag on these data. It is seen that at zero degrees, these effects are negligible and the excellent correlation with table motion is within the accuracy of the measurement. Frictional effects are evident on the 45 degree test as one would expect.

The coefficient of friction (μ) was measured at 0.62 using the gravity fall through test described in Section 5.1.1 (Reference Equation (5.1)). In desk top experiments, by carefully elevating one end of the gage to determine the angle of repose, the breakaway μ was measured to range from 0.3 to 0.4. A reason for the wide range of value for μ is the relatively rough finish on the sliding surfaces. One can readily sense a variable pressure on the fingertip as the slug is pushed slowly through the Crescent gage core.

With these test results and considerations in view it seems doubtful whether or not the Crescent gage would be any better than an accelerometer for long term measurements of ground motion. The Crescent gage tested did very well if the only acceleration is axial. Reference to the 45 degree test results indicates that a significant error could be expected at late times.

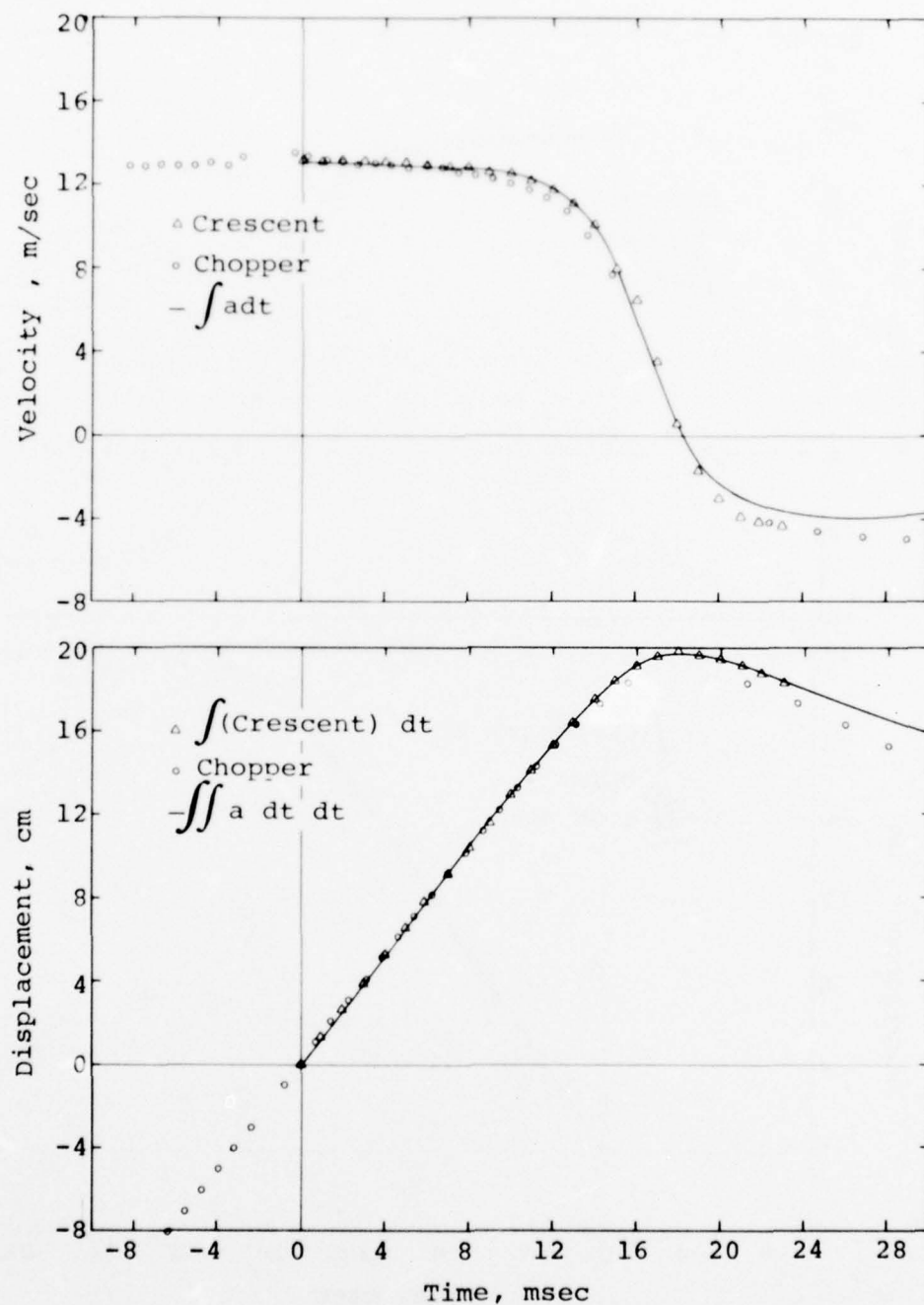


Figure 5.26. Crescent gage drop test results, 300 g at zero degrees.

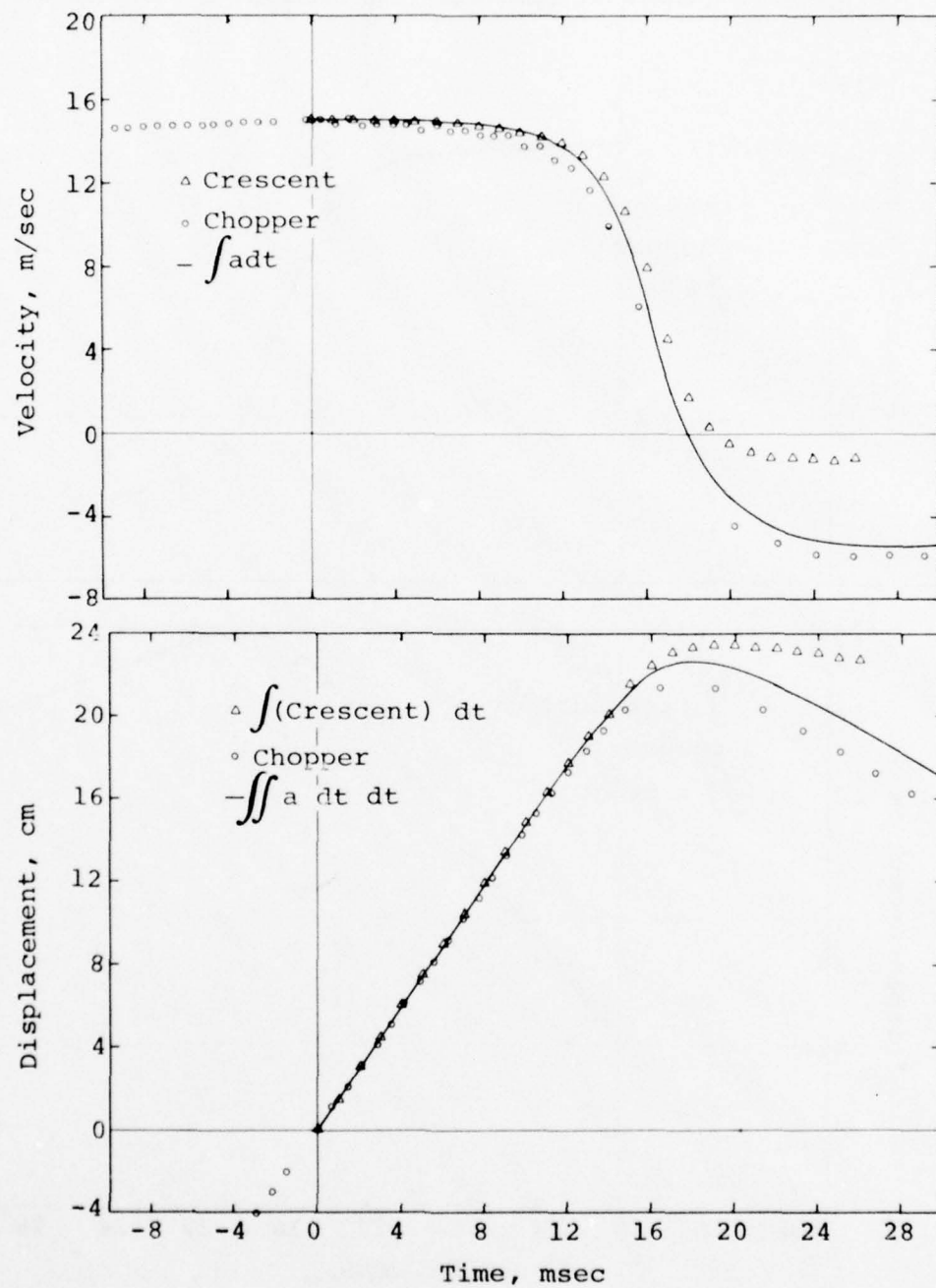


Figure 5.27. Crescent gage drop test results, 300 g at 45 degrees.

CHAPTER 6

HUSKY PUP UGT

The two EDS units fielded on event Husky Pup yielded no useful displacement or velocity information. The reason for the total failure of both channels can only be speculated without access to the EDS units for post-mortem inspection. After a studied analysis of the situation it appears that the most likely cause of failure is a pressure leakage path into the EDS interior through a hole in the cable overjacket. This design deficiency is discussed in some detail in Chapter 4, Section 4.2.2.

As a consequence of the total loss of information from both channels, many otherwise important aspects of the fielding are of academic interest and are not reported in any detail.

6.1 INSTALLATION

Two EDS systems were fielded by KSC on event Husky Pup for measurement of free-field radial particle displacement. The two gages were installed in 20 cm diameter drill holes MD-1 and MD-2 at locations shown in Figure 6.1. The gage located at the 137 meter range in MD-1 was installed according to plan. The geological media was sound and the grout was pressurized to 80 N/cm².

The close-in EDS emplacement was planned to be at a 95 meter range. The plan was to locate the sensor ahead of the perturbation to the free field that the DNA Auxiliary Closure (DAC) No. 2 crossdrift would introduce. Obstructions in the MD-2 drill hole prevented this and the EDS was finally located at 104 meters as shown in Figure 6.1. The tunnel wall was not geologically sound in the region of MD-2 and attempted pressurization of the grout resulted in blowout of a large section of the wall. Subsequently the grout was pressurized at 25 to 30 N/cm².

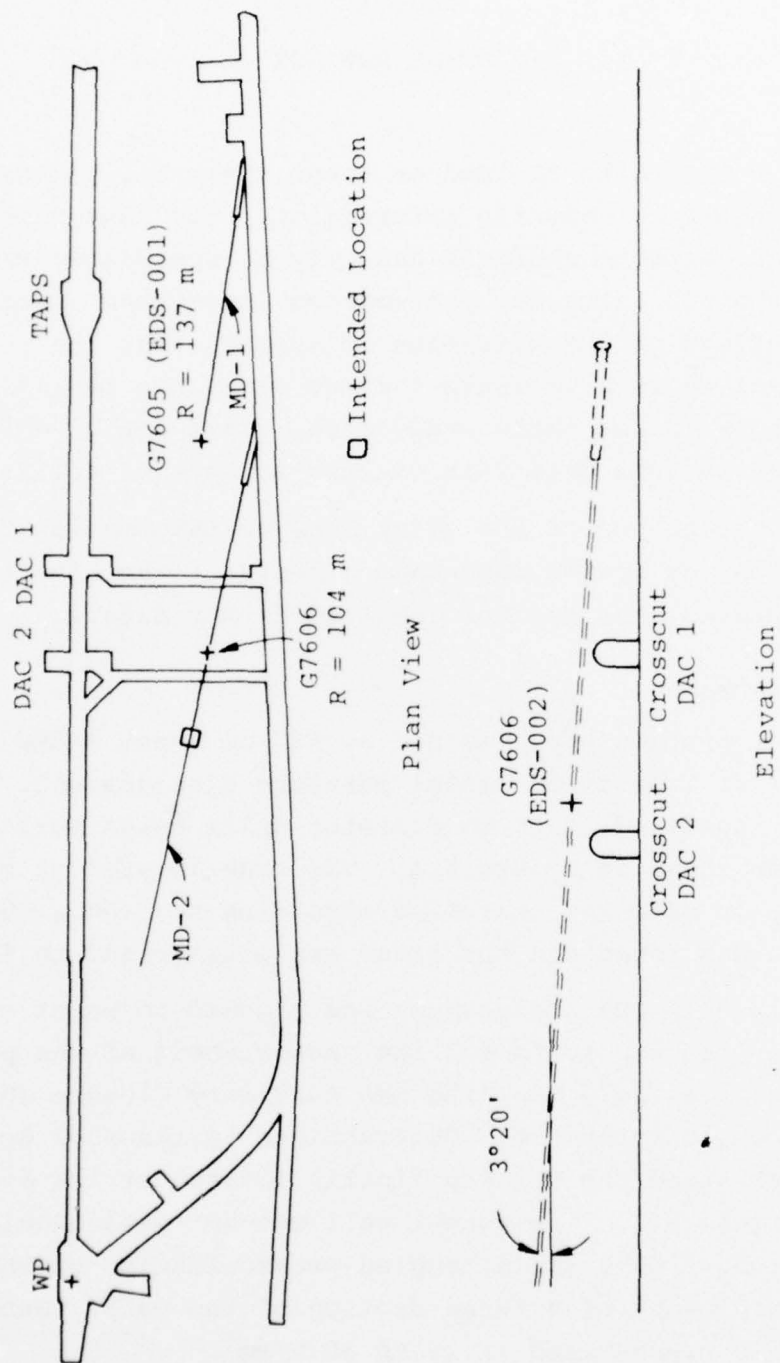


Figure 6.1.1. EDS placement on Husky Pup event.

It was learned that the most desirable grout, from an impedance and strength viewpoint, could not be used because of pumping constraints. Consequently, grout mixture HPNS-2 was substituted as an alternate.

Two regions in which the cables are especially vulnerable to damage are recognized as (1) immediately behind the EDS as the cable exits from the canister and (2) at the tunnel wall interface. Cable protection in the first region was covered by the transition on the EDS as well as the convoluted aluminum tubing extending behind the canister. At the wall interface flexible conduit was slipped over the cable from about 10 feet into the drill hole and up to the rigid conduit that crossed under the tracks on the tunnel floor.

Resistance readings before and after energizing the solenoids were unchanged, indicating a malfunction of the EDS priming mechanism. Prior to energizing the solenoids, EDS-1 at the 104 meter station indicated that the inertial slug was not properly seated. This syndrome would be expected if grout fluid had leaked into the EDS interior during the grouting operation.

6.2 RESULTS

The outputs of the EDS channels were recorded by KSC on a 20 kHz bandwidth tape recording system as a piggyback project in conjunction with another fielding effort by KSC. No data was recorded from either gage that could be interpreted as a meaningful displacement measurement.

Analysis of the noise signature on the recorded EDS channels gives encouragement that the cables survived for several hundred milliseconds. This provides a level of confidence that the transition and other protective measures for the cable functioned properly.

6.3 COMMENTS

The failure to record any data from either channel is naturally a big disappointment. However, it was known prior to the event day that the EDS was not a fieldworthy instrument, based on analysis of the shock test data. Installation schedules did not permit this determination before the commitment to field. In defense of the schedule it should be said that extrapolation of the design from TRIM to EDS was not expected to pose the problems actually encountered.

A major obstacle was found to be in the fabrication of the long coil tube with the degree of precision required to keep the coefficient of friction low enough for a useful gage. This stands as the primary engineering problem to be faced in development of a useful EDS.

CHAPTER 7

SELECTED BIBLIOGRAPHIES

7.1 COMMENTARY

A selected bibliography on pertinent topics is included as Chapter 7. These references were found to be the most useful and in general the best ones located by those working on the EDS project. They are presented here in addition to those referenced in the text in the expectation that the readers of this report will also find them helpful.

7.2 GROUND MOTION STUDIES

1. S. N. Burchett, J. A. Milloy, and W. A. Von Rieseemann; "Finite Element Analysis of an Underground Protective Test Station Subjected to Severe Ground Motion"; Sandia Laboratories, Albuquerque, New Mexico.
2. Y. H. Pao, R. R. Gajewski, and S. A. Thau; "Analysis of Ground Wave Propagation in Layered Media"; DASA 2697, February 1971; Department of Theoretical and Applied Mechanics, Ithaca, New York for Headquarters, Defense Nuclear Agency, Washington, D. c.
3. T. D. Riney and others; "Ground Motion Models and Computer Techniques"; DNA 2915Z, 3SR-1071, April 1972; Systems, Science and Software, La Jolla, California for Headquarters, Defense Nuclear Agency, Washington, D. C.
4. R. P. Swift; "Dynamic Response of Earth Media to Spherical Stress Waves"; DNA 2954F, PIFR-315, May 1973; Physics International Company, San Leandro, California for Headquarters, Defense Nuclear Agency, Washington, D. C.
5. A. T. Matthews and H. H. Bleich; "Dynamic Response of Cylindrical Shells in Bilinear Media - Axisymmetric Case"; DNA 3143F, 1 March 1973; Weidinger Associates, New York, New York for Director, Defense Nuclear Agency, Washington, D. C.

6. M. W. McKay and C. S. Godfrey; "Study of Spherically Diverging Shock Waves in Earth Media, DASA-2223, PIFR-064, March 1969; Physics International Company, San Leandro, California for Defense Atomic Support Agency, Washington, D. C.

7. W. R. Perret and R. C. Bass; "Free-Field Ground Motion Induced by Underground Explosions"; SAND74-0252, February 1975; Sandia Laboratories, Albuquerque, New Mexico.

8. H. C. Rodean; "Nuclear-Explosion Seismology"; TID25572, 1971; Lawrence Livermore Laboratory, University of California, Livermore, California for U. S. Atomic Energy Commission, Division of Technical Information.

7.3 GROUND MOTION MEASUREMENTS

1. F. M. Sauer and J. A. Kochly; "Ground Motion Measurements", Operation Diamond Mine, Final Report; POR 6573, PIFR-283, October 1972; Physics International Company, San Leandro, California.

2. P. Lieberman and others; "Close-in Pressure and Displacement Measurements in Mine Ore"; DASA 2321, August 1969; IIT Research Institute, Chicago, Illinois for Defense Atomic Support Agency, Washington, D. C.

7.4 SOIL STRUCTURE INTERACTION

1. J. R. Allgood; "Summary of Soil - Structure Interaction"; Technical Report R-771, Y-F008-08-02-108, DNA 13.018; Naval Civil Engineering Laboratory, Port Hueneme, California for Defense Nuclear Agency, Washington, D. C.

2. G. R. Boyer; "Investigation of Soil-Structure Interaction Models"; August 11, 1970; Bell Telephone Laboratories, Whippany, New Jersey.

3. T. K. Lew; "Soil/Structure Interaction: Horizontal Cylinders"; TR-816, October 1974; Civil Engineering Laboratory, Naval Construction Battalion Center, Port Hueneme, California.

4. J. K. Ingram; "Placement Effects on Ground Shock Instrumentation"; Miscellaneous Paper N-70-7, July 1970; U. S. Army Engineer Waterways Experiment Station, Vicksburg, Mississippi for Defense Atomic Support Agency, Washington, D. C.

5. D. E. Van Dillen and D. P. Reddy; "Interaction Between Gage and Soil"; R-7354-3616, April 1975; Agbabian Associates, El Segundo, California for Defense Nuclear Agency, Washington, D. C.

7.5 GEOLOGICAL MATERIALS

1. S. H. Schuster and J. Isenberg; "Equations of State for Geologic Materials"; DNA 2925Z, AA-R-7134-2283, September 1972; Agbabian Associates, Los Angeles, California for Defense Nuclear Agency, Washington, D. C.

2. I. Nelson, M. L. Baron, and I. Sandler; "Mathematical Models for Geological Materials for Wave Propagation Studies"; DASA 2672, March 1971; Paul Weidlinger, Consulting Engineer, New York, New York for Headquarters, Defense Nuclear Agency, Washington, D. C.

3. F. L. DiMaggio and I. Sandler; "Material Models for Soils"; DASA-2521, April 1970; Paul Weidlinger, Consulting Engineer for Defense Atomic Support Agency, Washington, D. C.

4. M. H. Wagner, M. Rosenblatt, and S. Timurtas; "Material Model Studies for Rocks and Soils"; DASA 2678, August 1971; Shock Hydrodynamics, Inc. Sherman Oaks, California for Defense Nuclear Agency, Washington, D. C.

5. S. W. Butters and others; "The Mechanical Behavior of Nevada Test Site Grouts"; TR 74-40, December 1974; Terra Tek, Salt Lake City, Utah for Defense Nuclear Agency, Washington, D. C.

6. C. W. Smith and others; "In Situ Constitutive Relations of Soils and Rocks"; DNA 3678F, November 1974; Stanford Research Institute, Menlo Park, California for Director, Defense Nuclear Agency, Washington, D. C.

7. S. W. Butters and others; "Material Properties of Grouts and of Tuffs from Selected Drill Holes"; DNA 3383F, 10 July 1974; Terra Tek, Salt Lake City, Utah for Defense Nuclear Agency, Washington, D. C.

7.6 GROUND MOTION INSTRUMENTATION

1. H. M. Fernandez; "Shock Effects, Volume II", Instrumentation for Nuclear Weapon Effects Simulation Symposium; AFSWC-TR-70-5, Vol. II, 6 March 1970; Air Force Special Weapons Center, Kirtland Air Force Base, New Mexico.

2. D. A. Dicke; "Status of Earth Motion Measurements on AEC Underground Nuclear Tests", Shock Effects, Volume II, Instrumentation for Nuclear Weapon Effects Simulation Symposium; AFSWC-TR-70-5, Vol. II, 6 March 1970; EG&G, Albuquerque, New Mexico for Air Force Special Weapons Center, Kirtland Air Force Base, New Mexico.

3. D. J. Newell, Lt., USAF; "Development of an Advanced Velocity Transducer", Shock Effects, Volume II, Instrumentation for Nuclear Weapon Effects Simulation Symposium, AFSWC-TR-70-5, Vol. II, 6 March 1970; Air Force Special Weapons Center, Kirtland Air Force Base, New Mexico.

4. Dr. P. Lieberman and G. Nagumo; "Particle Velocity History Measurement and Cannister/Medium Interaction", Shock Effects, Volume II, Instrumentation for Nuclear Weapon Effects Simulation Symposium; AFSWC-TR-70-5, Vol. II, 6 March 1970; TRW Systems, Redondo Beach, California and IIT Research Institute, Chicago, Illinois for Air Force Special Weapons Center, Kirtland Air Force Base, New Mexico.

5. P. L. Coleman: "A Particle Velocity Gauge for Ground Motion Studies"; SSS-R-75-2597; Systems, Science and Software, La Jolla, California.

6. P. Coleman, W. Ginn, and D. Grine; "Ground Motion Gauge Development"; DNA 3702F, September 1975; Systems, Science and Software, La Jolla, California for Director, Defense Nuclear Agency, Washington, D. C.

7. S. F. Pickett; "Development and Evaluation of Measurement Systems for Blast-Induced Motions in Buried Structures"; AFWL-TR-73-230, April 1974; The University of New Mexico CERF for Air Force Weapons Laboratory, Kirtland Air Force Base, New Mexico.

8. R. S. Bunker and others; "Middle Gust Instrumentation Evaluation"; AFWL-TR-72-238, February 1973; Air Force Weapons Laboratory, Kirtland Air Force Base, New Mexico.

9. Dr. R. A. Shunk; "Ground Motion Instrumentation Specifications Below One Kilobar"; DNA 3431F, 4 February 1975; Science Applications, Inc., Albuquerque, New Mexico for Director, Defense Nuclear Agency, Washington, D. C.

REFERENCES

1. Dale T. Stjernholm; "KSC MOD K-1 TRIM Gage User's Manual; Kaman Sciences Corporation, Colorado Springs, Colorado.
2. John B. Dobbins, Jr., CDR, USN; "Predicted Ground Motion Parameters; Letter, FCTD-T1; Defense Nuclear Agency, Field Command, Kirtland Air Force Base, New Mexico.
3. Robert Bass; Unpublished data; Sandia Laboratories, Albuquerque, New Mexico.
4. Raymond J. Roark; "Formulas for Stress and Strain"; 4th Edition, 1965; McGraw-Hill Book Company, New York.
5. Dr. P. Liebermann and G. Naguamo; "Particle Velocity History Measurement and Canister/Medium Interaction"; TRW Systems, Redondo Beach, California and IIT Research Institute, Chicago, Illinois.
6. S. W. Butters and others; "The Mechanical Behavior of Nevada Test Site Grouts"; TR 7440, December 1974; Terra Tek, Salt Lake City, Utah.
7. S. W. Butters and others; "Material Properties of Grouts and of Tuffs from Selected Drill Holes", DNA 3383F, 10 July 1974; Defense Nuclear Agency, Washington, D. C.
8. R. S. Bunker and others; "Middle Gust Instrumentation Evaluation"; AFWL-TR-72-283, February 1973; Air Force Weapons Laboratory, Kirtland Air Force Base, New Mexico.
9. Coye T. Vincent; "Stemming and Containment Diagnostics", Latch Key Series, Shot Dorsal Fin, Project Officers Report Project 9.62; POR6282 (WT-6282), 29 September 1969; Stanford Research Institute, Menlo Park, California.

PRECEDING PAGE BLANK-NOT FILMED

10. F. M. Sauer and J. A. Kochly; "Ground Motion Measurements", Operation Diamond Dust, Project 3.1; POR-6437, May 1971; Physics International Company, San Leandro, California.

11. F. M. Sauer and J. A. Kochly; "Ground Motion Measurements", Operation Diamond Mine, Final Report; POR-6573 (PIFR-283), October 1972; Physics International Company, San Leandro, California.

APPENDIX A
ANALYSIS OF EDS WITH DAMPING

A.1 INTRODUCTION

This appendix contains analysis of the EDS with viscous damping. Two preliminary investigations are included and felt to be pertinent to this report although a damped version was never made. The first analysis, Section A.2 is by Dr. B. A. Hartenbaum, Research and Development Associates (RDA), and Dr. Rey A. Shunk, Electromechanical Systems, Inc., and has been extracted from a memo to Major B. Ellis, Field Command, DNA dated 9 June 1975. The second analysis performed by R. E. Keeffe, KSC, is contained in Section A.3.

A.2 ANALYSIS BY HARTENBAUM AND SHUNK

A.2.1 Purpose of Analysis. To determine the damping coefficient and the step (frequency) response of the gage (Section A.2.2); to present the technique for unfolding data from the gage output (Section A.2.3); and to present an illustrative example (Section A.2.4).

A.2.2 Mathematical Model. Consider a horizontal frictionless shuttle acted on by velocity proportional damping (Figure A.1). The shuttle is initially at rest at the far end of the tube (away from the shot point). A step velocity \dot{z} equals $V_0 H(t)$ is applied to the case. The motion of the shuttle is given by

$$m\ddot{x} + c(\dot{x} - \dot{z}) = 0$$

where m is the mass of the shuttle and c is the damping constant.

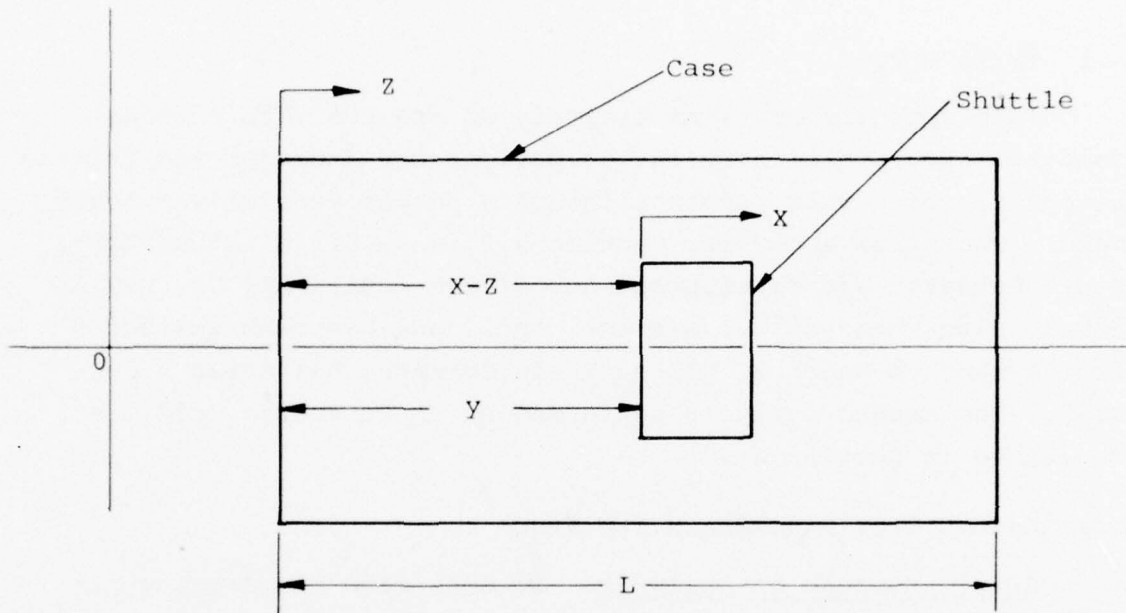


Figure A.1. EDS model for analysis.

Let

$$y = x - z$$

and

$$\alpha = c/m$$

Then

$$\ddot{y} + \alpha \dot{y} = -V_0 \delta(t)$$

The solution is

$$y = L - \frac{V_0}{\alpha} \left(1 - e^{-\alpha t} \right) : \text{displacement}$$

$$\dot{y} = -V_0 e^{-\alpha t} : \text{velocity}$$

To make damping worthwhile, the damping should allow the gage length to be decreased to at least 1/4 of the ground displacement; i.e., L equals $z_{\max}/4$. At the maximum displacement

$$y = 0$$

Thus

$$\alpha = \frac{V_0}{L} \left[1 - \exp \left(-\frac{4L\alpha}{V_0} \right) \right]$$

For a typical case:

material	wet tuff
yield	10 KT
range	260 feet (79 meters)
velocity	30 ft/s (9.1 m/sec)
displacement	4 feet (1.2 meters) ,

the damping coefficient, α , must have the value 29.40 sec^{-1} .

However, the velocity signal from the gage is

$$\dot{y} = -V_o \exp\left(-\frac{t}{0.034}\right)$$

where the time constant is 34 msec. The transform of the velocity is

$$\bar{\dot{y}} = -\frac{V_o}{p + \alpha}$$

so the lower 3 dB point is 4.7 Hz, which is rather high for underground testing.

The error in directly reading the displacement from the gage output is

$$\Delta z = \left(\frac{1}{1 - y'}\right) \Delta y'$$

where y' equals L minus y and $\Delta y'$ is the uncertainty in the gage output. For discrete coils wrapped at one inch (2.54 cm) intervals as proposed by KSC the error can be considerable (see Figure A.2).

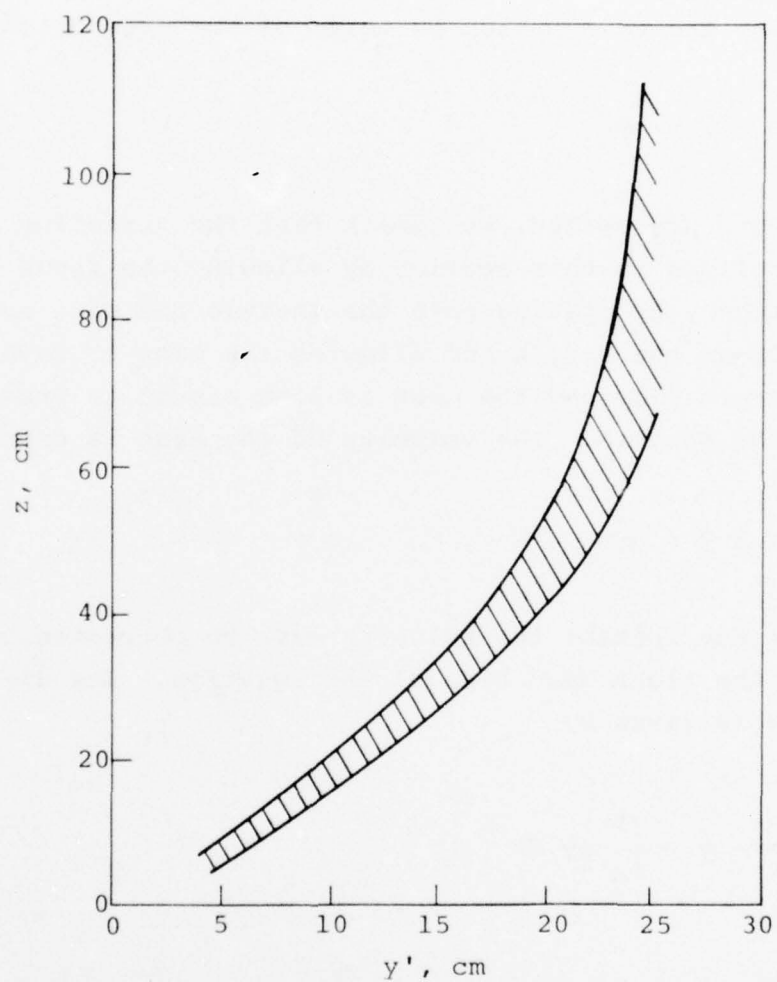


Figure A.2. Direct readout of ground displacement versus shuttle displacement for 2.54 cm coil spacing (uncertainty in shuttle position ± 1.27 cm).

A.2.3 Data Compensation. Because the damping has destroyed the direct read-out capabilities of the gage, the displacement and velocity must be inferred via manipulation of the measurand. The necessary operations can be determined from the equation describing the case motion in terms of the gage output,

$$\ddot{z} = -\ddot{y} - \alpha\dot{y}$$

Before proceeding, we remark that the preceding discussion is generalized in this section by allowing the input waveform to be arbitrary, by placing both the shuttle and case coordinates initially at the origin and allowing the case to have an arbitrary length provided the case is long enough to prevent bottoming of the shuttle. The velocity of the case is expressed as

$$\dot{z} = -\dot{y} - \alpha y$$

Thus, at any instant the velocity must be corrected by the second term on the right hand side of the equation. The displacement of the case is given by

$$z = -y - \int_0^t \alpha y \, dt$$

A correction term which is the integral of the gage output must be added to the gage output to infer the true displacement of the case. The accuracy with which the unfolding process can be done depends (within the assumptions of the analysis) on knowledge of the damping coefficient, the transit time of the shuttle through a coil, and the response of the coil circuitry. Other factors, not considered in the above analysis, may also affect

the unfolding process. These include friction, tilt in the gravitational field, and cross axis loading. A complete discussion of unfolding is beyond the scope of this note, but one of the authors has successfully used integral correction techniques to unfold data from underground and other explosive tests.

A.2.4 Example. As an illustration of the shuttle-gage output and the magnitude of the integral correction required to infer the displacement, consider the following example. The input velocity is a ramp for $0 \leq t \leq 0.01$ second and thereafter an exponential decay with an e-folding time of 0.2 second. The peak velocity is 9.1 m/sec. The gage damping coefficient is 40 sec^{-1} , which allows the gage length to be 20 percent of the true displacement of the case. The true displacement is plotted as a solid line in Figure A.3 while the quasi-digital output of the gage is denoted by o. The area under a curve fitted through the o's multiplied by α (40 in this example) is the correction term needed to obtain the displacement.

A.2.5 Conclusions. Various schemes can be devised to counter problems associated with a shuttle-type gage. We have explored but a few solutions to a small number of problems. An undamped gage gives an output that is directly proportional to velocity and displacement, but the gage is overly long and quite similar in operating principle to the Crescent gage which has often malfunctioned in underground tests. To decrease the length of the gage (and perhaps alleviate stiction) velocity proportional damping can be added to the shuttle action. However, this solution creates another problem; namely, correction terms that are often quite substantial must be added to the velocity and displacement signals. The gage is no longer direct reading for either velocity or displacement. In particular, the displacement measurement requires that the gage output be integrated to obtain the displacement.

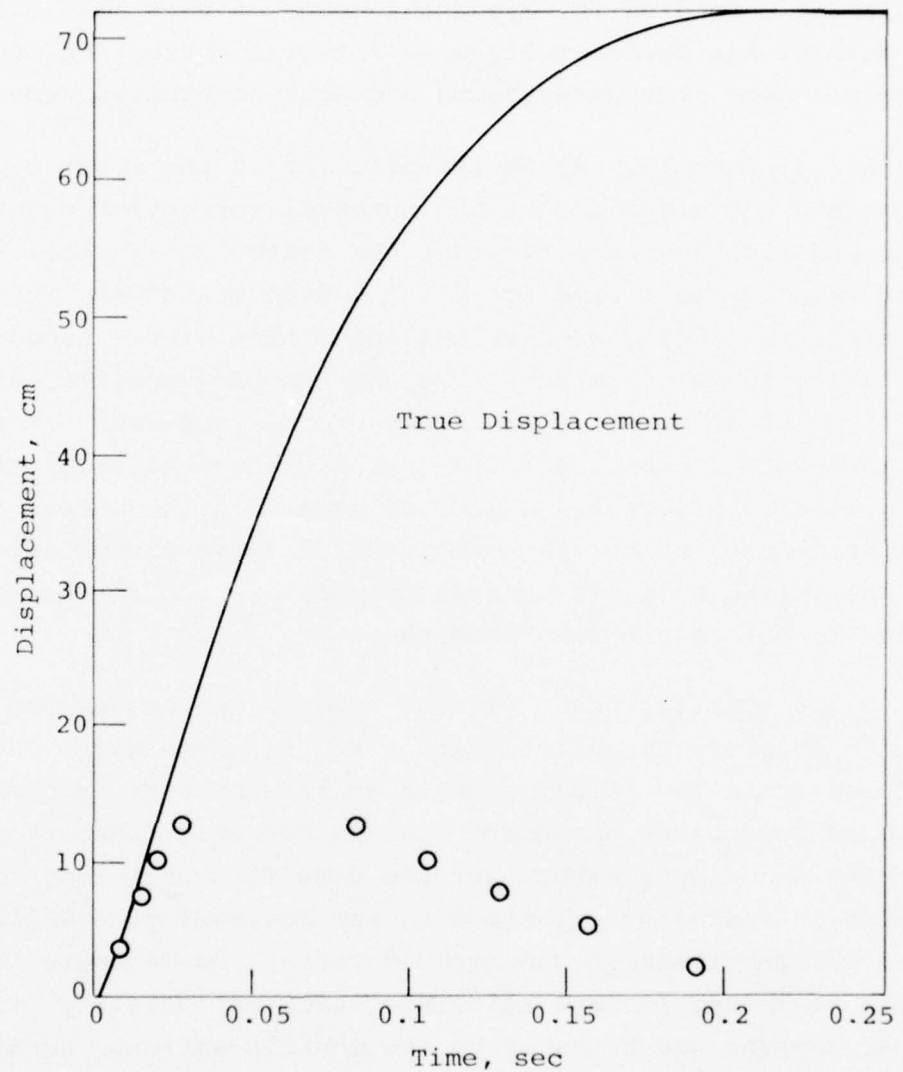


Figure A.3. Comparison of true displacement with shuttle output. Ramp velocity input for $0 \leq t \leq 0.01$ second. Exponential decay with e-folding time of 0.2 second for $t > 0.01$ second. Peak velocity: 9.1 m/sec. Shuttle damping coefficient: 40 sec^{-1} . o denotes gage output.

Direct reading velocity gages are currently in use. Of what advantage is a damped shuttle gage which requires a correction to be made to the output to obtain velocity and an integration to be made to obtain displacement?

A.3 ANALYSIS BY KEEFFE

The implementation of viscous damping in the EDS has been suggested as a method for decreasing gage length while maintaining the capability of measuring large displacements. Initial KSC thoughts on this concept are summarized below.

A.3.1 Analytic Predictions. The addition of a linear viscous damping term to the analytics used to predict EDS response to NTS environments is a straightforward task. The EDS equation of motion, after slug breakaway, without viscous damping is as follows:

$$\ddot{X} = \mu |g + \ddot{X}_1(t) \sin \alpha| \quad (\text{A.1})$$

where

X = slug displacement

X_1 = free field displacement

μ = coefficient of coulomb (sliding) friction

α = angle of direct induced wave front.

When the EDS tube is filled with a viscous fluid the equation of motion takes the following form.

$$\ddot{X} = -\frac{c}{m} \dot{X} + \mu |g + \ddot{X}_1(t) \sin \alpha| \quad (\text{A.2})$$

where:

c = viscous damping coefficient

m = mass of EDS slug.

Since these equations of motion are solved numerically the addition of the viscous damping does not present any real problem to solution methodology.

A.3.2 Evaluation of Viscous Damping Coefficient. For any given fluid the viscous damping coefficient can be determined by simple vertical free fall test as shown in Figure A.4. For this test configuration coulomb friction effects are essentially eliminated and the equation of motion for slug response becomes

$$\ddot{X} = g - \frac{c}{m} \dot{X} \quad (A.3)$$

(with zero initial conditions)

The solution for displacement and velocity is

$$X(t) = \frac{gm}{c} t - \frac{gm^2}{c^2} [1 - e^{-c/m t}]$$
$$\dot{X}(t) = \frac{gm}{c} [1 - e^{-c/m t}] \quad (A.4)$$

The velocity-time history is shown in Figure A.5.

Note that the velocity asymptotically approaches the constant value equals $(g m/c)$. Thus the EDS output which measures velocity can be directly used to evaluate the viscous damping coefficient, c , since m , and g are known.

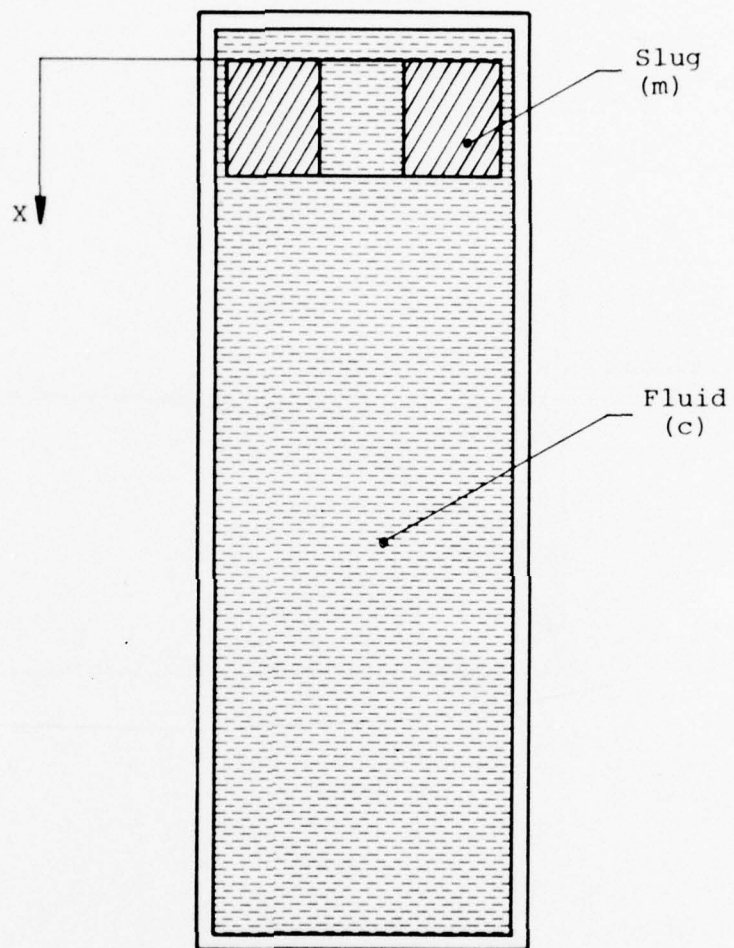


Figure A.4. Vertical free fall experiment.

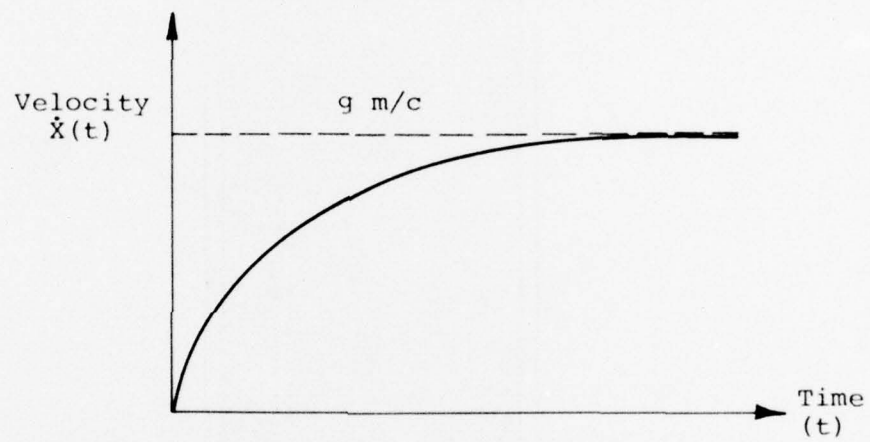


Figure A.5. EDS slug velocity-time history.

Note that Equations (A.3) and (A.4) can be used to find the free fall distance X_f and time t_f at which the velocity \dot{X} is within 0.1 percent of g m/c. For a value of c/m equals 29.4, the number derived by Hartenbaum and Shunk as a design requirement, the resultant values of X_f and t_f are:

$$X_f = 6.7 \text{ cm}$$

$$t_f = 0.235 \text{ second}$$

Therefore, the slug velocity will approach the desired asymptote well before reaching the end of the EDS tube.

A.3.3 Interpretation of Damped EDS Data. The output of the highly damped EDS gage to NTS or drop test environments will of course have to be subject to corrective data reduction methods to obtain actual free field motions. The technology to do this for linear systems is based upon established Fourier transform techniques which are commonly used for unfolding data.

Neglecting Coulomb damping effects, the transfer function of the viscously damped EDS slug is readily derivable as:

$$H(\omega) = - \frac{\omega}{\omega + i \frac{c}{m}} \quad (A.5)$$

where

$$\omega = \text{frequency (rad/sec)}$$

Given an EDS output from an actual environment, $X(t)$ with Fourier transform $X(\omega)$, the Fourier transform of the free field displacement is:

$$X_1(\omega) = \frac{X(\omega)}{H(\omega)} \quad (\text{A.6})$$

with $H(\omega)$ defined from Equation (A.5). The time history of free field displacement is then the inverse Fourier transform of the result obtained from Equation (A.6).

The real problem in this approach does not lie in the correction for viscous damping, but instead involves correcting for the non-linear coulomb damping resulting from sliding friction.

The absolute value term in Equation (A.2) leads to a non-linear effect on slug response. Since the Fourier transform manipulation of data strictly applies only to linear systems, the non-linear terms will result in non-correctable errors.

The secret of successful implementation of the EDS lies in minimization of the coulomb damping effect. If sliding friction is very small the resultant measurement error will also be small and the data correction technique described above will be adequate.

APPENDIX B

FREE-FIELD GROUND MOTION FOR EDS ANALYSIS

In order to facilitate response predictions for the KSC EDS, consistent definitions of free-field ground motion are required. Reference B.1 presents direct induced maximum acceleration, \ddot{X}_m , velocity, \dot{X}_m , and displacement, X_m , motions for a seven kiloton shot in saturated tuff along with temporal distributions for each type motion. However, at times later than the maximum displacement time, these temporal forms are not adequate. This appendix presents a consistent definition for the temporal distributions of direct induced free-field motion used for EDS response predictions.

The radial acceleration has the assumed form shown in Figure B.1. Up to time of maximum displacement, t_v , this pulse agrees reasonably well with that presented in Reference B.1. At later times the acceleration pulse has been modified to agree approximately with data presented in Reference B.2. Referring to Figure B.1, the acceleration pulse is analytically described as follows.

$$\ddot{X}_1 = 2\ddot{X}_m \frac{t}{t_g} ; \quad 0 \leq t \leq t_g/2$$

$$\ddot{X}_1 = 2\ddot{X}_m \left(1 - \frac{t}{t_g}\right) ; \quad \frac{t_g}{2} \leq t \leq t_g$$

$$\ddot{X}_1 = -\beta\ddot{X}_m ; \quad t_g < t \leq t_v$$

$$\ddot{X}_1 = \frac{\beta\ddot{X}_m}{(t_d - t_v)} [2t - (t_v + t_d)] ; \quad t_v \leq t \leq t_d$$

$$\ddot{X}_1 = 0 ; \quad t > t_d$$

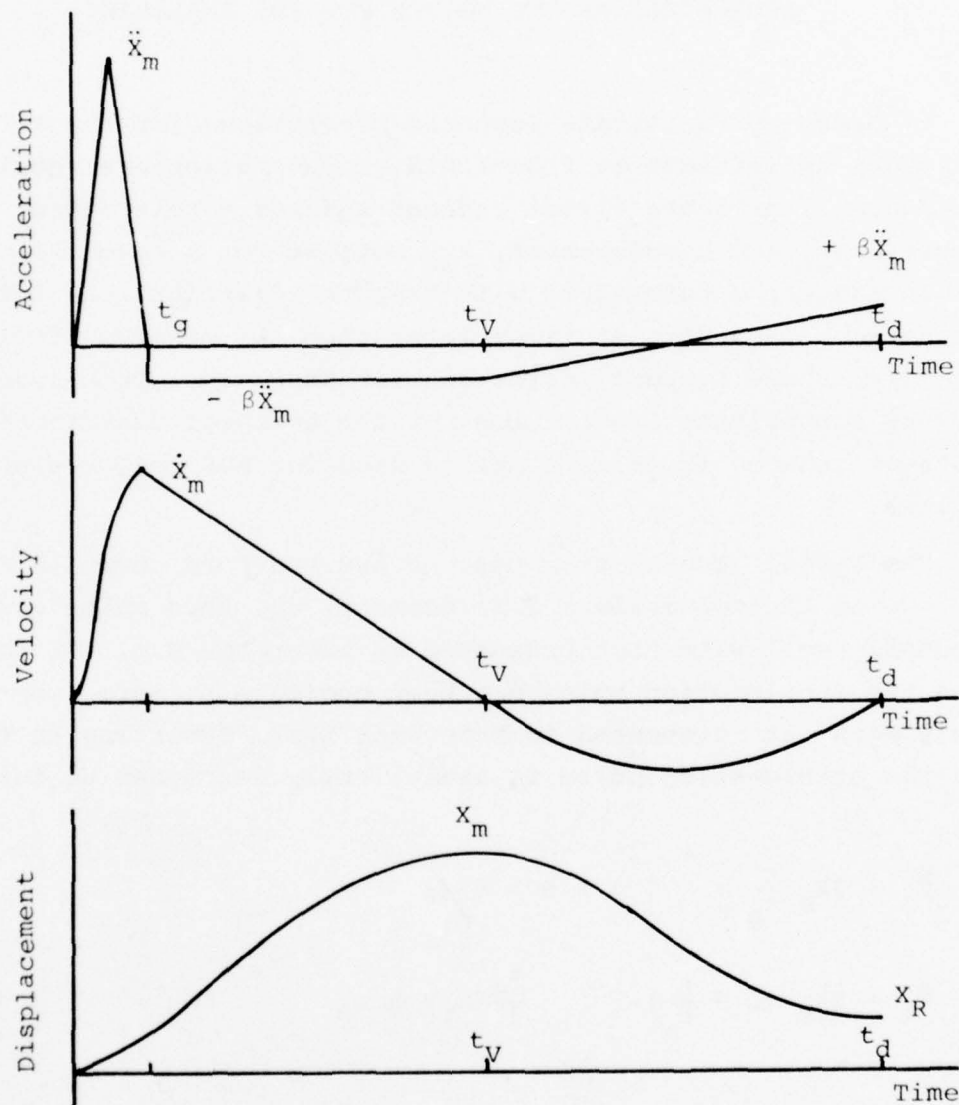


Figure B.1. Typical free-field motion.

Also shown in Figure B.1 are the radial velocity and displacement motions consistent with the assumed acceleration motion. Again, it may be noted that these waveforms are in substantial agreement with data presented in Reference B.2. The velocity may be analytically expressed as follows:

$$\dot{x}_1 = \frac{\ddot{x}_m t^2}{t_g} ; \quad 0 \leq t \leq t_g/2$$

$$\dot{x}_1 = \ddot{x}_m \left[2t - \frac{t^2}{t_g} - \frac{t_g}{2} \right] ; \quad \frac{t_g}{2} \leq t \leq t_g$$

$$\dot{x}_1 = \frac{\ddot{x}_m t_g}{2} - \beta \ddot{x}_m (t - t_g) ; \quad t_g \leq t \leq t_V$$

$$\dot{x}_1 = \frac{\beta \ddot{x}_m}{(t_d - t_V)} [t^2 - t(t_V + t_d) + t_V t_d] ; \quad t_V \leq t \leq t_d$$

$$\dot{x}_1 = 0 ; \quad t \geq t_d$$

With the displacements of the form:

$$x_1 = \frac{\ddot{x}_m t^3}{3t_g} ; \quad 0 \leq t \leq \frac{t_g}{2}$$

$$x_1 = \ddot{x}_m \left[t^2 - \frac{t^3}{3t_g} - \frac{t_g t}{2} + \frac{t_g^2}{12} \right] ; \quad \frac{t_g}{2} \leq t \leq t_g$$

$$x_1 = \ddot{x}_m \left[\frac{t_g^2}{4} + \frac{t_g}{2} (1 + 2\beta) (t - t_g) - \frac{\beta}{2} (t^2 - t_g^2) \right];$$

$$t_g \leq t \leq t_v$$

$$x_1 = x_m + \frac{\beta \ddot{x}_m}{(t_d - t_v)} \left[\frac{t^3}{3} - \frac{t^2}{2} (t_v + t_d) + t_v t_d t + \frac{t_v^2}{2} \left(\frac{t_v}{3} - t_d \right) \right]; \quad t_v \leq t \leq t_d$$

$$x_1 = x_R; \quad t \geq t_d$$

where:

maximum displacement = x_m at $t = t_v$

$$x_m = \frac{\ddot{x}_m}{2} \left[\frac{t_g^2}{2} + t_g (1 + 2\beta) (t_v - t_g) - \beta (t_v^2 - t_g^2) \right]$$

residual displacement = x_R at $t = t_d$

$$x_R = x_m - \frac{\beta \ddot{x}_m}{6} (t_d - t_v)^2$$

Similarly the maximum positive velocity = \dot{X}_m at $t = t_g$

$$\dot{X}_m = \frac{\ddot{X}_m t_g}{2}$$

and the maximum negative velocity = $\dot{\bar{X}}_m$ at $t = \frac{t_v + t_d}{2}$

$$\dot{\bar{X}}_m = - \frac{\beta \ddot{X}_m}{4} (t_d - t_v)$$

Given values for \ddot{X}_m , \dot{X}_m , and X_m (Reference B.1), a number of the early time parameters describing the waveforms are uniquely defined.

$$t_g = \frac{2\dot{X}_m}{\ddot{X}_m}$$

$$t_v = \frac{2X_m}{\dot{X}_m}$$

$$\beta = \frac{0.5}{\frac{X_m \ddot{X}_m}{\dot{X}_m^2} - 1}$$

By substitution of above it is seen that

$$\beta = \frac{t_g}{2(t_V - t_g)}$$

It should be noted that values obtained using these relationships compare very well with corresponding early-time data presented in Reference B.1.

Since residual displacement, X_R , data is not given it is not possible to uniquely define the final constant time t_d . However, based upon bounding values for X_R , a parametric representation of t_d and X_R may be obtained. The ratio of residual to maximum displacement is found to be:

$$\frac{X_R}{X_m} = 1 - \frac{(t_d/t_V - 1)^2}{3 \left(1 - \frac{\dot{X}_m^2}{X_m \ddot{X}_m} \right)}$$

For the waveforms shown the ratio of residual to maximum displacement falls within the bounds:

$$0 \leq \frac{X_R}{X_m} \leq 1$$

noting that when

$$x_R = x_m$$

$$t_d = t_V$$

and when

$$x_R = 0$$

$$t_d = (t_d)_{\max}$$

where:

$$(t_d)_{\max} = t_V \left\{ 1 + \left[3 \left(1 - \frac{\dot{x}_m^2}{\ddot{x}_m x_m} \right) \right]^{1/2} \right\}$$

In the extreme case

$$\frac{(t_d)_{\max}}{t_V} = 1 + \sqrt{3} = 2.732$$

A parametric plot $\frac{x_R}{x_m}$ as a function of $\left(\frac{t_d}{t_V}\right)$ for various values of $\frac{\dot{x}_m^2}{\ddot{x}_m x_m}$ is presented in Figure B.2. Given the free-field parameters \ddot{x}_m , \dot{x}_m , x_m , and either x_R or t_d the remaining unknown may be determined.

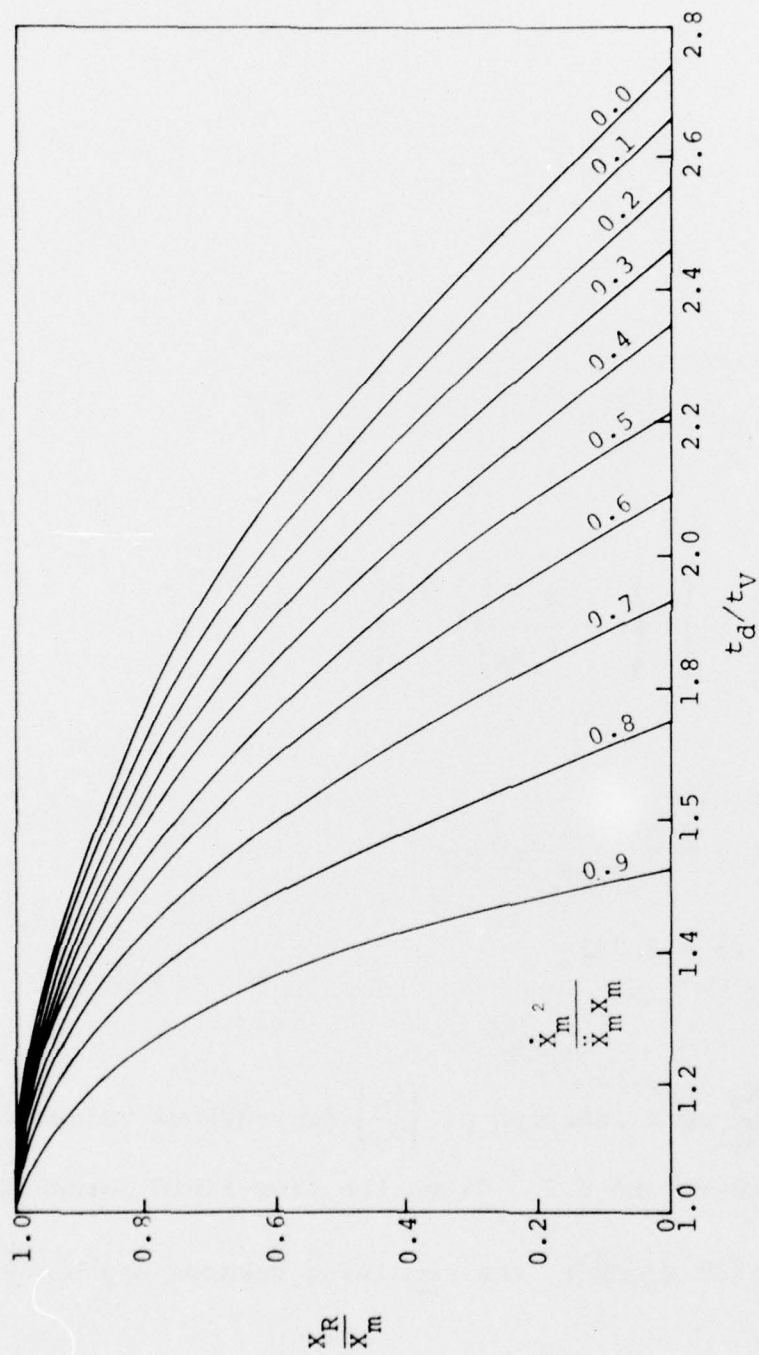


Figure B.2. Parametric plot for determining X_R or t_d .

APPENDIX C

NUMERICAL ANALYSIS OF DROP TEST RESULTS

C.1 CONFIGURATION OF EDS DROP TEST

Definitions for the parameters used in this analysis are shown in Figure C.1 and are given as follows:

\ddot{Y}_C = transverse acceleration of canister (measured)

\ddot{X}_C = axial acceleration of canister (measured)

x = EDS slug displacement

m = mass of EDS slug

α = test angle

R = clip restraining force

f = coulomb friction force

C.2 CANISTER MOTIONS

Given $\ddot{X}_C(t)$ and $\ddot{Y}_C(t)$ from accelerometer records, numerically integrate to obtain $\dot{X}_C(t)$, $\dot{Y}_C(t)$ and $\dot{X}_C(f)$, $\dot{Y}_C(f)$ over time range of interest; starting at time of impact (t equals zero). Note that initial conditions are as follows:

$$X_C(0) = 0,$$

$$Y_C(0) = 0$$

$$\dot{X}_C(0) = \dot{X}_V \cos \alpha,$$

$$\dot{Y}_C(0) = \dot{X}_V \sin \alpha$$

where:

$$\dot{X}_V = \text{table impact velocity}$$

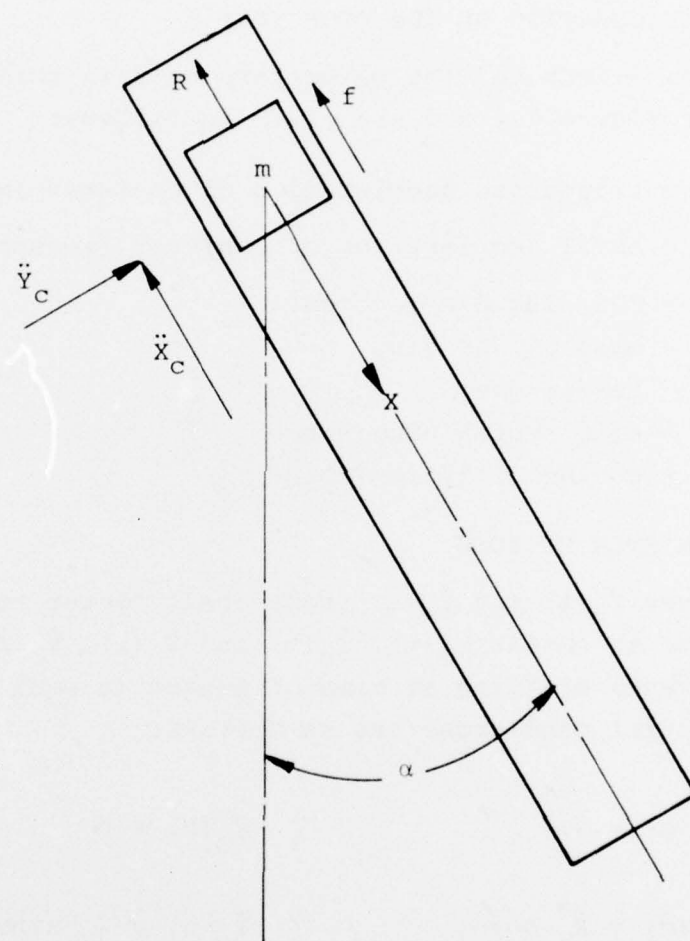


Figure C.1. EDS drop test configuration.

Store:

$x_c(t)$ and $\dot{x}_c(t)$ for later use.

C.3 EDS EQUATIONS OF MOTION

C.3.1 Slug Free-Body. A free body drawing of the EDS slug is shown in Figure C.2. Definitions for the parameters identified in the figure follow:

$$R = mg\zeta$$

where

$$\zeta = \text{constant}$$

$$f = \mu N$$

$$\mu = \text{coefficient of friction}$$

$$N = |mg \sin \alpha + \ddot{y}_c(t)m|$$

$$f = \mu m |g \sin \alpha + \ddot{y}_c(t)|$$

C.3.2 Equations of Motion.

$$m\ddot{x} = mg \cos \alpha - R - F$$

$$m\ddot{x} = mg \cos \alpha - mg\zeta - \mu m |g \sin \alpha + \ddot{y}_c(t)|$$

$$\ddot{x} = g(\cos \alpha - \zeta) - \mu |g \sin \alpha + \ddot{y}_c(t)| \quad (C.1)$$

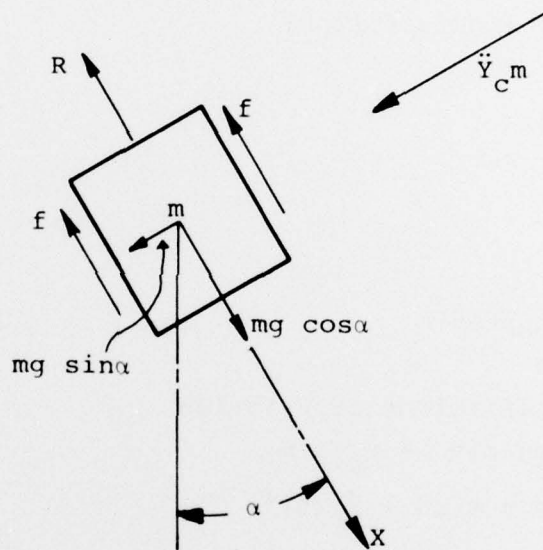


Figure C.2. Slug free-body diagram.

Equation C.1 is used to determine when the slug breaks away from the canister, i.e.,

$$\dot{x} > \dot{x}_c$$

C.3.3 Slug Breakaway. Breakaway occurs when:

$$\ddot{x}_c \geq -\dot{x}$$

or

$$\ddot{x}_c(t) \geq \mu |g \sin \alpha + \ddot{y}_c(t)| - g(\cos \alpha - \zeta)$$

Let

$$t = t_b = \text{breakaway time}$$

then

$$\ddot{x}_c(t_b) = \mu |g \sin \alpha + \ddot{y}_c(t_b)| - g(\cos \alpha - \zeta) \quad (C.2)$$

Given $\ddot{x}_c(t)$ and $\ddot{y}_c(t)$, with ζ , μ , and α constant, the breakaway time t_b can be determined using Equation C.2.

At t equals t_b look up $\dot{y}_c(t_b)$, and $y_c(t_b)$ from Section C.2 calculations and save.

C.4 SLUG RESPONSE

Starting at breakaway time t_b with initial conditions $\dot{Y}_c(t_b)$ and $Y_c(t_b)$ numerically solve the following equation of motion for the slug:

i.e.,

$$t \geq t_b$$

$$\ddot{X}(t) = g \cos \alpha - \mu |g \sin \alpha + \ddot{Y}_c(t)| \quad (C.3)$$

for

$$\dot{X}(t), \text{ and } x(t) .$$

At each time step compare $\dot{X}(t)$ to $\dot{X}_c(t)$.

As long as $\ddot{X}(t)$ is greater than $\ddot{X}_c(t)$, Equation C.3 holds as given. However, at late times the canister velocity may equal and become greater than the slug velocity. When this occurs, continue on the numerical integration with the following revised equation of motion:

$$\ddot{X}(t) = g \cos \alpha + \mu |g \sin \alpha + \ddot{Y}_c(t)|$$

with initial conditions on $\dot{X}(t)$, $x(t)$, $\dot{Y}_c(t)$, $Y_c(t)$ determined at the time the inequality takes place.

Again, compare $\dot{X}(t)$ to $\dot{X}_c(t)$ at each time step.

If at some later time $\dot{X}(t)$ exceeds $\dot{X}_c(t)$ the equation of motion reverts to the form given in Equation C.3 with correct initial conditions at this time.

Continue calculations using this procedure until slug response is completely determined.

C.5 DATA PRESENTATION

Print and punch cards for the following parameters:

- $X_c(t)$, canister displacement
- $X(t)$, slug displacement
- $X(t) - X_c(t)$, EDS displacement output
- $\dot{X}_c(t)$, canister velocity
- $\dot{X}(t)$, slug velocity
- $\dot{X}(t) - \dot{X}_c(t)$, EDS velocity output
- $X(t)/X_c(t)$, gage error.

These data will be used for possible further analysis and final reporting.

DISTRIBUTION LIST

DEPARTMENT OF DEFENSE

Assistant Secretary of Defense
Cmd., Cont., Comm. & Intell.
Department of Defense
ATTN: ODASD IA

Assistant to the Secretary of Defense
Atomic Energy
Department of Defense
ATTN: Honorable Donald R. Cotter
ATTN: Colonel R. N. Brodie

Director
Defense Advanced Rsch. Proj. Agency
ATTN: Technical Library
ATTN: NMRO
ATTN: PMO
ATTN: STO

Director
Defense Civil Preparedness Agency
Assistant Director for Research
ATTN: Staff Dir. Resr., George N. Sisson
ATTN: Admin. Officer

Director
Defense Communications Agency
ATTN: CCTC/C672, Franklin D. Moore
ATTN: Code 930

Defense Documentation Center
Cameron Station
12 cy ATTN: TC

Director
Defense Intelligence Agency
ATTN: Technical Library
ATTN: DB-4C3
ATTN: DT-2, Wpns. & Sys. Div.
ATTN: DB-4C2, Timothy Ross
ATTN: DB-4C1, Paul Castleberry
ATTN: DT-1C

Director
Defense Nuclear Agency
2 cy ATTN: SPAS
ATTN: TISI, Archives
ATTN: DDST
2 cy ATTN: SPSS
3 cy ATTN: TITL, Tech. Library

Dir. of Defense Rsch. & Engineering
Department of Defense
ATTN: S&SS (OS)

Commander
Field Command
Defense Nuclear Agency
ATTN: FCTMOF
ATTN: FCPR

Director
Interservice Nuclear Weapons School
ATTN: Document Control

DEPARTMENT OF DEFENSE (Continued)

Director
Joint Strat. Target Planning Staff, JCS
ATTN: JLTW-2
ATTN: XPFS
ATTN: STINFO, Library
ATTN: DOXT

Chief
Livermore Division, Field Command, DNA
Lawrence Livermore Laboratory
ATTN: FCPRL

Chief
Test Construction Division
Field Command Test Directorate
Defense Nuclear Agency
ATTN: FCTC

DEPARTMENT OF THE ARMY

Director
BMD Advanced Tech. Center
Huntsville Office
ATTN: CRDABH-X
ATTN: CRDABH-S

Program Manager
BMD Program Office
ATTN: CRDABM-NE

Commander
BMD System Command
ATTN: BDMSC-TEN, Noah J. Hurst

Director
Construction Engineering Rsch. Lab.
ATTN: CERL-SL

Dep. Chief of Staff for Rsch. Dev. & Acq.
Department of the Army
ATTN: Technical Library
ATTN: DAMA(CS), Major A. Gleim
ATTN: DAMA-CSM-N, LTC G. Ogden

Chief of Engineers
Department of the Army
ATTN: DAEN-MCE-D
ATTN: DAEN-RDM

Deputy Chief of Staff for Ops. & Plans
Department of the Army
ATTN: Technical Library
ATTN: Dir. of Chem. & Nuc. Ops.

Chief
Engineer Strategic Studies Group
ATTN: DAEN-FES, LTC Hatch

Commander
Harry Diamond Laboratories
ATTN: DRXDO-TI, Tech. Lib.
ATTN: DRXDO-NP

PRECEDING PAGE BLANK-NOT FILMED

DEPARTMENT OF THE ARMY (Continued)

Commander
Picatinny Arsenal
ATTN: B. Shulman, DR-DAR-L-C-FA
ATTN: Technical Library

Commander
Redstone Scientific Information Center
US Army Missile Command
ATTN: Chief, Documents

Commander
US Army Armament Command
ATTN: Tech. Lib.

Director
US Army Ballistic Research Labs.
ATTN: Charles Kingery
ATTN: W. Taylor
ATTN: DRXBR-X, Julius J. Meszaros
ATTN: DRDAR-BLE, J. H. Keefer
ATTN: A. Ricchiazzi
2 cy ATTN: Tech. Lib., Edward Baicy

Commander
US Army Comb. Arms Combat Dev. Acty.
ATTN: LTC G. Steger
ATTN: LTC Pullen

Commander
US Army Communications Command
ATTN: Technical Library

Commander
US Army Electronics Command
ATTN: DRSEL-TL-IR, Edwin T. Hunter

Commander
US Army Engineer Center
ATTN: ATSEN-SY-L

Division Engineer
US Army Engineer Div. Huntsville
ATTN: HNDED-SR

Division Engineer
US Army Engineer Div. Ohio River
ATTN: Technical Library

Commandant
US Army Engineer School
ATTN: ATSE-CTD-CS
ATTN: ATSE-TEA-AD

Director
US Army Engr. Waterways Exper. Sta.
ATTN: John N. Strange
ATTN: Guy Jackson
ATTN: Leo Ingram
ATTN: James Ballard
ATTN: Technical Library
ATTN: William Flathau

Commander
US Army Foreign Science & Tech. Center
ATTN: Research & Concepts Branch

DEPARTMENT OF THE ARMY (Continued)

Commander
US Army Mat. & Mechanics Rsch. Center
ATTN: Technical Library
ATTN: John Mescall
ATTN: Richard Shea

Commander
US Army Materiel Dev. & Readiness Command
ATTN: Technical Library
ATTN: DRCDE-D, Lawrence Flynn

Commander
US Army Missile Command
ATTN: DRSMI-XS, Chief Scientist
ATTN: J. Hogan

Commander
US Army Mobility Equip. R & D Center
ATTN: Al Tolbert
ATTN: Technical Library

Commander
US Army Nuclear Agency
ATTN: ATCA-NAW
ATTN: Tech. Lib.

Commander
US Army Training & Doctrine Command
ATTN: LTC J. Foss
ATTN: LTC Auveduti, COL Enger

Commandant
US Army War College
ATTN: Library

US Army Mat. Command Proj. Mngr. for Nuc. Munitions
ATTN: DRCPM-NUC

DEPARTMENT OF THE NAVY

Chief of Naval Material
Navy Department
ATTN: MAT 0323

Chief of Naval Operations
Navy Department
ATTN: OP 982, LCDR Smith
ATTN: Code 604C3, Robert Placesi
ATTN: OP 981
ATTN: OP 03EG
ATTN: OP 982, LTC Dubac
ATTN: OP 982, CAPT Toole

Chief of Naval Research
Navy Department
ATTN: John Haycock
ATTN: Code 464, Thomas P. Quinn
ATTN: Code 464, Jacob L. Warner
ATTN: Nicholas Perrone
ATTN: Technical Library

Officer-in-Charge
Civil Engineering Laboratory
Naval Construction Battalion Center
ATTN: Stan Takahashi
ATTN: R. J. Odello
ATTN: Technical Library

Commandant of the Marine Corps
Navy Department
ATTN: POM

DEPARTMENT OF THE NAVY (Continued)

Commander
David W. Taylor Naval Ship R & D Center
ATTN: Code L42-3, Library

Commanding General
Development Center
Fire Support Branch
MCDEC
ATTN: CAPT Hartneady
ATTN: LTC Gapenski

Commander
Naval Air Systems Command
Headquarters
ATTN: F. Marquardt

Commander
Naval Electronic Systems Command
Naval Electronic Systems Command Hqs.
ATTN: PME 117-21A

Commanding Officer
Naval Explosive Ord. Disposal Fac.
ATTN: Code 504, Jim Petrousky

Commander
Naval Facilities Engineering Command
Headquarters
ATTN: Technical Library
ATTN: Code 03A
ATTN: Code 04B

Commander
Naval Ocean Systems Center
ATTN: Technical Library

Superintendent (Code 1424)
Naval Postgraduate School
ATTN: Code 2124, Tech. Rpts. Librarian

Director
Naval Research Laboratory
ATTN: Code 2600, Tech. Lib.
ATTN: Code 8440, F. Rosenthal

Commander
Naval Sea Systems Command
Navy Department
ATTN: Code 03511
ATTN: ORD-01313, Lib.
ATTN: ORD-033
ATTN: SEA-9931G

Commander
Naval Ship Engineering Center
Department of the Navy
ATTN: NSEC 6105G
ATTN: Technical Library

Commander
Naval Ship Resch. & Development Center
Underwater Explosive Research Division
ATTN: Technical Library

Officer-in-Charge
Naval Surface Weapons Center
ATTN: Code WA501, Navy Nuc. Prgms. Off.
ATTN: G. L. Matteson
ATTN: Code 240, C. J. Aronson
ATTN: M. Kleinerman

DEPARTMENT OF THE NAVY (Continued)

Commander
Naval Surface Weapons Center
Dahlgren Laboratory
ATTN: Technical Library

President
Naval War College
ATTN: Technical Library

Commander
Naval Weapons Center
ATTN: Code 533, Tech. Lib.

Commanding Officer
Naval Weapons Evaluation Facility
ATTN: R. Hughes
ATTN: Technical Library

Director
Strategic Systems Project Office
Navy Department
ATTN: NSP-273
ATTN: NSP-43, Tech. Lib.
ATTN: NSP-272

DEPARTMENT OF THE AIR FORCE

Commander
ADCOM/XPD
ATTN: XP
ATTN: XPQDQ

AF Geophysics Laboratory, AFSC
ATTN: LW, Ker C. Thompson
ATTN: SUOL, Rsch. Lib.

AF Institute of Technology, AU
ATTN: Library AFIT Bldg. 640, Area B

AF Weapons Laboratory, AFSC
ATTN: DES-C, Robert Henny
ATTN: DEP, Jimmie L. Bratton
ATTN: DES-S, M. A. Plamondon
ATTN: DED
ATTN: DES-G, Mr. Melzer
ATTN: SUL

Headquarters
Air Force Systems Command
ATTN: Technical Library
ATTN: DLCAW
ATTN: R. Cross

Commander
ASD
ATTN: Technical Library

Assistant Secretary of the Air Force
Research & Development
Headquarters, US Air Force
ATTN: Col R. E. Steere

Deputy Chief of Staff
Research & Development
Headquarters, US Air Force
ATTN: Col J. L. Gilbert

DEPARTMENT OF THE AIR FORCE (Continued)

Commander
Foreign Technology Division, AFSC
ATTN: NICD, Library
ATTN: ETD
ATTN: PDBG
ATTN: PDBF, Mr. Spring

Hq. USAF/IN
ATTN: IN

Hq. USAF/PR
ATTN: PRE

Hq. USAF/RD
ATTN: RDPS, Lt Col A. Chiota
ATTN: RDQSM
ATTN: RDQRM, Col S. C. Green
ATTN: RDP
ATTN: RDQPN, Maj F. Vajda

Commander
Rome Air Development Center, AFSC
ATTN: EMREC, R. W. Mair
ATTN: EMTLD, Doc. Library

SAMSO/DE
ATTN: DEB

SAMSO/DY
ATTN: DYS

SAMSO/MN
ATTN: MNNH
ATTN: MMH

SAMSO/RS
ATTN: RSS/Col Donald Dowler

SAMSO/XR
ATTN: XRTB

Commander in Chief
Strategic Air Command
ATTN: NRI-STINFO, Library
ATTN: XPFS

ENERGY RESEARCH & DEVELOPMENT ADMINISTRATION

Division of Military Application
US Energy Rsch. & Dev. Admin.
ATTN: Doc. Con. for Test Office

University of California
Lawrence Livermore Laboratory
ATTN: Larry W. Woodruff, L-96
ATTN: J. R. Hearst, L-205
ATTN: M. Fernandez
ATTN: Ted Butkovich, L-200
ATTN: Jerry Goudreau
ATTN: D. M. Norris, L-90
ATTN: Richard G. Dong, L-90
ATTN: Robert Schock, L-437
ATTN: Tech. Info. Dept. L-3
ATTN: Jack Kahn, L-7

Los Alamos Scientific Laboratory
ATTN: Doc. Con. for Reports Lib.
ATTN: Doc. Con. for G. R. Spillman
ATTN: Doc. Con. for Al Davis

ENERGY RESEARCH & DEVELOPMENT ADMINISTRATION
(Continued)

Sandia Laboratories
Livermore Laboratory
ATTN: Doc. Con. for Tech. Library

Sandia Laboratories
ATTN: Doc. Con. for W. Roherty
ATTN: Doc. Con. for 3141, Sandia Rpt. Coll.
ATTN: Doc. Con. for A. J. Chaban
ATTN: L. Hill
ATTN: Doc. Con. for M. L. Merritt
ATTN: Doc. Con. for Luke J. Vortman

US Energy Rsch. & Dev. Admin.
Albuquerque Operations Office
ATTN: Doc. Con. for Tech. Library

US Energy Rsch. & Dev. Admin.
Division of Headquarters Services
Library Branch G-043
ATTN: Doc. Con. for Class Tech. Lib.

US Energy Rsch. & Dev. Admin.
Nevada Operations Office
ATTN: Doc. Con. for Tech. Lib.

Union Carbide Corporation
Hollifield National Laboratory
ATTN: Civil Def. Res. Proj.
ATTN: Doc. Con. for Tech. Lib.

OTHER GOVERNMENT AGENCIES

Central Intelligence Agency
ATTN: RD/SI Rm. 5G48, Hq. Bldg. for NED/OSI-
5G48 Hqs.

Department of the Interior
Bureau of Mines
ATTN: Tech. Lib.

Department of the Interior
US Geological Survey
ATTN: Cecil B. Raleigh
ATTN: J. H. Healy

NASA
Ames Research Center
ATTN: Robert W. Jackson

Office of Nuclear Reactor Regulation
Nuclear Regulatory Commission
ATTN: Robert Heineman
ATTN: Lawrence Shao

DEPARTMENT OF DEFENSE CONTRACTORS

Aerospace Corporation
2 cy ATTN: Tech. Info. Services
ATTN: Prem N. Mathur
ATTN: Larry Selzer

Agbabian Associates
ATTN: M. Agbabian
ATTN: Carl Bagge

Analytic Services, Inc.
ATTN: George Hesselbacher

DEPARTMENT OF DEFENSE CONTRACTORS (Continued)

Applied Theory, Inc.
2 cy ATTN: John G. Trulio

Artec Associates, Inc.
ATTN: Steven Gill

Avco Research & Systems Group
ATTN: William Broding
ATTN: Research Lib., A830, Rm. 7201

Battelle Memorial Institute
ATTN: Technical Library
ATTN: R. W. Klingsmith

The BDM Corporation
ATTN: A. Lavagnino
ATTN: Technical Library

The BDM Corporation
ATTN: Richard Hensley

Bell Telephone Laboratories
ATTN: J. P. White

The Boeing Company
ATTN: R. H. Carlson
ATTN: Aerospace Library
ATTN: Robery Dyrdaahl

Brown Engineering Company, Inc.
ATTN: Manu Patel

California Institute of Technology
ATTN: Thomas J. Ahrens

California Research & Technology, Inc.
ATTN: Sheldon Shuster
ATTN: Ken Kreyenhagen
ATTN: Technical Library

Calspan Corporation
ATTN: Technical Library

Center for Planning & Rsch., Inc.
ATTN: R. W. Shnider

Civil/Nuclear Systems Corp.
ATTN: Robert Crawford

University of Dayton
Industrial Security Super KL-505
ATTN: Hallock F. Swift

University of Denver
Colorado Seminary
Denver Research Institute
ATTN: Sec. Officer for J. Wisotski

EG&G, Inc.
Albuquerque Division
ATTN: Technical Library

Electric Power Research Institute
ATTN: George Sliter

Electromechanical Sys. of New Mexico, Inc.
ATTN: R. A. Shunk

DEPARTMENT OF DEFENSE CONTRACTORS (Continued)

Engineering Decision Analysis Company, Inc.
ATTN: Robert Kennedy

The Franklin Institute
ATTN: Zenons Zudans

Gard, Incorporated
ATTN: G. L. Neidhardt

General Dynamics Corp.
Pomona Division
ATTN: Keith Anderson

General Dynamics Corp.
Electric Boat Division
ATTN: Michael Pakstys

General Electric Company
Space Division
Valley Forge Space Center
ATTN: M. H. Bortner, Space Sci. Lab.

General Electric Company
Re-Entry & Environmental Systems Div.
ATTN: Arthur L. Ross

General Electric Company
TEMPO-Center for Advanced Studies
ATTN: DASIAC

General Research Corporation
ATTN: Benjamin Alexander

Geocenters Incorporated
ATTN: Edward Marram

H-Tech. Laboratories, Inc.
ATTN: B. Hartenbaum

Honeywell Incorporated
Defense Systems Division
ATTN: T. N. Helvig

III Research Institute
ATTN: R. E. Welch
ATTN: Technical Library

University of Illinois at Chicago
College of Engineering
Dept. of Materials Engineering
ATTN: Ted Belytschko

Institute for Defense Analyses
ATTN: IDA Librarian, Ruth S. Smith

J. H. Wiggins, Company, Inc.
ATTN: Jon Collins

Kaman AvIDyne
Division of Kaman Sciences Corp.
ATTN: Norman P. Hobbs
ATTN: E. S. Criscione
ATTN: Technical Library

Kaman Sciences Corporation
ATTN: Paul A. Ellis
ATTN: Frank H. Shelton
ATTN: Library
ATTN: Herb Hollister
ATTN: Eldine L. Cole
ATTN: Michael A. Lew

DEPARTMENT OF DEFENSE CONTRACTORS (Continued)

Karagozian & Case
ATTN: John Karagozian

Lockheed Missiles & Space Company, Inc.
ATTN: Technical Library

Lockheed Missiles & Space Company, Inc.
ATTN: Tom Geers, D/52-33, Bldg. 205

Lovelace Foundation for Medical Education & Rsch.
ATTN: Technical Library
ATTN: Asst. Dir. of Res., Robert K. Jones

Martin Marietta Aerospace
Orlando Division
ATTN: G. Fotieo

McDonnell Douglas Corporation
ATTN: Robert W. Halprin

McMillian Science Associates, Inc.
ATTN: Robert Oliver

Merritt Cases, Incorporated
ATTN: J. L. Merritt
ATTN: Technical Library

Meteorology Research, Inc.
ATTN: William D. Green

The Mitre Corporation
ATTN: Library

University of New Mexico
Dept. of Campus Security & Police
ATTN: G. E. Triandafalidis

Nathan M. Newmark
Consulting Engineering Services
B106A Civil Engineering Building
University of Illinois
ATTN: Nathan M. Newmark

Pacifica Technology
ATTN: G. Kent
ATTN: R. Bjork

Physics International Company
ATTN: Doc. Con. for E. T. Moore
ATTN: Doc. Con. for Charles Godfrey
ATTN: Doc. Con. for Dennis Orphal
ATTN: Doc. Con. for Fred M. Sauer
ATTN: Doc. Con. for Larry A. Behrmann
ATTN: Doc. Con. for Coye Vincent
ATTN: Doc. Con. for Robert Swift
ATTN: Doc. Con. for Tech. Lib.

Prototype Development Associates, Inc.
ATTN: T. K. McKinley

The Rand Corporation
ATTN: Armas Laupa
ATTN: C. C. Mow
ATTN: Technical Library

Science Applications, Inc.
ATTN: David Bernstein
ATTN: D. E. Maxwell

DEPARTMENT OF DEFENSE CONTRACTORS (Continued)

R & D Associates
ATTN: Paul Rausch
ATTN: Arlen Fields
ATTN: Robert Port
ATTN: Technical Library
ATTN: J. G. Lewis
ATTN: Jerry Carpenter
ATTN: Henry Cooper
ATTN: William B. Wright, Jr.
ATTN: Cyrus P. Knowles
ATTN: Albert L. Latter
ATTN: Harold L. Brode

Science Applications, Inc.
ATTN: Technical Library

Science Applications, Inc.
ATTN: James Cramer

Science Applications, Inc.
ATTN: Steve Oston

Science Applications, Incorporated
ATTN: Burt Chambers
ATTN: William M. Layson

Southwest Research Institute
ATTN: A. B. Wenzel
ATTN: Wilfred E. Baker

Stanford Research Institute
ATTN: George R. Abrahamson

Systems, Science & Software, Inc.
ATTN: Technical Library
ATTN: Donald R. Grine
ATTN: Thomas D. Riney
ATTN: Ted Cherry
ATTN: Robert Sedgewick

Terra Tek, Inc.
ATTN: Technical Library
ATTN: A. H. Jones
ATTN: Sidney Green

Tetra Tech., Inc.
ATTN: LI-San Hwang
ATTN: Technical Library

Texas A & M University System
Texas A & M Research Foundation
ATTN: Harry Coyle

TRW Defense & Space Sys. Group
ATTN: Norm Lipner
ATTN: Tech. Info. Center/S-1930
2 cy ATTN: Peter K. Dai, R1/2170
ATTN: Pravin Bhutta, R1-1104
ATTN: Donald Jortner, R1-2144

TRW Defense & Space Sys. Group
San Bernardino Operations
ATTN: E. Y. Wong, 527/712
ATTN: G. D. Hulcher

Universal Analytics, Inc.
ATTN: E. I. Field

DEPARTMENT OF DEFENSE CONTRACTORS (Continued)

URS Research Company
ATTN: Ruth Schneider
ATTN: Technical Library

The Eric H. Wang Civil Engineering Rsch. Fac.
University Station
ATTN: Larry Bickle
ATTN: Neal Baum

Washington State University
Administrative Organization
ATTN: Arthur Miles Bohorf for George Duval

DEPARTMENT OF DEFENSE CONTRACTORS (Continued)

Weidlinger Assoc. Consulting Engineers
ATTN: Melvin L. Baron
ATTN: J. M. McCormick

Weidlinger Assoc. Consulting Engineers
ATTN: J. Isenberg

Westinghouse Electric Corp.
Marine Division
ATTN: W. A. Volz